Multiport Power Electronics Circuitry for Integration of Renewable Energy Sources in Low Power Applications

A thesis presented in partial fulfilment of the requirements for the degree of

Doctor of Philosophy

In

Electrical Engineering

at Massey University, Palmerston North

New Zealand

Zubair Rehman

2017

Abstract

The increasing demand for electricity and the global concern about environment has led energy planners and developers to explore and develop clean energy sources. Under such circumstances, renewable energy sources (RES) have emerged as an alternative source of energy generation. Immense development has been made in renewable energy fields and methods to harvest it. To replace conventional generation system, these renewable energy sources must be sustainable, reliable, stable, and efficient. But these sources have their own distinguished characteristics. Due to sporadic nature of renewable energy sources, the uninterrupted power availability cannot be guaranteed. Handling and integration of such diversified power sources is not a trivial process. It requires high degree of efficiency in power extraction, transformation, and utilization. These objectives can only be achieved with the use of highly efficient, reliable, secure and cost-effective power electronics interface. Power electronics devices have made tremendous developments in the recent past. Numerous single and multi-port converter topologies have been developed for processing and delivering the renewable energy.

Various multiport converter topologies have been presented to integrate RES, however some limitations have been identified in these topologies in terms of efficiency, reliability, component count and size. Therefore, further research is required to develop a multiport interface and to address the highlighted issues.
In this work, a multi-port power electronics circuitry for integration of multiple renewable energy sources is developed. The proposed circuitry assimilates different renewable sources to power up the load with different voltage levels while maintaining high power transfer efficiency and reliability with a simple and reliable control scheme.

This research work presents a new multiport non-isolated DC-DC buck converter. The new topology accommodates two different energy sources at the input to power up a variable load. The power sources can be employed independently and concurrently. The converter also has a bidirectional port which houses a storage device like battery to store the surplus energy under light load conditions and can serve as an input source in case of absence of energy sources.

The new presented circuitry is analytically examined to validate its effectiveness for multiport interface. System parameters are defined and the design of different components used, is presented.

After successful mathematical interpretation, a simulation platform is developed in MATLAB/Simscape to conduct simulations studies to verify analytical results and to carry out stability analysis.

In the final stage, a low power, low voltage prototype model is developed to authenticate the results obtained in simulation studies. The converter is tested under different operating modes and variable source and load conditions.

The simulation and experimental results are compiled in terms of converter's efficiency, reliability, stability.

The results are presented to prove the presented topology as a highly reliable, stable and efficient multiport interface, with small size and minimum number of components, for integration of renewable energy sources.

Research Outputs

Journal Publications

1. Z. Rehman, I. H. Al-Bahadly and S. C. Mukhopadhyay "Multi input DC-DC Converters in Renewable Energy Applications- An Overview," Journal of Renewable and Sustainable Energy Reviews, 41, pp 521-539 January 2015. (Cited by 18 till 29th March 2017). Journal Impact Factor: 6.798 (29th March 2017).
2. Z. Rehman, I. H. Al-Bahadly and S. C. Mukhopadhyay "Renewable Energy Harvesting for low Power Wireless Monitoring Networks", Journal of Clean Energy Technologies vol. 5, No 6, pp. 448-453, November 2017.

Journal (In Press)

1. Z. Rehman, I. H. Al-Bahadly and S. C. Mukhopadhyay "A Single Stage-Single Inductor Multiport DC-DC Converter for low power Electronics Devices" Submitted to Journal of Power Electronics, 2017.

Conference Publications

1. Z. Rehman, I. H. Al-Bahadly and S. C. Mukhopadhyay "Dual Input-Dual Output Single Inductor dc-dc Converter", Proceedings of 41st International Annual Conference of the IEEE Industrial Electronics Society, IECON 2015, pp 004848-004853, 2015.
2. Z. Rehman, I. H. Al-Bahadly and S. C. Mukhopadhyay "Dual Input-Dual Output Single Inductor dc-dc Converter for Renewable Energy Applications," Proceedings of 4th International Conference on Renewable Energy and Research Applications ICRERA, pp 783-788, 2015.
3. Z. Rehman, I. H. Al-Bahadly and S. C. Mukhopadhyay, "A Non-Isolated DC-DC converter for Renewable Energy Based Portable Measuring Instruments," Proceedings of IEEE Instrumentation and Measurement Technology Conference I^2MTC pp. 936-941, 2013.
4. I. H. Al-Bahadly, Z. Rehman, and Joshua Pirihi, "Combining small scale Wind and Hydro Generation," Proceedings of International Conference on

Sustainability, Green Buildings, Environmental Engineering & Renewable Energy SGER, pp 122-133, 2016.

5. I. H. Al-Bahadly, James Tingey and Z. Rehman "Portable Energy Unit for Natural Energy disaster" Proceedings of International Conference on Sustainability, Green Buildings, Environmental Engineering & Renewable Energy SGER, pp 134-140, 2016.

Seminars and Presentations

1. Z. Rehman "Renewable Energy Harvesting for low Power Wireless Monitoring Networks". Presented at the 5th International Conference on Power Science and Engineering, (ICPSE 2016), Venice, Italy.
2. Z. Rehman, "Combining small scale Wind and Hydro Generation," Presented at International Conference on Sustainability, Green Buildings, Environmental Engineering & Renewable Energy (SGER, 2016), Kuala Lumpur, Malaysia.
3. Z. Rehman, "Portable Energy Unit for Natural Energy disaster" Presented at the International Conference on Sustainability, Green Buildings, Environmental Engineering & Renewable Energy (SGER, 2016), Kuala Lumpur, Malaysia.
4. Z. Rehman "Dual Input-Dual Output Single Inductor dc-dc Converter", Presented at 41st International Annual Conference of the IEEE Industrial Electronics Society, IECON 2015, Yokohama, Japan.
5. Z. Rehman, "Dual Input-Dual Output Single Inductor dc-dc Converter for Renewable Energy Applications," Presented at the 4th International Conference on Renewable Energy and Research Applications (ICRERA, 2015), Palermo, Italy.
6. Z. Rehman, "A Non-Isolated DC-DC converter for Renewable Energy Based Portable Measuring Instruments," Presented at the IEEE Instrumentation and Measurement Technology Conference (I^2MTC 2013), Montevideo, Uruguay.
7. Z. Rehman "Multi-port converters for Renewable Energy Applications", Presented at SEAT PG Seminar Day Program, 2015.
8. Z. Rehman "Design of a non-isolated DC-DC converter" Presented at SEAT Doctoral Seminar Day Program, 2014.

9. Z. Rehman "A Non-Isolated DC-DC Converter for Renewable Energy Based Portable Measuring Instrument", Presented at EICS Cluster Seminar Series, SEAT, 2013.
10. Z. Rehman "Multi Input Power Electronics Circuitry for Integration of Renewable Energy Sources" PhD Conformation Seminar 2013.
11. Z. Rehman "A Single Inductor Dual Input-Dual Output DC-DC Buck Converter for Standalone Hybrid Energy System" Presented at IEEE Post Graduate Seminar, SEAT, Massey University, 2013.

Awards

1. Massey University Doctoral Completion Bursary 2016.
2. Universities New Zealand Claude McCarthy Fellowship 2015.
3. HEC Pakistan MS leading to PhD Scholarship (2012-2017).

Acknowledgements

All the praise and thanks to Almighty Allah for His countless blessings.

I would like to acknowledge the contributions of all the people who have helped and supported me throughout my PhD studies.

I would like to express sincere gratitude to my Supervisors, Associate Professor Ibrahim H. Al-Bahadly and Professor Subhas Chandra Mukhopadhyay for their valuable guidance, help and support in my studies. I sincerely thank my supervisors for their able supervision, optimism inspiration, and confidence to conduct and complete this research work.

I am grateful to Dr. Jesus M. Corres from Public University of Navarra, Pamplona, Spain for his help, guidance, and support in this study. I am also thankful to Mr. Ken Mercer and SEAT administrative staff for their help and support.

Thanks to all my family members for their love and care.

Special thanks to my wife Beenish, daughter Romesa and son Abdul Mohaiman, for their love, patience, care, and support to successfully complete this research work.

I am thankful to Massey University Palmerston North for providing a wonderful research atmosphere, equipment, and resources.

I am also grateful to Higher Education Commission Pakistan (HEC) for providing me the opportunity for higher studies abroad and for providing all the financial support to complete this project.

Table of Contents

List of Figures

List of Tables

Abbreviated Terms

School of Engineering and Advanced Technology	SEAT
Higher Education Commission	HEC
Giga Watt	GW
Annual Energy Outlook	AEO
Hybrid Energy System	HES
Renewable Energy System	RES
Photovoltaic	PV
Power Electronics	PE
Single input-Single Output	SISO
Dual input-Single Output	DISO
Single input-Dual Output	SIIDO
Dual input-Dual Output	DIDO
Pulsating Source Cells	PSC
Multi-Input Converter	MIC
Three Port Converter	TPC
Multiport Converter	MPC
Pulsating Voltage-Source Cell	PVSC
Pulsating Current-Source Cell	PCSC
Pulse Width Modulation	PWM
Pulse-Skipping Modulation	PSM
Pulse-Frequency Modulation	PFM
Single input Multi Output	SIMO
Single Inductor Multi Output	SIMO
Continuous Conduction Mode	CCM

Multi Input Multi Output	MIMO
Multi Input	MI
Multi Output	MO
Discontinuous Conduction Mode	DCM
State Space Averaging	SSA
Relative Gain Array	RGA

Chapter 1

1 Introduction

1.1 Background

Electricity consumption around the globe is increasing day by day. Use of electricity throughout the world is expected to increase at an average of 0.8% from 2010 to 2040 [1]. To meet this immense energy demand, more electricity is required to be generated. The electricity generation is expected to increase by 24% from 2013 to 2040 [1]. The conventional methods of power generation using fossil fuels have lost their utility due to the emission of harmful gases, depletion of fossil fuels and environmental regulations. Thus clean, reliable, viable and sustainable sources of energy are of great importance to match the growing industrialization needs. In recent years, the focus of energy generation has shifted towards alternate methods using renewable energy sources. Noticeable technological advancements have been made in developing these energy sources. These are the solution to ever increasing power demand problem. The main factors behind the diversion of power generation methods from conventional to alternate generations are the fast depletion of fossil fuels, technical and environmental regulations, international agreements on climate change and awareness of people on green technologies based electric power generation systems.

1.2 Electricity Generation

According to International Energy Agency report (AEO 2015), the total electricity generation increases from 1065 GW to 1261GW in 2040. However, electricity generation from conventional sources like coal drops from 39% in 2013 to 34% in 2040 whereas the natural gas share of electricity generation grows from 27% to 31%. In case of Nuclear power plants, the share of electricity generation decreases from 19% to 15%. On the other hand, there is a substantial growth in the share of renewable energy generation from 2013 to 2040 as indicated in Figure 1-1 [1]. It is expected that by 2040, nearly 60% of all the power generation is to come from renewable sources [2].

Among the renewable energy sources, Hydropower is the largest contributor of the electricity in the category of renewable electricity generation. However, a tremendous growth is also seen in Wind and Solar powered generation system. Figure 1-2 reflects that by 2040, it is expected that two-third of the electricity generation by renewable energy sources will be contributed by wind and solar generation. In addition to that, the contribution of geothermal and biomass energy is also increasing at faster average rates.

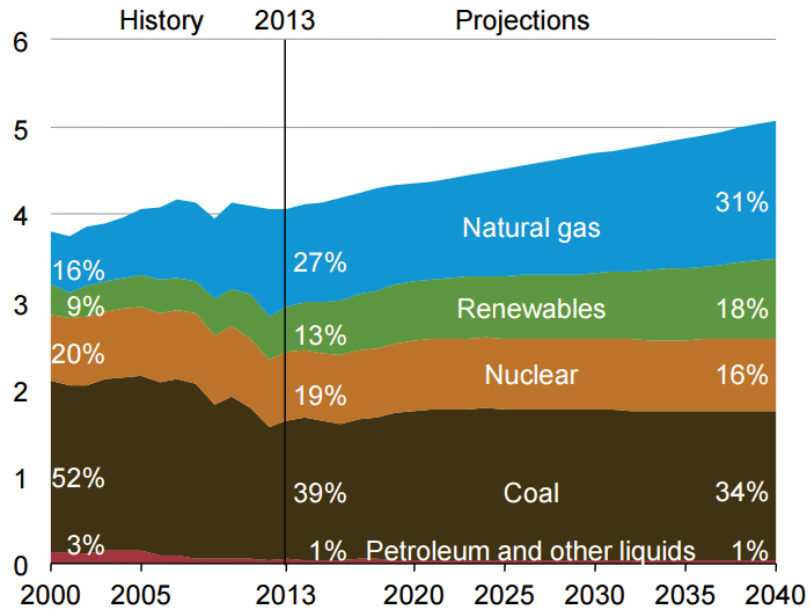

Figure 1-1 Share of electricity generation by fuel (2000-2040) [1]

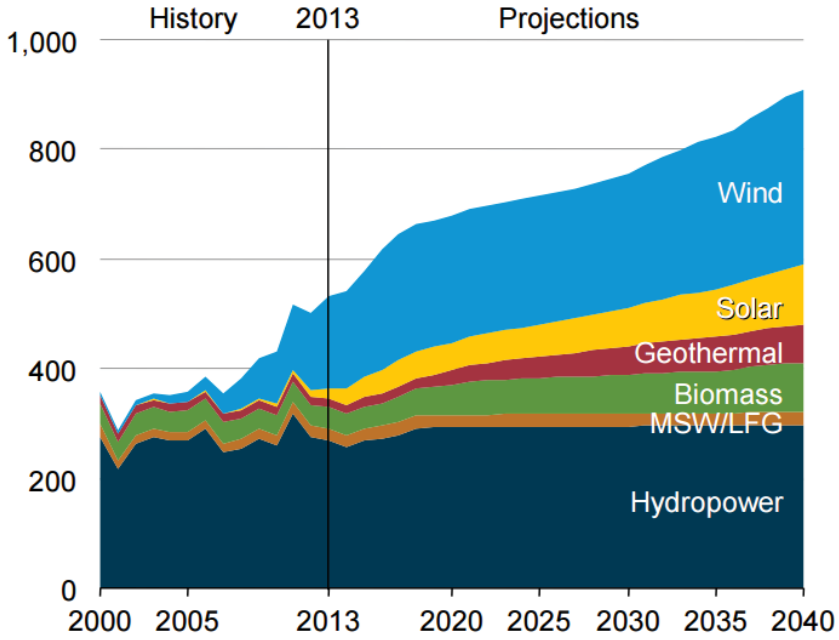

Figure 1-2 Share of Renewable Energy Generation by source [1]

Despite of decline in the electricity generation share from conventional sources and predictions of considerable growth in the share of renewable sources, yet the renewable sources are not considered as the most reliable source of electricity generation due to their inherited drawbacks. The major disadvantage of wind and solar energy sources is their dependence on weather which makes them intermittent in nature. They may be present at one time but can completely disappear at the other. This drawback can be removed by integrating these energy sources to develop a hybrid energy system [3]-[5].

1.3 Integration of Multiple Sources

In the recent years, tremendous improvements have been made to have alternate energy sources mainstream. Although renewable energy is the source of efficient and clean energy, yet this has some disadvantages due to the stochastic nature. For instance, wind and solar energy, which are not constantly available. Some, like fuel cells, exhibit slow response. Therefore, these are required to be integrated and/or connected to the utility grid to constitute a multi-source power generation or Hybrid Energy System (HES) wherein these energy sources complement each other to provide a reliable source of power [6]. A Hybrid Energy System is defined as "small set of co-operating units, generating electricity or electricity and heat, with diversified primary energy carriers (renewable and non-renewable), and while the co-ordination of their operation takes place by utilization of advanced power electronics systems" [7]. Figure 1-3 shows layout of a typical hybrid energy system utilizing renewable energy sources. Several workable combinations of distributed energy sources to constitute HES have been identified, among them the most common form of HES is wind-solar hybrid energy system which addresses the problems associated with independent wind and solar energy generations. In this combination, both the sources complement each other to enhance reliability of the overall system. The wind generation can be obtained round-the-clock depending upon availability and speed of wind while solar energy can support it during day time when usage is at its peak. To further enhance the reliability, a storage device can also be added to the system so that if the demand is less than supply, the excess energy can be stored which later can be used during peak consumption periods or in absence of RES [8]-[12]. Other possible combinations are wind-solar with Pumped hydro system [13], wind-solar with bio mass [14],[15] and wind photovoltaic with fuel cell system [16]-[18]. The hybrid

energy system can operate as a standalone power generation system in the areas where no utility power is available or the extension of transmission lines and construction of additional grid stations is not a viable option [19][20][21]. HES can also be connected to a utility grid to enhance the capacity, efficiency and reliability of the power distribution system [22]-[27].

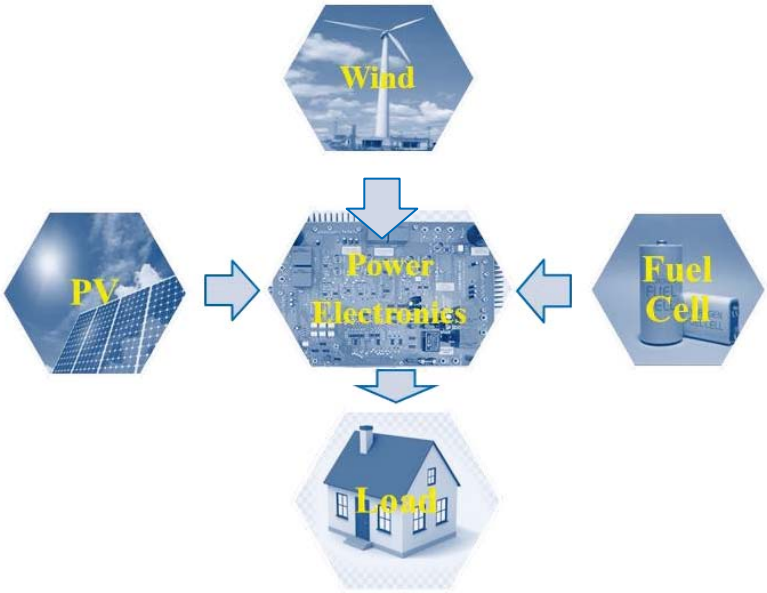

Figure 1-3 Typical Hybrid Energy System

1.4 Challenges in integration of Multiple Sources

Even though integration of multiple sources overcomes the irregular supply of power from RES but there are some additional challenges associated with this multisource interface. For instance, in a standalone hybrid energy system, due to the intermittency of power from wind and solar sources and variable load conditions, the overall system stability, reliability and continuity of this combination to power up the loads is still relatively low. Therefore, an energy storage unit needs to be connected to compensate or absorb the difference between the generated and required power [28].

As far as grid connected system is concerned, the integration of RES with utility grid has even more consequences. Renewable energy interface can cause power quality issues due to supply voltage variations. If RES is connected to the feeder with less loading, there are chances of reverse power flow. Likewise, a rapid variation in load current causes variation in feeder current which has adverse effects like dips and flickering in system voltage. Another problem is harmonics currents which can cause distortion in voltage wave form which can travel up to distribution grid [29]-[31].

Conventional utility grids usually imply protection scheme depending on single source of supply. When the sources are multiple they also contribute to fault currents. Which are difficult to detect and can create protection problems. The detection and setting of protective devices is made as per value of fault currents of the system. Addition of RES may increase this value therefore the interrupting capabilities of protective devices must be very carefully selected [32].

Overhead transmission lines are usually equipped with an auto re-closer system. As the temporary fault on overhead line does not persist for longer duration therefore the line is not permanently switched off rather it is switched off for shorter period and is reenergized after clearance of fault. The auto re-closer makes several attempts and if the problem persists then line is completely de energized. If RES is connected to the system, the line remains permanently energized and hence a temporary fault is sensed as permanent fault which is an undesirable scenario [33].

RE source connected to the utility grid is required to trip off in case of any abnormal voltage conditions. The feeders adjacent to the one where RES is connected may create similar situation of abnormal voltages. Under such conditions it is difficult for RES source protection scheme to discriminate between actual over /under voltage fault and impact of other feeders, as a result it trips off unnecessarily [29].

Under any fault conditions, Renewable energy source and utility grid both contribute to the fault current thus current at fault increases. The combined fault current may increase but the contribution from renewable energy source may be more than that from grid therefore the protective devices at the grid are not able to pick the fault and fault remains unnoticed which can lead to failure and system damage [33].

1.5 Power Electronics Interface

Irrespective of all the advantages the RES may have, their penetration and integration into an electrical network is not a trivial process, rather it is a very challenging task. Increasing number of these generating sources would require new methods and strategies to maintain the regulation of electric power in hybrid energy system [34]. To increase the usefulness of RES and to reduce their potential negative impacts, as highlighted above, power electronics (PE) interface can be used to integrate RES with the existing electrical power network [35]. Due to the unique capabilities of PE

interface, it is becoming more prevalent in use with all types of RES. The quality and reliability of electric power depends upon the efficiency, reliability, and sustainability of PE devices. PE interface can deal with conversion and control of electric power with the help of switch mode power converters. With the introduction of reliable and low-cost power electronics devices, most of the problems induced by the infiltration of renewable energy sources can be minimized or eliminated. Some of the advantages of PE devices are emphasized as,

- The issues like power quality of hybrid energy system due to their integration with existing distribution system, can be improved through effective PE interface. As it not only controls the harmonics contents of current and voltage but also provides fast operation and minimizes reactive power requirements of the grid. RES interface through PE allows the control of voltage and reactive power at the source of generation as the inverters of HES are self-commutated and are able to produce AC voltage, this allows HES to produce power at any power factor which provides reactive power support to the grid [36].
- Addition of RES to utility networks does have some adverse effects on the system protection which requires modification in selection and setting of protection devices. Power electronics devices have resolved this problem by enabling the devices to respond quickly to the faults contributed by renewable source and instantly rectifying them before having any impact on existing grid protection system.
- Power electronics devises have been found very effective in interfacing the multiple energy sources. The use of common DC bus allows the integration of several renewable energy sources and storage devices which enhances system reliability.
- An important property of hybrid energy system is the formation of micro grid. During the micro grid formation, HES must have the ability to quickly switch between stand alone to grid connected mode. To do this, an extremely fast switching will be required which is only possible through power electronics devices [37].

Various power electronics converters have been developed to integrate renewable energy sources and to control of power from source to load. These converters perform the following functions in hybrid energy system [38]-[41].

- Conversion of power from variable input voltages to regulated output voltages.
- To ensure the high-quality output power with low voltage and frequency deviation.
- Perform electrical isolation between source and load.
- Track Maximum power in wind and solar energy system.
- Power conditioning and control flow of Power from source to load
- Conversion of power to the required voltage and frequency

Numerous power electronics converters have been presented for renewable energy interface in hybrid electrical system. These converters can perform AC to DC, DC to DC and DC to AC conversion and can be classified into several groups as single stage converters like AC-AC, AC-DC, DC-DC, DC-AC or multiple stage converters like AC-DC-AC converters [39]. The application of power electronics converters depends on renewable energy source and requirement of load. For an instance wind energy generation system, may require single stage AC-AC conversion or AC-DC conversion or multiple stage AC-DC-AC conversion. Similarly, Solar energy system may employ DC-DC conversion or DC-AC conversion depending upon the connected load. Power electronics interface in DC and AC type of renewable energy sources is shown in Figure 1-4. This research work is primarily associated to DC-DC conversion.

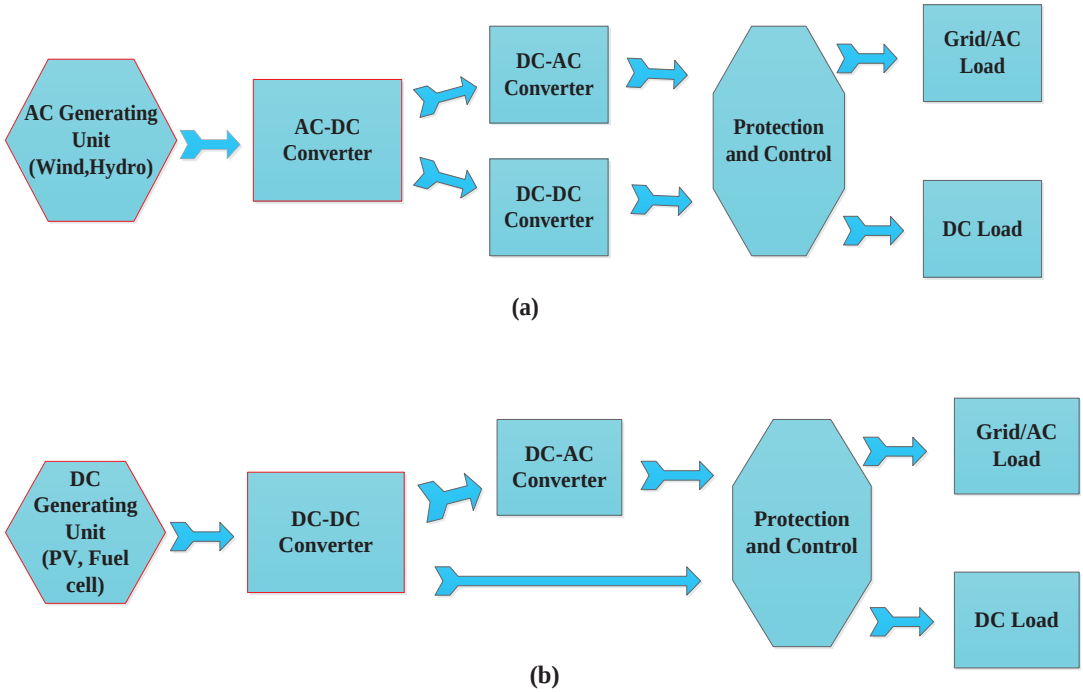

Figure 1-4 PE interface for RES (a) AC Generating units (b) DC generating Units

1.6 DC-DC Converters

DC-DC converters are most common and are widely used in renewable energy systems to provide a controlled and regulated supply from an uncontrolled and unregulated renewable energy source [42]. There are two main types of DC-DC converters used in renewable energy applications. One is the isolated type of converters where a high frequency transformer is used to provide isolation between source and load [43],[44]. These types of converters are used in medium to high power renewable energy applications. The other type is non-isolated converters. These converters are used in low power applications where high frequency transformer is not required for input and output isolation. These are very popular in RES applications due to their smaller size and less components and high conversion efficiency [45],[46]. Non-isolated converters can be further divided into two categories i.e. Single-port converters and Multi-port converters. The focus of this work is on non-isolated, Multiport DC-DC converters.

1.7 Statement of Research Problem

The incremental need of electricity, increasing economic/environmental challenges in conventional power generation system and safety concerns about nuclear power plants has shifted the focus of future power generation towards renewable energy resources. Although these sources are inexhaustible and can provide clean and green energy however these have their own distinguished features. The renewable energy sources are highly unpredictable and intermittent in nature therefore integration of these sources to existing network is not an easy task. To effectively utilize these sources, power electronics interface plays a vital role. Power Electronics converters are used to integrate renewable energy sources. Numerous converter topologies (single port and multiple-port) have been used in renewable energy applications in the past decade. Multi-port power converter topologies are preferred over single port converter topologies due to the use of fewer components, decreased size and reduced cost. Several multiport converters have been proposed in the literature to integrate different renewable energy sources. Comprehensive review of multiport topologies, presented in chapter two of this dissertation, has identified some drawbacks in the existing topologies. Table 2-2 presents the summery of the limitations, spotted during the

literature review for non-isolated multiport DC-DC converters. Literature review reveals that there is a need to conduct further research in the area and further development of a multiport power electronics interface is required. The interface which could assimilate multiple renewable energy sources and power up multiple loads and the surplus energy could also be stored and utilized in case of absence of RES.

1.8 Aims and Objectives

The objective of this research is to develop a multi-port power electronics circuitry for integration of multiple renewable energy sources with variable input voltage and load characteristics. The proposed circuitry will assimilate different renewable sources to power up the load with regulated output while maintaining high power transfer efficiency and reliability with a simple and reliable existing control scheme. The performance of the proposed circuitry will be analysed on the bases of conversion efficiency, reliability and number of components in the circuit. The proposed circuitry will be examined analytically and computer simulations will be carried out. The results obtained will then be verified by performing experiments on prototype circuit. The research work will be divided into groups to achieve the different sub objectives which will lead to accomplish the main objective.

Objectives 1: To conduct an extensive literature review of available power conversion topologies to design and refine the research for the achievement of main goal. This will be an ongoing process during the whole course of research work.

Objective 2: New topology of multi-port DC-DC non-isolated converters for low voltage low power applications will be proposed on the bases of literature review and identified research problems. Design, mathematical modelling, simulation, and experimental results will be presented to support the utility of new topology. Control system analysis will also be conducted using existing control schemes.

Objective 3: Multi input-Multi output power electronics circuitry for low voltage and power applications will be designed and developed for standalone low power applications.

1.9 Scope of Work

Renewable energy sources may be integrated by using various converter topologies, however, this work is focused on low power, non-isolated DC-DC buck converter.

1.10 Research Methodology

The methodology to successfully complete this research project is composed of different phases. In each phase, certain predefined objectives will be achieved. The research methodology is comprised of the following steps.

- Identify
- Model
- Simulate
- Develop
- Test

1.10.1 Mathematical Modelling

Based on the literature review and identified research gaps, new topology of a non-isolated multiport DC-DC buck converters is proposed. Mathematical model of proposed topology is presented and analysed as per different parameters.

1.10.2 Simulation Studies

After the successful mathematical modelling and analysis, the circuitry is simulated in MATLAB/Simscape. The operating conditions are defined, rating and capacity of the system is determined by defining the input power and load requirements. Circuit components are designed accordingly. The obtained simulation results are compared with the analytical results to demonstrate the feasibility of the proposed topology. Several simulation programs are run based on different operating conditions and performance is evaluated as per different parameters.

1.10.3 Experimental Studies

A prototype model of proposed topologies is developed and experiments are conducted as per different operating conditions. The obtained results are critically evaluated and compared with the existing topologies to demonstrate the novelty of the proposed topology.

Based on the analytical, simulation and experimental results, a novel multiport power electronics circuitry is developed and presented. The presented circuitry is compared with the existing converter circuits in low voltage and power applications and the

performance is evaluated with respect to reliability, efficiency, number of components, and size of the circuitry.

1.11 Research Contribution

The major contribution of this research work is to develop a multi-port power electronics circuitry for integration of multiple renewable energy sources. The proposed circuitry will integrate different renewable sources to power up the load with regulated output while maintaining high power transfer efficiency and reliability with a simple control scheme. In addition to energize the load, the circuitry also supports the storage of excess energy which can be later used, in absence of renewable energy sources. The contributions of this research work can be summarised as

- Design a novel multiport non-isolated DC-DC buck converter circuit to interface multiple sources and loads for low power application
- Conduct mathematical analysis to prove the effectiveness of the converter circuit
- Develop a simulation platform to test the newly designed circuit and to conduct simulation studies for different mode of operation and variable source and load conditions using the control system already presented in the literature.
- Develop a low power prototype model for multiport converter.
- Test prototype model under different operating conditions.
- Present simulation and experimental results to prove the novelty and uniqueness of the developed circuitry.

1.12 Applications

The proposed topology will find its possible applications in harvesting of renewable energy for low voltage low power portable electronic devices, measuring instruments, low power house holds equipment and remotely deployed wireless sensors networks.

1.13 Thesis Organisation

The dissertation is organised in eight chapters

Chapter 1

This chapter enlightens the background of the research area. It briefly describes the drivers, opportunities and challenges for renewable power generating sources and their possible integration in electricity network. The importance of Power Electronics (PE) interface and some basic components of PE are also briefly discussed. Research problem is apprised, Research objectives are demarcated, research methodology is formulated and research contributions are also summarized in this chapter.

Chapter 2

A review of non-isolated PE converters is presented in this chapter. Single-port converters are briefly discussed whereas Multiport converters are comprehensively explored.

Chapter 3

A new topology of multi-port non-isolated DC-DC buck converter is introduced in this chapter. Merits of the new topology are highlighted its structure is presented and mathematical analysis are conducted. Guidelines for selection of different components to design and develop the presented topology are also presented in this chapter.

Chapter 4

This chapter explores different control schemes adopted to control the multiport converters in renewable energy applications. An overview of control scheme adopted for this research work is presented and a small signal model of the converter for linear analysis is presented.

Chapter 5

This chapter covers the development of simulation platform, selection and finalization of design parameters and simulation studies of the converter in different modes of operation. Open loop and closed loop simulation results are presented in this chapter.

Chapter 6

To validate the analytical and simulation results presented in chapter 3 and chapter 5, experiments are conducted on prototype model. The presented topology is tested for different operating conditions and results are presented in this chapter.

Chapter 7

The results obtained in chapter 3,5 and 6 are critically analysed in this chapter. Power transfer efficiency of the new topology is presented for different modes and under different conditions. Results of stability analysis of the converter are presented. Finally, the comparison of the presented topology, in terms of its efficiency, reliability, size and components count is made with the topologies cited in the literature.

Chapter 8

Final conclusions are drawn in this chapter and opportunities of further research work in the area are identified.

Chapter 2

2 Non-Isolated DC-DC Converter Topologies

2.1 Introduction

Non-isolated DC-DC converter topologies are extensively used in low power renewable energy interface. The purpose of these converters is to connect the generating the source to load by stepping up or stepping down the generated voltage and to provide the regulated output from an irregular supply source. In addition, these converters also track maximum power point in case of PV and wind energy applications. Non-isolated DC-DC converters used is renewable energy application can be further divided to into two categories i.e. Single port converter and Multiport converter. The former is used to connect a single source to a solitary load whereas later is utilized to connect the multiple RES to a single or single RES to multiple loads,

2.2 Single-Port Non-Isolated DC-DC converters

2.2.1 DC-DC Boost Converters

In DC–DC boost or step-up converter, the magnitude of output voltage is always higher than the magnitude of input voltage. This topology is used where the requirement of load voltage is higher than the generating source voltage. Boost converters are commonly used in photovoltaic generation in standalone and grid operated systems. In order to achieve high gain and high efficiency, the conventional boost converters have been modified, and the topologies like Boost converter with coupled inductor, Boost converter with switched capacitor, Boost converter with inductor and switched capacitor and Boost converter with coupled inductor and switched capacitor, have been introduced [47]. A comprehensive literature review of DC-DC boost converters used to interface RES can be found in [47] and [48].

2.2.2 DC-DC Buck Converters

In DC–DC buck converter also known as or step-down converter, the magnitude of output voltage is always lower than the magnitude of input voltage. This topology is used to interface high generating voltage renewable energy source to low voltage load or low voltage storage devices. In this topology voltage modulation is generally

performed by PWM signal to charge the batteries or to track the maximum power point in case of wind and solar systems. In order to achieve the high step down voltage ratio, the conventional buck converters are modified to an interleaved two phase buck converter [49], coupled inductor synchronous buck converter [50],[51] and interleaved buck converters [52].

2.2.3 DC-DC Buck-Boost Converters

The buck–boost is a step-up or step-down converter. In this topology, the magnitude of output voltage can be lower or higher than the magnitude of input voltage. This topology is used to connect nearly-matched load and source voltage. This topology can be constructed by cascading two basic converters (boost and buck converter). The conversion ratio of output and input voltages is the ratio of the two converters in cascade when the switches of both the converters have the same duty ratio [53]. The voltage-conversion range of the converter is widen by proposing a synchronous rectifier technique [54]. To achieve zero voltage switching and high step up, step down ratio a bidirectional LCL resonant converter is introduced in [55].

2.2.4 DC-DC Cuk Converter

This type of DC-DC converter performs the function of stepping up or down input voltage like buck–boost converter and is used for connecting nearly-matched load to source voltages. Major advantage of this topology is its continuous current at the input and output. Whereas the disadvantage is high electrical stress on components and higher number of passive components [56]. This topology is extensively used for maximum power extraction from PV panel using several control algorithms such as PI, sliding mode control and fuzzy-logic control [57],[58].

2.2.5 DC-DC SEPIC Converter

Single-Ended Primary Inductor Converter (SEPIC) is like buck-boost converter capable of stepping up or down input voltage and has non-inverting characteristics. The difference being that it has two inductors. SEPIC converter as like Cuk converter, has the requirement of the switch control terminal connected to ground similarly the input current is continuous like cuk converters and draws ripple-free current from a PV panel which is important for effective MPPT. The drawback being this topology

is only applicable where the battery voltage is higher than the PV source voltage [59],[60].

2.3 Multi-Port Non-Isolated DC-DC converters

Recent developments in renewable energy based power systems, hybrid vehicles, aerospace systems and hand held portable devices have brought challenges to the design a new DC-DC power conversion systems. This new system will be composed of several input energy sources, integrated through a multi input power electronics converters, that could accommodate a variety of input sources and combine their advantages to deliver a controlled output for diversified applications [61]-[65]. Two structures for DC-DC conversion have been reported in the literature. In the conventional structure, as shown in Figure 1, multiple sources are combined at a common DC bus and separate DC–DC conversion stages are employed for individual sources and converters are controlled independently [27],[66] in some cases, a communication bus is also added for exchange of information between sources. As this system involves power conversion at multiple stages and communication devices are sometimes required, therefore the resulting cost of the converter is on higher side. The independent control of several converters also makes the system complex.

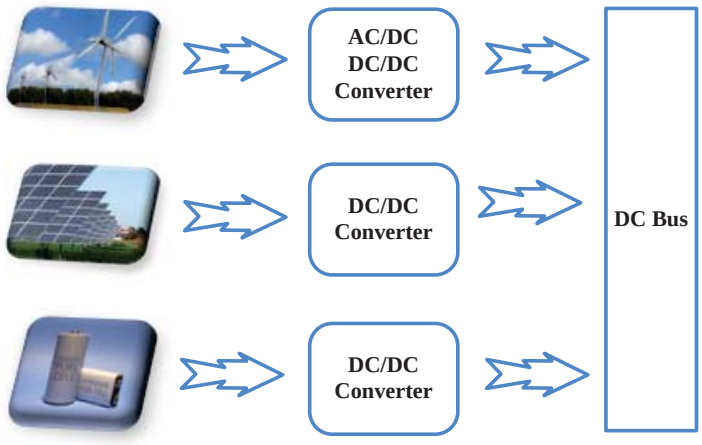

Figure 2-1 Conventional single-port Structure

To overcome these disadvantages, a multiport structure is adopted as shown in Figure 2. In this system, the whole structure is treated as a single power converter, which combines multiple sources [67]. In this structure, all the sources share the output circuitry of the converter. Due to their simple structure, minimum number of

conversion stages and less devices, these multiport power electronics converters have been proposed for a number of applications like hybrid energy systems [68]-[70], hybrid vehicles [71]-[75], satellite/aerospace applications and uninterrupted power supplies [76]-[78]. These are further divided into two categories (a) isolated and (b) non-isolated converters. Isolated converters [79]-[82] are used to isolate Low voltage DC side from high voltage side to avoid shock hazard, to achieve high voltage conversion, for voltage matching and to avoid large current and voltage rating semiconductor devices. High Frequency transformers are used for this purpose. But the disadvantage of this system is that it needs to accommodate transformer core which makes it bulky and in terms increases the cost. The non-isolated converters on the other hand are simple in structure and are used where the galvanic isolation between source and load is not required. The advantage of this topology is low cost due to less number of components and it can achieve high power density.

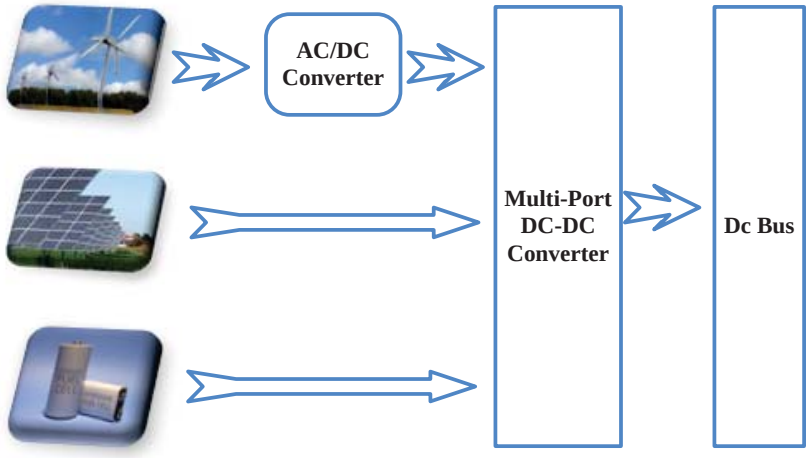

Figure 2-2 Multiport DC-DC converter structure

The non-isolated multiport converters can be further classified into dual input-single output converters, Single input-dual output converters and dual input-dual output converters.

2.4 Dual Input-Single Output DC-DC Converters (DISO)

The use of dual input-Single output converter is found in several renewable energy based power systems. A dual-input non-isolated converter, with central capacitor capable of boosting multiple PV strings and tracking two MPP with reduced voltage stress, integrates several PV panels and operates in wide voltage range [61]. A non-isolated DC-DC converter is presented for PV and battery Hybrid energy system in

[83]. Similarly use of Dual input-single output converter is also found in mobile devices [84]. A new family of multi-input converters based on three switched leg is presented for low-voltage applications. In this topology, the number of input sources are increased without using transformers and can simultaneously power up the common load with a bidirectional operation [85]. Dual input-Single Output DC-DC converters are proposed and analysed for a high and a low voltage source in [86] and [87], as shown in Figure 2-3. This converter is a combination of the buck-boost and the buck converter. Four modes of operation are defined which are based on availability of input voltage sources and conduction state of their respective switches (S_1& S_2). Low voltage source (V_{low}) is considered as the primary input source to provide the base load whereas the high voltage source (V_{hi}) caters the additional load demand. Input voltage sources (individually and simultaneously) charge the inductor during the ON state of their switches. When switches are ON, the diodes are reverse biased and when the switches are OFF, diodes (D_1& D_2) provide path for discharge of inductor current. Typical waveforms of Inductor voltage (V_L), Inductor current (I_L), and duty cycles (d_1 & d_2) are shown in Figure 2-4. If one of the voltage sources is not available, other source will provide energy to the load. The input-output voltage relationship is derived from the volt-second balance analysis of the inductor in steady state conditions. The output voltage (V_o) can be expressed as,

$$V_o = \frac{d_1}{1-d_2} V_{hi} + \frac{d_2}{1-d_2} V_{low} \tag{2-1}$$

Where d_1 and d_2 are the duty ratios of switches S_1 and S_2 respectively. To minimize the switching loss and to improve the overall efficiency, a passive lossless switching is added in the circuit.

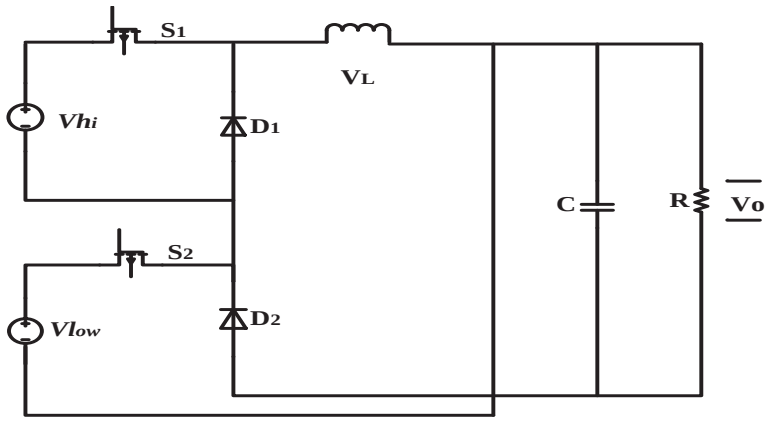

Figure 2-3 Double Input Buck-Buck Boost Converter

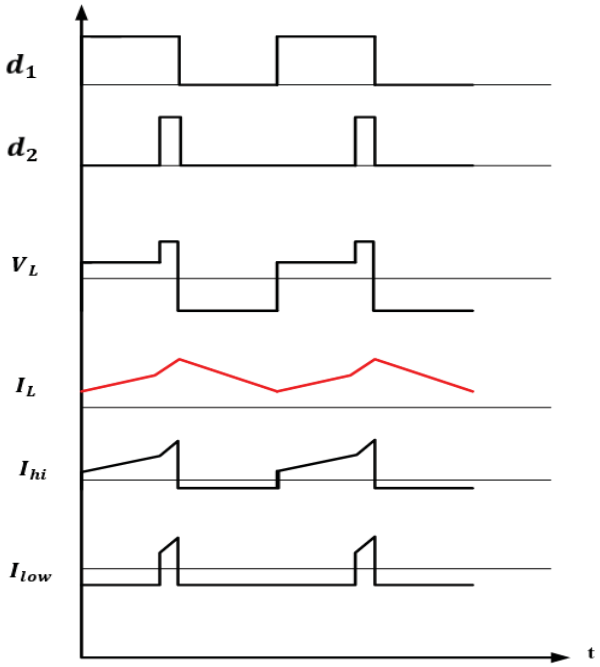

Figure 2-4 Typical current and voltage waveforms of double input converter

A topology with multiple inputs based on buck-boost converter is proposed in [88], as shown in Figure 2-5. This converter has reduced the circuit components but its drawback is negative reference output which can be reversed by using a transformer, with the addition to the cost and size of the topology. The converter operates in one direction and another converter is required for bidirectional operation. Another drawback of this topology is that only one source can deliver the power at a time. These drawbacks are removed by a bidirectional multi input DC-DC converter topology, introduced in [89], as shown in Figure 2-6. In addition to the advantages described in [88], this topology provides positive output voltage without any additional transformer. It can also operate in bidirectional mode without the requirement of any additional converter. It operates in three modes i.e. buck, boost, and buck–boost. But the number of devices has increased which increases the conduction losses and makes the converter costly. The conduction losses of switches in dual power state can be greatly reduced in the boost converter proposed in [90]. In this topology, bidirectional operation is achieved by applying less number of controllable switches. However, the reverse recovery current in output diode reduces the overall efficiency of the converter. The issue is addressed in a Zero Voltage Switching multi-input converter investigated in [91]. This converter utilizes current sources at input. Conduction losses of the switches are reduced due to series connected

input cells and Pulse Width Modulated (PWM) signals in the dual-power-supply state. An auxiliary circuit is added in the discontinuous conduction mode (DCM) to achieve turn-on zero voltage switching of all switches. Reverse-recovery current of the output diode in boost converter is removed by an auxiliary inductor, connected in series with Schottky diode. In this converter, two power sources with different voltage levels are converted to a single stable DC output. Another high-efficiency ZVS dual-input converter is investigated and experimental tested in [92], utilizing zero current switching turn OFF of all active switches by a modified auxiliary cell proposed in [93]. The reverse-recovery currents of the diodes and the switching losses of the switches are reduced. A high overall conversion efficiency has been achieved and the converter can be used for high voltage applications. However, this converter can induce electromagnetic interference (EMI) problems if used for non-isolated Photo Voltaic (PV) applications.

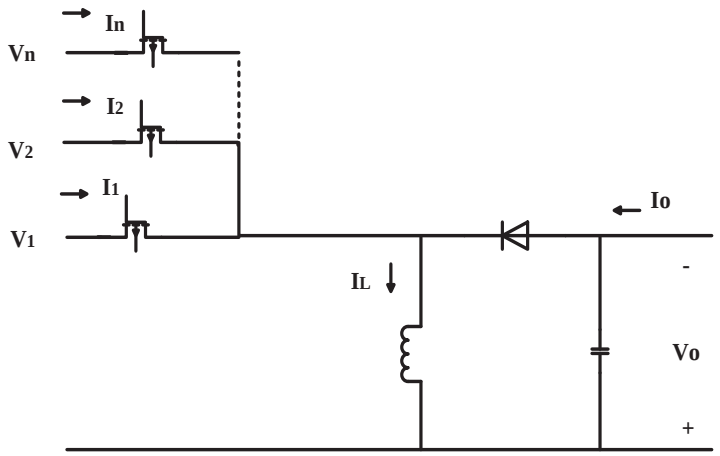

Figure 2-5 Unidirectional Multi input buck-boost converter

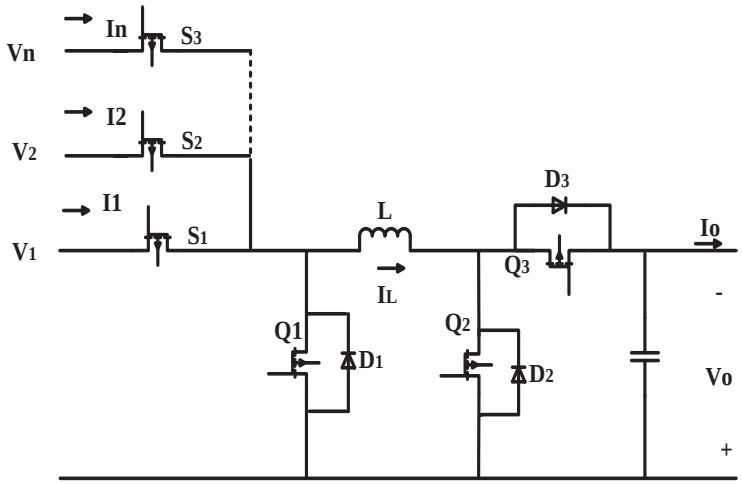

Figure 2-6 Bidirectional multi input converter

Two topologies like integrated buck-buck (Figure 2-7) and integrated buck boost-buck boost (Figure 2-8) are presented in [94] and [95]. The former topology can deliver the output power individually and simultaneously with both the sources whereas in the later topology voltage sources are unable to feed the load simultaneously. Four modes operation are defined for buck-buck converter topology (Figure 2-7) depending on the condition of switches.

Mode I $[M_1: ON / M_2: OFF]$: As M_1 conducts in this mode therefore diode D_1 is reverse biased whereas diode D_2 provides a bypass path for inductor current I_L. Voltage source V_1 provides power to inductor and the load.

Mode II $[M_1: ON / M_2: ON]$ both the switches are conducting and both the diodes are blocking. Both the voltage sources connected in series and both energize inductor and provide energy demand for load.

Mode III $[M_1: OFF / M_2: ON]$): In this mode switch M_2 and diode D_1 are in the state of conduction while diode D_2 is OFF. Voltage source V_2 is responsible to energize inductor and powers up the load.

Mode IV $[M_1: OFF / M_2: OFF]$ As both the switches are OFF therefore the diodes D_1 and D_2 provide the path for flow of current and the inductor discharges to release stored energy to the load. If a single source operates, the power conversion operation is same as in the conventional buck converter. By applying volt-second balance theorem, the input-output voltage relation can be obtained and is given by

$$V_o = V_1 d_1 + V_2 d_2 \tag{2-2}$$

Where d_1 and d_2 are the duty ratios of switches S_1 & S_2 respectively and V_o is output voltage. Typical current and voltage waveforms are shown in Figure 2-9.

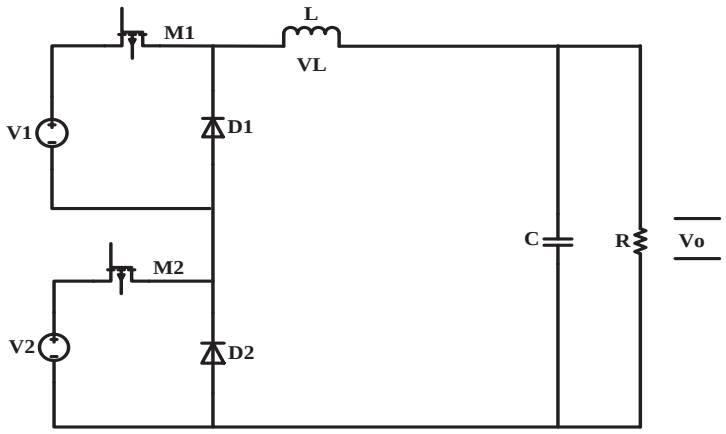

Figure 2-7 Dual Input Buck-Buck Converter

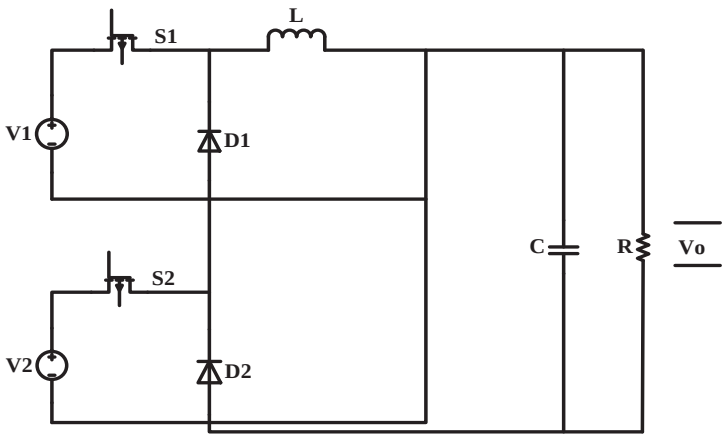

Figure 2-8 Dual input buck boost-buck boost converter

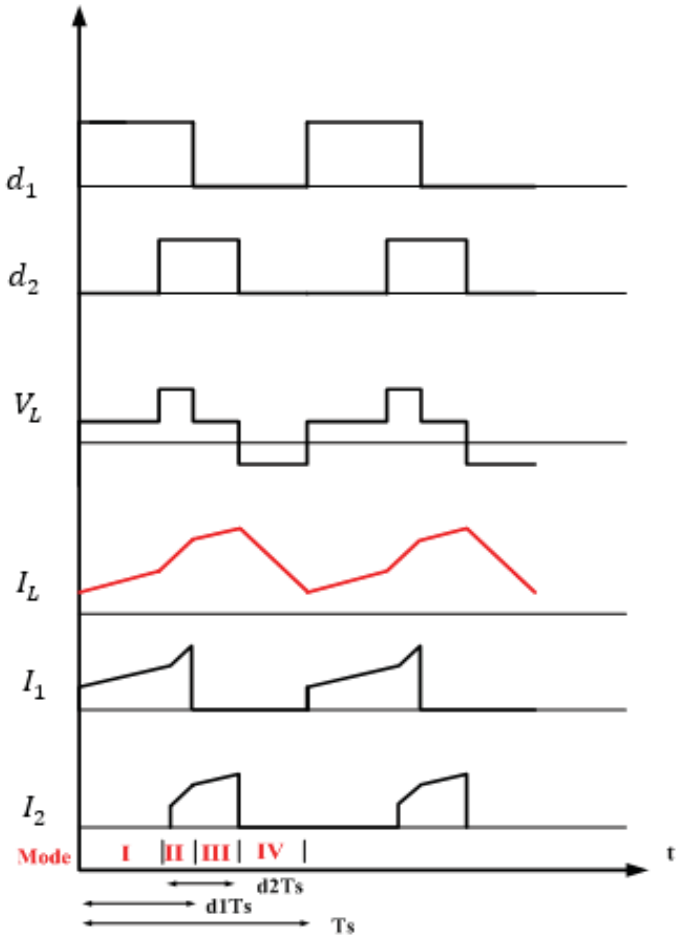

Figure 2-9 Typical waveforms of dual input buck-buck converter

In the topologies reported above, the method of developing dual or multi input converters from single input converter has not been explained. This method is explained in detail by the authors of work [96] and [97]. In this work, the concept of the pulsating voltage-source cell (PVSC) and the pulsating current-source cell (PCSC)

has been introduced. These pulsating source cells (PSCs) are extracted from the six basic non-isolated converters like buck, boost, buck–boost, Cuk, Zeta, and SEPIC converters. Two families of multi input converters (MICs) have been generated by inserting these PSCs into the six basic non-isolated converters. The input sources of the generated non-isolated MICs can transfer energy to the load individually or simultaneously. However, the topologies with time-multiplexing control scheme are not considered in this approach. Feasible topologies of multi input DC-DC converters based on some conditions, assumptions and restrictions are identified and several multi input converters are derived with time multiplexing control scheme [98]. Multi input converters (MICs) are also synthesized by using six basic pulse width modulated DC-DC converters by a systematic method [99]. Two types of MICs are considered one which allows only single source to transfer power to output load at a time, and the other allows both the input sources to deliver energy to output load either individually or simultaneously. The basic cells for constructing DC–DC converters have been discussed first and then basic Pulsating voltage source Cells and, basic pulsating current source cells, and hybrid Pulsating Source Cells (PSCs) are proposed and the rules for connecting PSCs are defined and finally two families of MICs are developed.

Nicole et al., [100] proposed a hybrid Multi-input DC-DC converter for high step-down conversion voltage ratio. In this topology, the output voltage can vary in a wider range. The proposed dual input hybrid DC-DC converters are obtained using hybrid and classical buck structures. The output/ Input relationship is being given as

$$V_O = \frac{2d_1 - d_2}{2 - d_2} V_1 + \frac{d_2}{2 - d_2} V_2 \quad \text{for } d_1 > d_2 \tag{2-3}$$

$$V_O = \frac{d_1}{2 - d_2} V_1 + \frac{d_2}{2 - d_2} V_2 \quad \text{for } d_1 \leq d_2 \tag{2-4}$$

Where V_O is Output voltage, $V_1 \& V_2$ are the input voltages for source 1 & 2 and $d_1 \& d_2$ are the duty ratios of the switches. The output voltage in this topology is reduced by a factor of (2- d_2) which is lower than normal buck converter. Similar approach has been adopted in [101] and [102] using a multi input hybrid buck LC converter for a standalone small hybrid wind turbine and PV with battery storage system. Analysis, simulations, and experimental results show that this topology has the advantage of a high input to output voltage conversion ratio without using a transformer, which facilitates the connection of a low voltage battery to the renewable

sources at a higher voltage. Three operating modes have been discussed and the results show that the system operation is stable in each operating mode. However, efficiency of the converter has not been taken into account in experiments.

Ashok and Kumaravel [103] proposed a multi input power conditioner with two inputs and one output DC-DC boost converter for a hybrid electric system. The proposed system overcomes capacitor voltage imbalance problem associated with single sourced converters. This converter has the advantages like lower voltage stress on the power switch employed in DC/DC converter, less switching loss of the switch, regulated output and can deliver reliable output power. Simulation has been carried out using the real weather data. The obtained results show that the topology can be highly beneficial in renewable energy applications. Multi input DC-DC converter is proposed with the integration of Cuk and SEPIC converters in [66]. The advantages of this topology are there is no need of separate input filters, can support step up/down operations for each renewable energy source, can ensure maximum power point tracking MPPT for each source and supports individual and simultaneous operation modes.

2.5 Single Input-dual output DC-DC Converters (SIDO)

Single input-dual output converters (SIDO) with the advantage of fewer components and multiple output voltages are being broadly used in electric vehicles [104], Power factor correction [105], USB links [106], portable applications like digital cameras, cellular phones, hand held devices, MP3 players and LED drivers [107]-[110]. A series of non-isolated multioutput converters is developed from single-inductor converters with addition of switched capacitor techniques and three dual-output pulse width modulation (PWM) converters are derived by integrating the switched capacitor based inverting technique and boots trap technique with the basic boost circuitry. More topologies are then derived from this basic converter series [111]. A non-isolated Single Input Multi output dc–dc Converter that can deliver step-up and step-down outputs from a single dc source. In this topology control switch of a boost converter are replaced by switches connected in series and using the resulting switch nodes to get extra outputs [112]. Various SIDO converters have been reported in the literature. Figure 2-10 shows a circuit of a SIDO converter. Q_1& Q_2 are the controlled switches, V_{in} is the input voltage, V_{01} and V_{02} are the two output voltages and two diodes are

represented by D_A and D_B. Three classes are investigated in continuous conduction mode depending on input-output voltages, duty cycles d_1 and d_2 of respective switches [113],[114].

Class-1: $\boldsymbol{d_1 > d_2}$: In this case, during time period t_1, both the switches are turned ON. The inductor is charged with the current $I_L = \frac{V_{in} - V_{o1}}{L}$ and the diode D_B is reverse biased due to the fact $V_{o2} > V_{o1}$. During the next time period t_2 , Q_1 is still on but Q_2 is turned OFF, the inductor current ramps up with the slope $\frac{V_{in} - V_{o2}}{L}$ and flows through diode D_B to the output V_{o2}. During the time period t_3 when both $Q_1$and Q_2 are off, the inductor current I_L flows through both the diodes $D_A$and D_B and discharges through V_{o2} . In this class of operation, the inductor is charged through two periods and is discharged to output voltage V_{o2} in the last period.

Class-2: $\boldsymbol{d_1 = d_2}$: In this case both the switches are turned ON. The inductor is charged with the current $I_L = \frac{V_{in} - V_{o1}}{L}$ and the diode D_B is reverse biased due to the fact $V_{o2} > V_{o1}$. In the next time duration, when both Q_1 and Q_2 are turned OFF, the inductor current flows through both diodes and discharges to output V_{o2}. In this class of operation, the inductor is charged through one period and is discharged to output voltage in the last period.

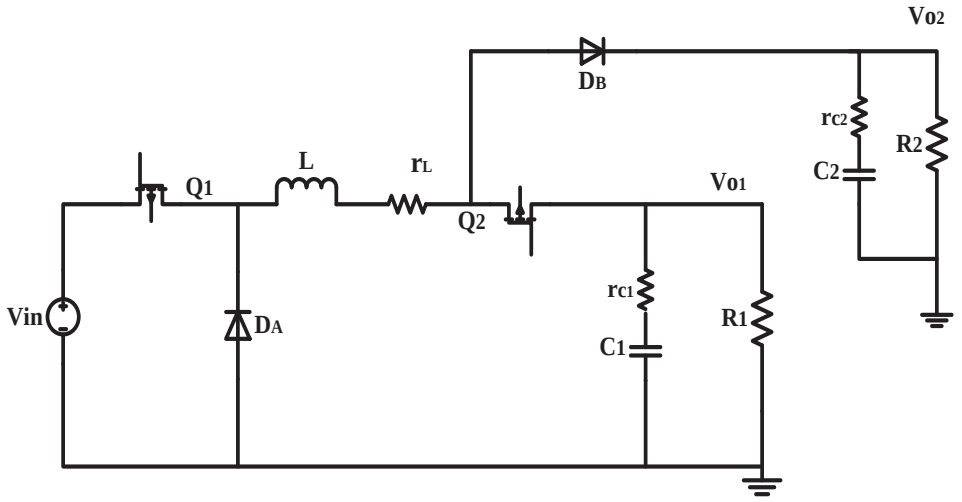

Figure 2-10 Single input-dual output buck converter

Class-3: $\boldsymbol{d_1 < d_2}$**:** Both the switches are ON during the time period t_1. The inductor is charged with the current $I_L = \frac{V_{in} - V_{o1}}{L}$ and the diode D_B is reverse biased due to the fact $V_{o2} > V_{o1}$. During the time period t_2, switch Q_2 is still on but Q_1 is turned OFF. The inductor current flows down to V_{o1} with the slope of V_{o1}/L through diode D_A.

During the time period t_3, both $Q_1$and $Q_2$are off, the inductor current is flows through diodes $D_A$and D_B with the slope V_{o2}/L. In short, when the switch $Q_1$is in ON state, energy is stored in the inductor; when $Q_1$is in OFF state, power is delivered to one of the outputs, depending on the state of switch Q_2.

Three different methods of converting single out converter to dual output converter are discussed and compared [38]. A simple method is to use time multiplexing of inductor current. In this method, different switches conduct inductor current to their output voltages for a fraction of time. In the other method, output energy is drawn from the complementary terminals of the inductor. The third method is to use switched nodes to charge capacitors. Furthermore, concept a single energizing cycle and multiple energizing cycles per switching period for smooth flow of energy is also discussed in [115]. Design and control of a dual output buck converter is explained in [116]. In this approach, the number of switches is reduced thus reducing the overall cost of the converter. The problems like large ripple and cross regulation of output voltages associated with single inductor dual output buck converter have been addressed and methods to supress these problems have been discussed in [117]. A single inductor multi output buck converter with two outputs V_{01} and V_{02} is shown in Figure 2-11. These output voltages are regulated by adjusting duty cycles d_1 & d_2. Steady state output input relation is given by

$$\frac{V_{o1}}{V_{in}} = \frac{d_1 d_2 R_1}{d_2^2 R_1 + (1-d_2)^2 R_2} \tag{2-5}$$

$$\frac{V_{o2}}{V_{in}} = \frac{d_1 (1-d_2) R_2}{d_2^2 R_1 + (1-d_2)^2 R_2} \tag{2-6}$$

And duty cycles are determined by

$$d_1 = \frac{I_{o1}}{I_{o1} + I_{o2}} \text{ , where } I_{o1} + I_{o2} = I_L \tag{2-7}$$

$$d_2 = \frac{V_{o1}[d_2^2 R_1 + (1-d_2)^2 R_2]}{V_{in} d_2 R_1} \tag{2-8}$$

The main focus of this approach to reduce cross regulation problem by using a multivariable digital controller [118] and satisfactory performance is verified by simulation and experimental results. Design methodologies of a multi-output converter are presented and verified for four outputs converter with 86% efficiency.

These methodologies are claimed to be suitable for unlimited number of outputs [119]. The authors in [120] and [121] present design and control of a dual output buck converter with reduced devices and unidirectional/bidirectional characteristics for motor drive system applications as shown in Figure 2-12 and 2-13. Simulation and experimental results are provided to prove better power loss distribution and high efficiency with low count switching devices. The drawback of this converter is that it requires high current rating switches.

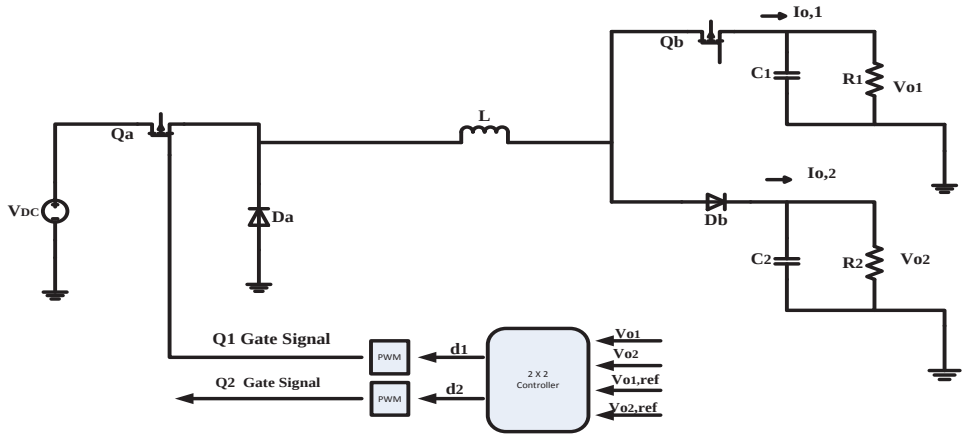

Figure 2-11 Single inductor dual output converter with multi variable control

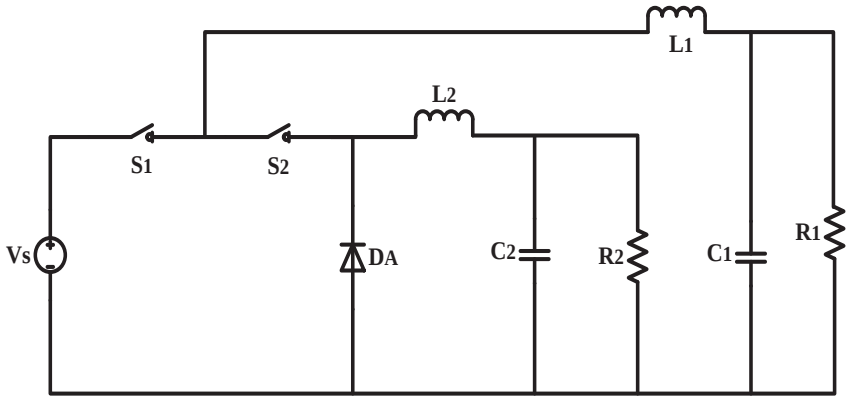

Figure 2-12 Single input-double output unidirectional buck converter

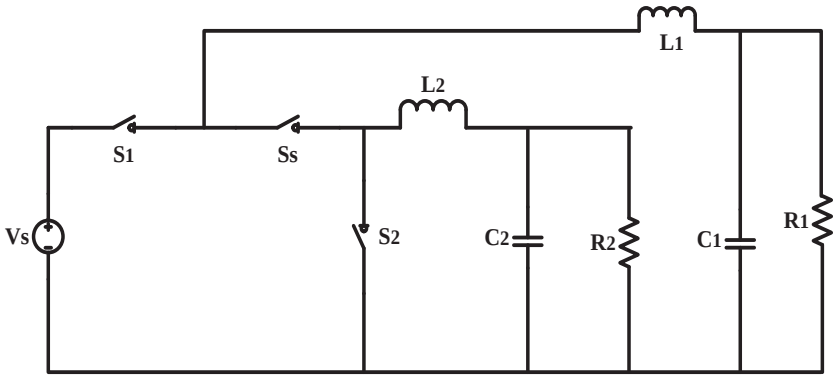

Figure 2-13 Single input-double output bidirectional buck converter

2.6 Multi Input-Multi Output Converters

Multi input Multi output converters are generally used for hybridization of renewable energy sources and electric vehicles for higher efficiency, low cost and greater reliability [122],[123]. A Multi Input Multi Output DC–DC boost converter using different voltage-current characteristics input energy sources is proposed. In this topology the voltage stress on switches is reduced by increasing the level of output voltage [124]. A dual input–tri-outputs buck–boost converter capable of single step transfer of power from source to load is proposed in [125]. The output power is regulated by using a combination of pulse-skipping modulation (PSM) and pulse-frequency modulation (PFM) techniques. Multi input and a multi out-put converters are combined to produce a new multi-input multi-output non-isolated converter having less number of elements and several outputs is proposed [126]. A multi input multi-output Buck-Boost DC-DC converter derived from Buck-Boost Converters in matrix format is suggested in [35]. This converter is used to interface DC loads and various DC input sources in a micro grid on controlled power sharing concept. The input sources are used in various range of power and voltage and output voltages varies from the values lower than the minimum input or greater than the maximum value. Analysis with simulation results has been presented. Figure 2-14 shows the circuit diagram of the proposed system. The number of inputs and outputs are claimed to be unlimited. However, the input sources are unable to power up outputs simultaneously.

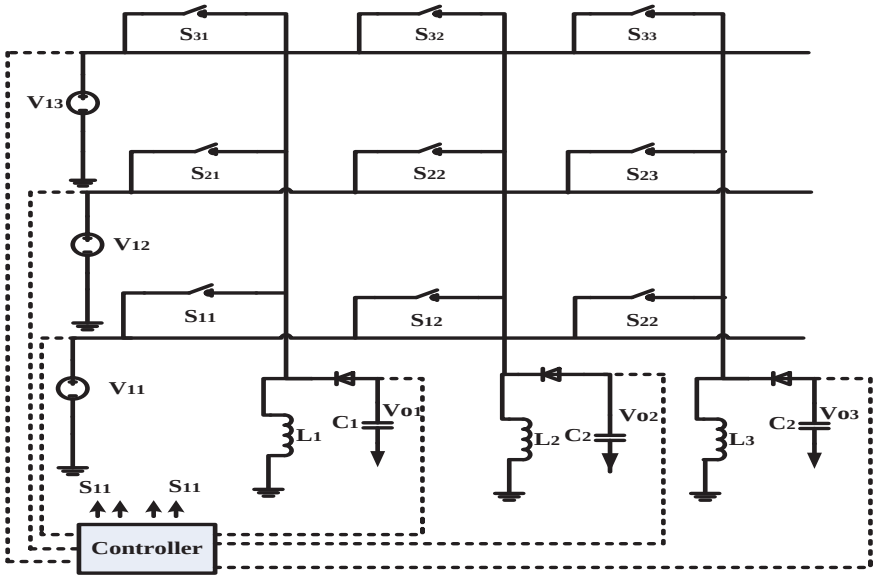

Figure 2-14 Multi input-Multi output converter topology

Three port converters have attracted interest in the recent research. A typical three port converter consists of a voltage source port, a storage unit port and an output or load port. This converter can operate in three modes i.e. dual input, dual output and Single Input-Single output mode. It acts as a dual input converter if both battery and input source are delivering the power to the load. If the power is consumed by the load and battery, the converter is in its dual output state. Input source or battery can power up the load in single input-Single output mode. This topology has advantages like high efficiency, compact size, reliability, and good power management. Due to these advantages, these are widely used in renewable energy systems. A non-isolated three-port converter to interface PV, battery and load is presented in [128]. With less conversion stages, higher power density and reliability are achieved and are verified by experimental results. A family of non-isolated three port converters is introduced in [129] and [130]. These three port converters are generated by introducing a single input-single output converter in a dual input converter or dual output converters. A systematic approach for derivation of three port converters from dual input and dual output converters is explained in [131]. Several three port converter topologies (TPC) have been generated by this procedure and a boost type TPC as shown in Figure 2-15 is analysed in dual input, dual output and single input-single output mode.

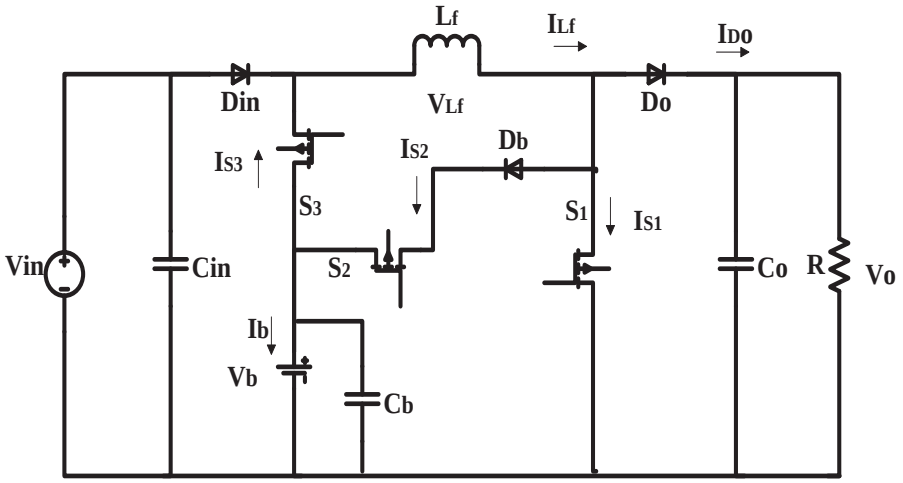

Fig. 2-15 Three-port Converter

2.6.1 Dual Output Mode

A three Port Converter in dual output mode is shown in Figure 2-16. In this mode, switch S_3 is kept OFF. Three switching states are explained in one switching period. Current and voltage waveforms are shown in Figure 2-17.

Switching State I: Switch S_1 is ON and S_2 is OFF. Inductor L_f absorbs energy from Input voltage V_{in} and its current I_{Lf} increases.

$$\frac{dI_{L_f}}{dt} = \frac{V_{in}}{L_f} \tag{2-9}$$

Switching State II: Switch S_1 is OFF and S_2 is ON. Battery is charged by both V_{in} and inductor L_f and its current I_{Lf} decreases.

$$\frac{dI_{L_f}}{dt} = \frac{V_{in} - V_b}{L_f} \tag{2-10}$$

Switching State III: Both the Switches are OFF. Load is powered by V_{in} and release of energy by inductor L_f and its current I_{Lf} decreases.

$$\frac{dI_{L_f}}{dt} = \frac{V_{in} - V_o}{L_f} \tag{2-11}$$

By applying inductor volt second balance theorem on inductor in steady state continuous-conduction mode we get the input output voltage relationship as,

$$(V_{L_f})_{Ts} = V_{in} - V_b d_2 - V_o(1 - d_1 - d_2) = 0 \tag{2-12}$$

$$V_{in} = V_o(1 - d_1) - V_b d_2 \tag{2-13}$$

$$V_o = \frac{V_{in} - V_b d_2}{1 - d_1 - d_2} \tag{2-14}$$

$$V_b = \frac{V_{in} - V_o(1 - d_1 - d_2)}{d_2} \tag{2-15}$$

Where d_1 and d_2 are the duty cycles of the switches S_1 and S_2, V_b is battery voltage and V_o is output voltage

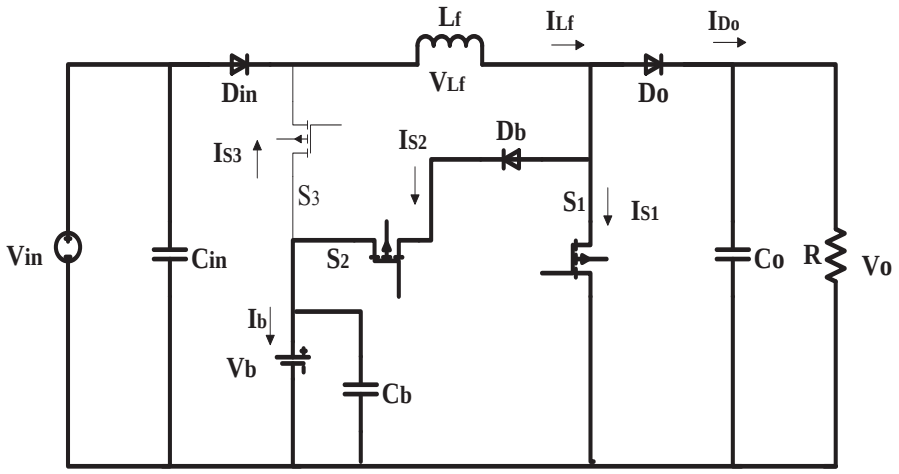

Figure 2-16 Equivalent circuit of three ports converter in Dual Output mode

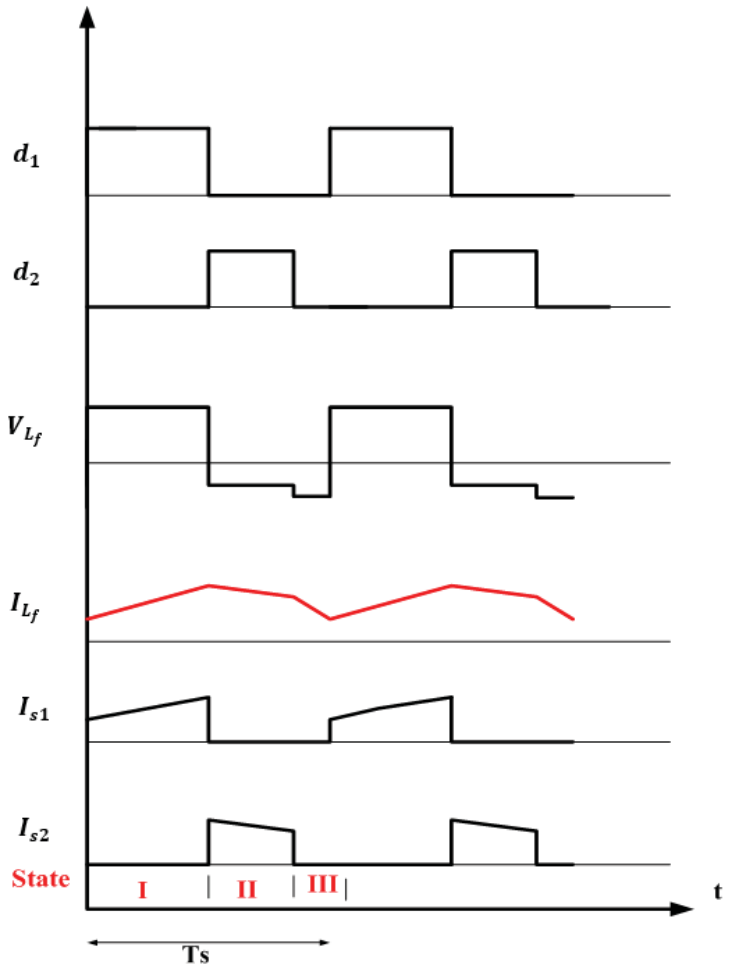

Figure 2-17 Typical waveforms of three ports converter in Dual Output mode

2.6.2 Dual Input Mode

A three-port converter in dual output mode is shown in Figure 2-18. Four switching states are explained in one switching period. Voltage and current waveforms for $d_1 > d_3$ are shown in Figure 2-19.

Switching State I: Switch S_1 and S_3 are ON. Inductor L_f absorbs energy from battery voltage V_b and its current I_{L_f} increases

$$\frac{dI_{L_f}}{dt} = \frac{V_b}{L_f} \tag{2-16}$$

Switching State II: Switch S_1 is ON and S_3 is OFF. Inductor L_f absorbs energy from Input voltage V_{in} and its current I_{Lf} increases.

$$\frac{dI_{L_f}}{dt} = \frac{V_{in}}{L_f} \tag{2-17}$$

Switching State III: Switch S_1 is OFF and S_3 is ON. Load is powered by V_b and release of energy by inductor L_f and its current I_f decreases.

$$\frac{dI_{L_f}}{dt} = \frac{V_b - V_o}{L_f} \tag{2-18}$$

Switching State IV: Both the Switches are OFF. Load is powered by V_{in} and release of energy by inductor L_f and its current I_{L_f} decreases.

$$\frac{dI_{L_f}}{dt} = \frac{V_{in} - V_o}{L_f} \tag{2-19}$$

By applying inductor volt second balance theorem on inductor in steady state continuous-conduction mode we get the input output voltage relationship as,

$$V_{in} = \frac{V_o(1-d_1) - V_b d_3}{1-D_3} \tag{2-20}$$

$$V_o = \frac{V_{in}(1-d_3) - V_b d_3}{1-d_1} \tag{2-21}$$

2.6.3 Single Input Single Output Mode

The equivalent circuit in the Single Input Single Output mode is shown in Figure 2-20. In this mode switch S_2 is kept OFF and S_3 is kept ON. The battery supplies the load alone and converter acts as a conventional boost converter.

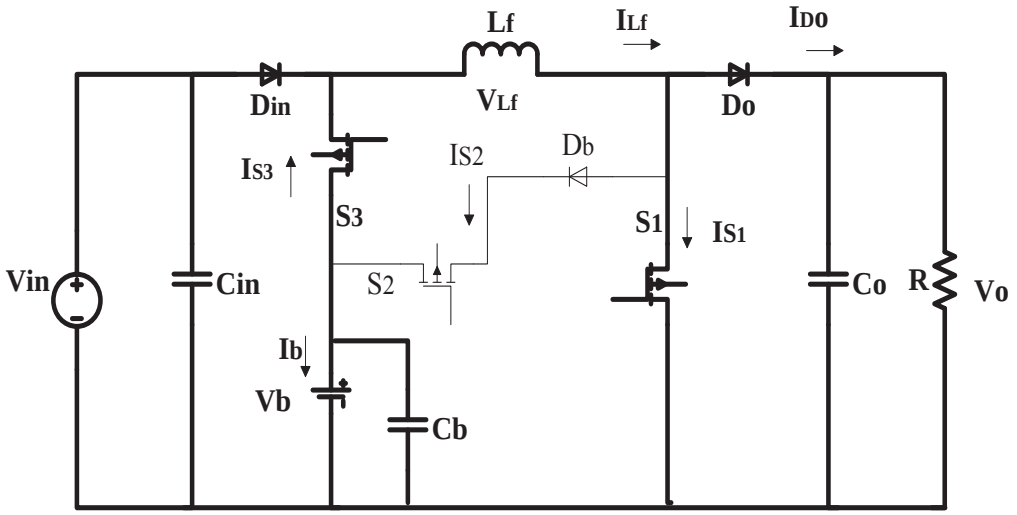

Figure 2-18 Equivalent circuit of three ports converter in Dual Input mode

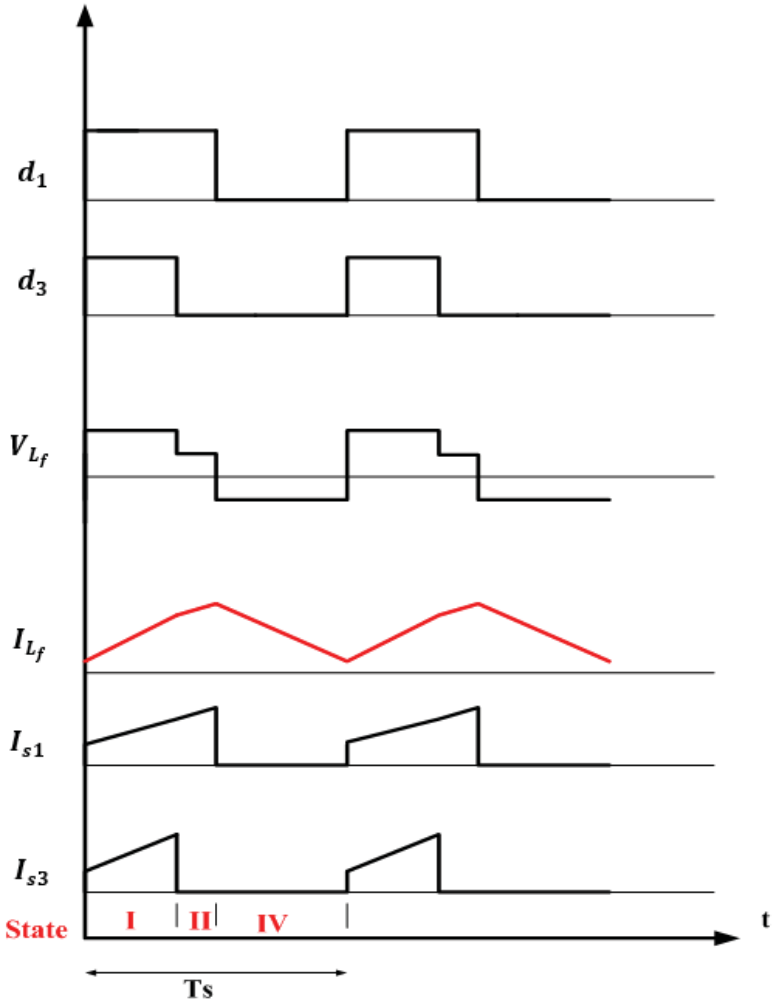

Figure 2-19 Typical waveforms of three ports converter in Dual Input mode

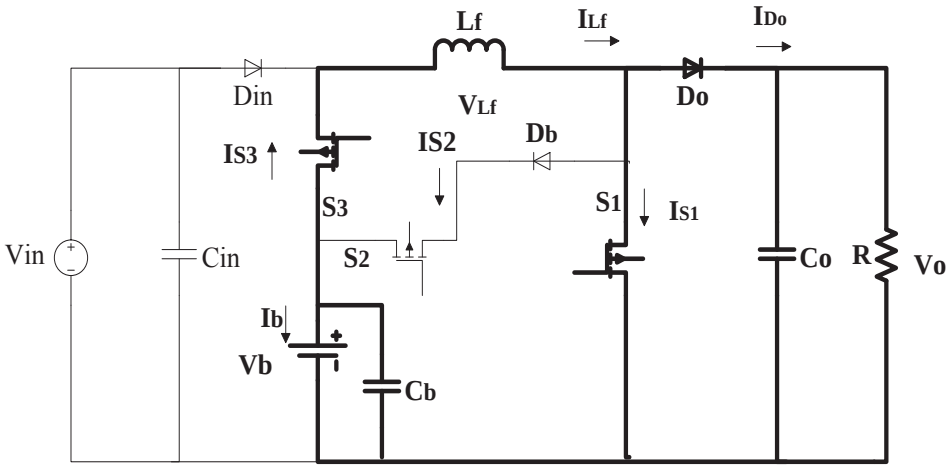

Figure 2-20 Three port converter in single input-single output mode

A multi input DC-DC boost converter combining the multiple sources in a unified structure with five switching periods is introduced in [132]. This system is also capable of providing reactive power to the load and grid. Simulation results have verified different features. A three-input dc–dc boost converter (Figure 2-21) is

presented in [133]. It has one bidirectional port in addition to two one directional input ports. This topology has been reported useful for integration of hybrid energy system having storage element and supplying the load individually or simultaneously. Four power switches are used with independent control and different duty cycles to provide regulated output. The validity of this converter and control system has been verified by simulation and experimental results for different conditions of operation. Simulation results show good transient and steady state responses of the converter with respect to step changes in generation and the load requirement. A low power prototype with an acceptable efficiency verifies simulation result. A single inductor dual input-dual output converter considering battery as a second source is presented in [134]. However, battery charging circuit is not controlled in this topology.

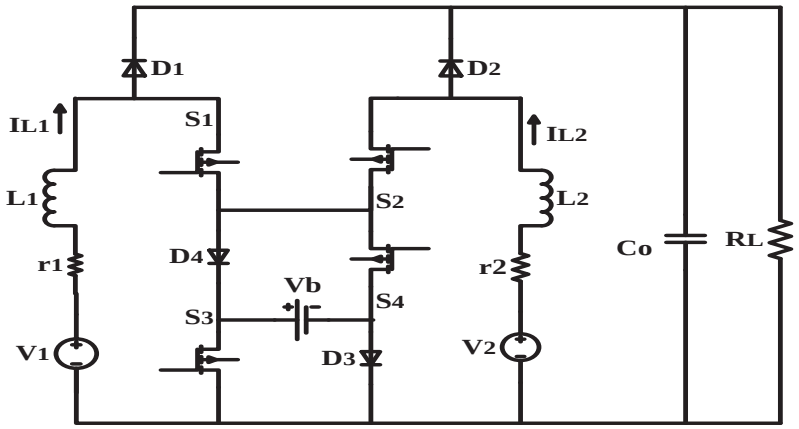

Figure 2-21 Three input DC-DC Converter

2.7 Comparison of Multi Input Non-Isolated DC-DC Converter Topologies

Each non-isolated DC- DC converter topology has its own merits and demerits therefore there are no specified selection criteria to choose any specific topology for any application. However, these topologies can be compared under certain characteristics like cost, reliability, flexibility and efficiency. The comparison is made only on the bases of simple synthesized topology. Control schemes and extra cells added components to achieve additional benefits are not taken into account in this comparison.

2.7.1 Cost of Converter

The expected cost of the converter can be worked out by the number of components being used in the particular topology. Multi input converters share the components in their input and output stages therefore they have advantage of less cost as compared

to the independent single input converters. Similarly non-isolated converters do not require bulky transformers for input output isolation therefore their cost is less as compared to isolated converters. Among non-isolated topologies, buck and boost converters are less costly as compared to the others due to less number of components in their circuitry. Among these two topologies, boost converters have an edge over the buck. Xiao et al., found that the boost converter has the following advantages over the buck in photo voltaic applications [135].

- Current rating of MOSFET in boost converter is lower as compared to buck converters.
- Boost converters require high inductance to achieve current ripple as compared to buck converters.
- Buck converters require a large capacitor to smooth discontinuous input current
- Freewheeling diode can serve as blocking diode in boost converter however this is an additional component in buck.

2.7.2 Reliability

Reliability of the converters can be determined by two factors. One factor is the number of common components in the circuit and other is the stress on each component. Buck-boost, Cuk and SEPIC converters have more number of passive devices and have high electrical stress on components like switches, diodes and capacitors, therefore these topologies are less reliable as compared to buck and boost converters [136],[137].

2.7.3 Flexibility

Flexibility can be defined as the compatibility of the topology with different kinds of input sources. As the main objective of multi input converters are to combine different input sources to provide the desired output therefore the topology input interface is very important. The topology should be able to integrate different input sources and provide wide range of output voltages. Cuk and SEPIC converters are better in flexibility as their input currents are continuous and ripple free and at the same time these are able to step up or step down the input voltage [59],[138].

2.7.4 Efficiency

In terms of efficiency buck and boost converters are considered as the most efficient topologies among the non-isolated category [59],[139]

Table 1 shows a comparison of non-isolated DC- DC converter topologies. The table is explained as, the "*" sign shows the attribute of topology under each heading. More numbers of "*" signs indicate that the topology is better as compared to others i.e. "***" is better than "**" which is better than "*".

Table 2-1 Comparison of MI DC-DC Converter Topologies

Topology	Cost	Reliability	Flexibility	Efficiency
MI Buck	**	**	**	***
MI Boost	***	**	***	****
MI Buck-Boost	*	*	**	*
MI Cuk	*	*	****	*
MI SEPIC	*	*	****	**

2.8 Limitations in Multiport Topologies

Several multi Input DC-DC converters topologies have been studied in this chapter. Literature suggests that multi input converters have reduced the problems associated with single input converters and enhanced the interface of different renewable sources which can deliver power individually and simultaneously to the load. The use of Multi port converters in renewable energy applications has reduced the cost for integration due to their minimum components and reduced switching losses with the use of lossless soft switching circuits and has increased reliability and power security. However, the study of different multi-port dc-dc converter topologies reveals that there is no single topology which can independently handle the entire goals of cost, reliability, flexibility and modularity. The following limitations have been identified in multi-port power electronics converters.

- Multi input converters can deliver the power individually and simultaneously to the load, however during the light load conditions and/or when both the sources are available, no storage device is present to store the extra available

energy. Furthermore, only a single load is energized in this system [66],[72], [84]-[101].

- Only one source can power up the load at a time. If the other source is also present, it is not utilized [83],[88]-[90], [122]-[125].
- High power loss, low efficiency, more number of switches [88],[89],[127].
- Only one renewable energy source is used to power up the load and to charge the battery. In case of absence of source, battery charging is discontinued and load is without power. Hence the system is less reliable [104]-[121],[128]-[131].

Table 2-2 Identified Limitations in existing Multiport topologies

Converter Topology	Cited Reference	Limitations
Multi Input-Single Output	[66],[72][84]-[103]	No Energy Storage Device
	[71]-[73],[83]-[85] [88]- [90],[103]	No Simultaneous Energy Transfer
	[88], [89]	High power loss, low efficiency, High number of components
	[100]- [102]	low efficiency
	[127]	Complex Control, bigger size, high cost
Single input-Multi Output	[104]- [121] [120],[121]	No Storage, only one input Bigger size, two inductors
Multi input-Multi Output	[122], [124], [125], [126]	No storage, no simultaneous power transfer two inductors
Three Port	[69], [124], [128]-[131],	Less Reliable (only one source)

2.9 Need of Further Research

Drawbacks in the existing multiport topologies, as highlighted in the above section, unveil the research gap in the area and establish a very strong motive to conduct further research work and to carry out additional development in the area of multiport power electronics interface. The interface which could integrate multiple renewable

energy sources and power up multiple loads and the surplus energy could also be stored and utilized later.

2.10 Conclusion

A comprehensive literature review of non-isolated single port and multiport converters is presented in this chapter. Comparison of several multiport converters is presented. Limitations in the existing multiport topologies are highlighted. The extensive literature review led to the identification of research gap and formulated the base to conduct further research.

Chapter 3

3 New Multiport Converter Topology

A comprehensive literature review of non-isolated multiport converter topologies has been presented in Chapter 2. The literature review reveals that there are some limitations in the existing multiport converter topologies and there is need of further research in the field. In this work a new non-isolated multiport DC-DC converter topology for a hybrid energy system in low power applications is proposed. The new topology assimilates multiple renewable energy sources and power up multiple loads with different output levels. This new topology has ability to cope with different voltage level requirements and can integrate several energy sources to satisfy the variable load demands. The sources can be utilized independently or simultaneously. Surplus energy can also be stored and made available in case of absence of renewable energy sources. The advantages of the proposed topology over the topologies in the cited literature are

- It can accommodate multiple sources at the input.
- Input sources can be employed independently and concurrently.
- It can power up multiple loads with different voltage levels.
- In addition to provide regulated output to the load, this converter can harvest maximum power from the input sources.
- Surplus energy can be stored in the battery and made available in the absence of renewable energy sources.

In this chapter detailed mathematical analysis of new topology in Continuous Conduction Mode (CCM), is presented. In the following sections, structure of new converter is explained followed by detailed analysis in different modes of operation to demonstrate the suitability of the converter in low power hybrid energy applications.

3.1 Architecture of New Topology

The multiport DC-DC buck converter is shown in Figure 3-1. The converter interfaces two input sources represented by voltage sources V_1 & V_2, a storage element port represented by V_b and an output load port represented by V_o. A single inductor with

inductance ‘L’ draws current from both the sources individually and simultaneously. ‘R’ is the load resistance. The converter has five controllable switches Q_1, Q_2, Q_3 , Q_4 and Q_5. These switches are responsible for the control of power flow from source to load through their duty cycles d_1, d_2, d_3, d_4 and d_5 respectively. Switches Q_1 and Q_2 are responsible to extract maximum power from the input renewable energy sources. Two Diodes D_1 and D_2 conduct complementary to the switches $Q_1$and Q_2. Diodes are reverse biased during the ‘ON’ state of the switches $Q_1$and Q_2 and are in the state of conduction during the ‘OFF’ time of switches $Q_1$and Q_2. Switches Q_3 and Q_4 are responsible for the control of battery charging and discharging process respectively and the switch Q_5 regulates the output voltage to a reference value.

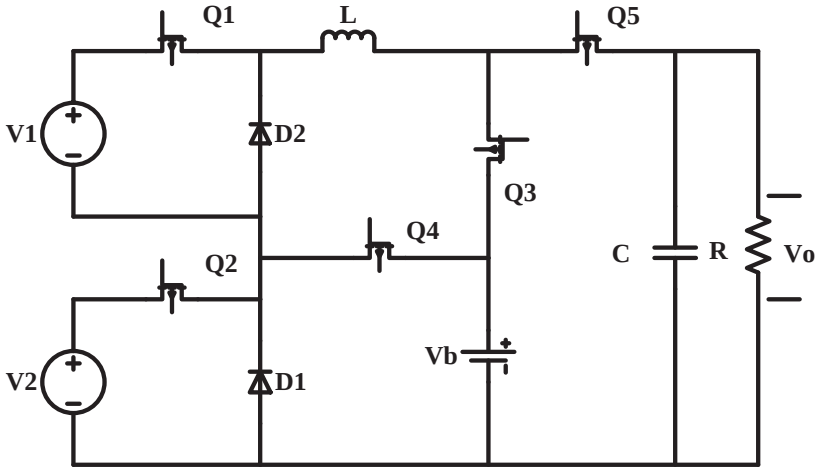

Figure 3-1 Dual input-Dual output DC-DC Buck Converter

3.2 Modes of Operation

In order to analyse the proposed converter, certain assumptions are made i.e.

- All the switches are ideal forward conducting reverse blocking.
- All the losses are neglected
- V_1 , V_2 & $V_b > V_o$.
- Output capacitor ‘C’, is large enough to smooth the output voltage ‘V_o’.
- It is assumed that the all the connected renewable energy sources are providing DC voltage corresponding to their maximum power point

The following are the different modes of operation for this new converter.

- Dual input-Single output
- Dual input- Dual output
- Single input-Dual output
- Single input- Single output

Each mode of converter operating in steady state will be analysed independently in the subsequent sections.

3.2.1 Dual input-Single output mode

This mode of operation is applicable when a single voltage source in not able to satisfy the load demand and needs to be complemented by the second source and if the second voltage source is also not available, the energy stored in the battery can be utilized. This mode is further divided into two sub-modes. Energy transfer action from source to load depends on the control strategy adopted to generate the gate drive signals (Gs) to turn ON the switches Q_1, Q_2 and/or Q_4. There are numerous different arrangements to turn ON/ OFF the control switches in different switching states (t_1, t_2, t_3, t_4), however, six main switching schemes are defined here and shown in Table 3-1 and Figure 3-2.

- The switches Q_1 & Q_2 turned ON and OFF at the same time (Figure 3-2 a).
- The switches Q_1 & Q_2 turned ON at the same time but turn OFF time is different Q_2 turns OFF first (Figure 3-2 b).
- The switches Q_1 & Q_2 turned ON at the same time but turn OFF time is different Q_1 turns OFF first (Figure 3-2 c).
- The switches Q_1& Q_2 are turned ON at different time (Q_1first) and turned OFF at the same time (Figure 3-2 d).
- Switch Q_1 turns ON and after an interval of time switch Q_2 is turns ON. Switch Q_1 turns OFF first and switch Q_2 turns OFF later (Figure 3-2 e)
- Switch Q_1 turned ON for a period and then it is turned OFF. Whereas switch Q_2 is turned on when Q_1 is turned OFF (Figure 3-2 f).

Table 3-1 Switching Schemes for Dual input -Single output mode

SWITCHING SCHEME FOR DUAL INPUT MODE									
Scheme	**Switching State**								**Description**
	t_1		t_2		t_3		t_4		
	ON	OFF	ON	OFF	ON	OFF	ON	OFF	
(a)	Q_1&Q_2			Q_1&Q_2	Not Applicable		Not Applicable		Switches Q_1 & Q_2 turned ON and turned OFF at the same time Figure (3-2 a)
(b)	Q_1&Q_2		Q_1	Q_2		Q_1&Q_2	Not Applicable		Switches Q_1 & Q_2 turned ON at the same time but turn OFF time is different. Q_2 turns OFF first (Figure 3-2 b)
(c)	Q_1&Q_2		Q_2	Q_1		Q_1&Q_2	Not Applicable		Switches Q_1 & Q_2 turned ON at the same time but turn OFF time is different Q_1 turns OFF first (Figure 3-2 c)
(d)	Q_1	Q_2	Q_1&Q_2			Q_1&Q_2	Not Applicable		Switches Q_1& $Q_2$are turned ON at different time but turn OFF at the same time (Figure 3-2 d)
(e)	Q_1	Q_2	Q_1&Q_2		Q_2	Q_1		Q_1&Q_2	Switch Q_1 turned ON and after an interval of time switch Q_2 is turned ON. Switch Q_1 turns OFF first and switch Q_2 turns OFF later (Figure 3-2 e).
(f)	Q_1	Q_2	Q_2	Q_1	Q_1&Q_2		Not Applicable		Switch Q_1 turned ON for a period and then it is turned OFF. Switch Q_2 is turned ON when Q_1 is OFF (Figure 3-2 f).

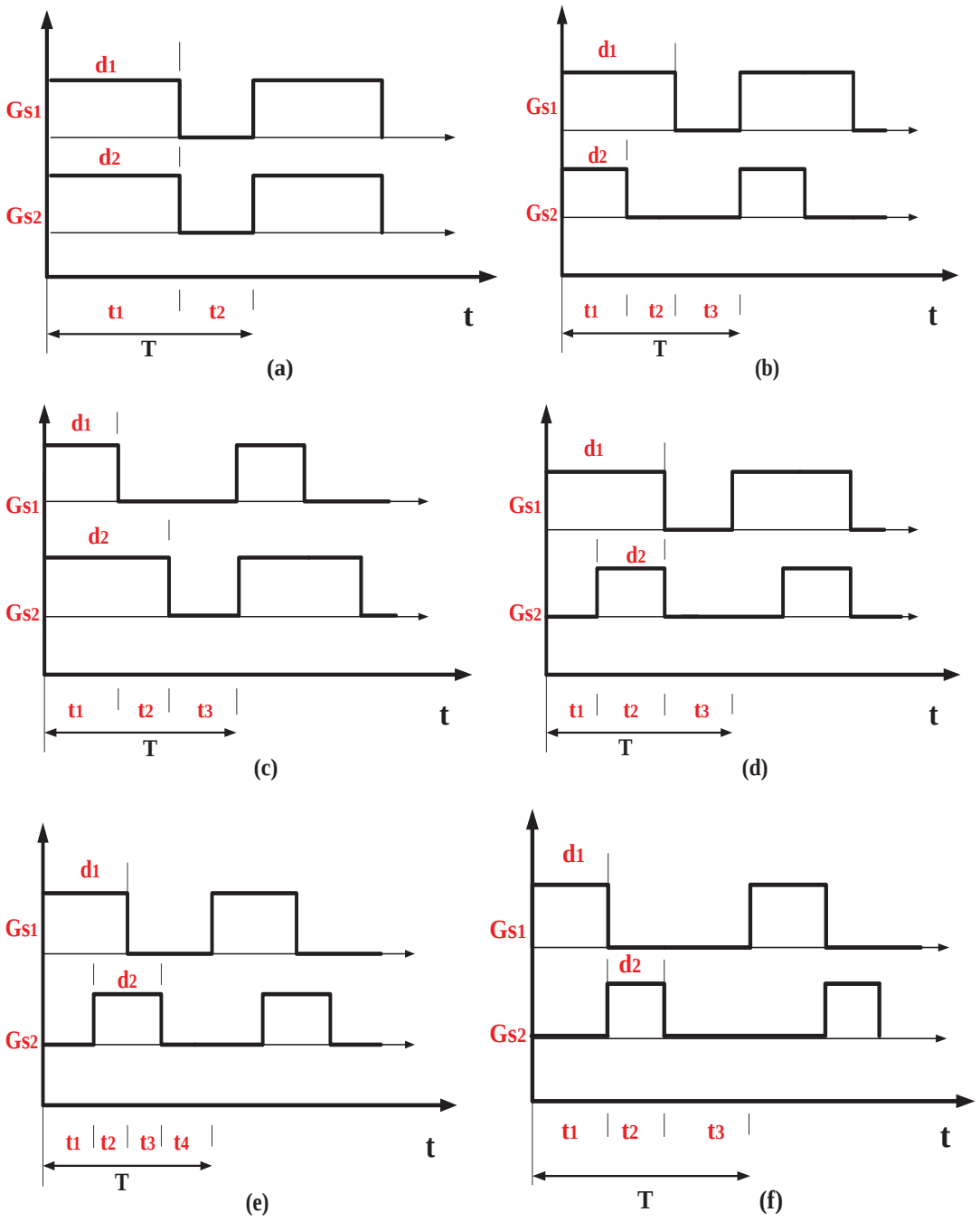

Figure 3-2 Switching Schemes for Dual Input-Single Output mode

3.2.1.1 Sub Mode 1 Voltage Sources V_1 and V_2 powering up the load

In this sub mode both the voltage sources (V_1& V_2) are available. However, Source one is unable to power up the load individually therefore needs a supplementary source to fulfill the load demand. The converter at this state is dual input buck converter. Switches Q_1 & Q_2 are utilized to track maximum power from the input renewable energy source. As the battery charging/discharging is not available in this mode, therefore the switches Q_3 and Q_4 will remain OFF all the times whereas the

switch Q_5 will regulate the output voltage to reference value. The equivalent circuit is shown in Figure 3-3 and the key waveforms are shown in Figure 3-4. Switching scheme as shown in Figure 3-2 (e) is used to control the flow of power from source to load. In this analysis, only one switching scheme is applied however the other schemes would have the same results. Depending on adopted switching scheme there are four switching states in one switching period (T).

3.2.1.1.1 Switching state 1

At time interval $\mathrm{t} = \mathrm{t}_1$, switch Q_1 is ON and Q_2 is OFF. See Figure 3-3 (a). The power demanded by load is provided by source one (V_1). The voltage across the inductor is associated with the rise of inductor current and is given.

$$\mathrm{V}_L = L\frac{di_L}{dt} \tag{3-1}$$

The voltage across the inductor can be calculated as

$$\mathrm{V}_L = V_1 - V_o \tag{3-2}$$

Equating 3-1 and 3-2 and rearranging for time interval t_1 gives

$$\frac{di_L(t_1)}{dt} = \frac{V_1 - V_o}{L} \tag{3-3}$$

3.2.1.1.2 Switching state 2

At time interval $t = t_2$, Switch Q_2 is also turned ON. See Figure 3-3 (b). Load demand is satisfied by both the sources as these are connected in series. The voltage across the inductor in this state is

$$\frac{di_L(t_2)}{dt} = \frac{(V_1 + V_2) - V_o}{L} \tag{3-4}$$

3.2.1.1.3 Switching state 3

For time interval $t = t_3$, switch Q_1 is turned OFF whereas Q_2 is still ON. See Figure 3-3 (c). At this state voltage source V_2 is responsible for provision of load demand. And the equation of inductor voltage becomes

$$\frac{di_L(t_3)}{dt} = \frac{V_2 - V_o}{L} \tag{3-5}$$

3.2.1.1.4 Switching state 4

For time interval $t = t_4$, both the switches are OFF. See Figure 3-3 (d). Diodes D_1 and D_2 are forward biased due to change in the polarity of voltage across the inductor and start conducting to provide a freewheel path for flow of current. Inductor current discharges through output capacitor 'C' and the voltage across the inductor becomes as shown in equation (3-6).

$$\frac{di_L(t_4)}{dt} = \frac{-V_o}{L} \tag{3-6}$$

Here V_1 = input voltage source 1

V_2 = input voltage source 2

V_o = output voltage

L = Inductance of the inductor

According to volt-second balance theorem the average voltage across the inductor for a switching period (T), is zero hence for all the four states. The inductor voltage equation in steady state continuous conduction mode can be obtained by.

$$V_L = (V_1 - V_o)(t_1) + [(V_1 + V_2) - V_O](t_2) + (V_2 - V_O)(t_3) - V_O(t_4) = 0 \tag{3-7}$$

The time interval when switch Q_1 is ON $= d_1T = t_1 + t_2$

The time interval when switch Q_2 is ON $= d_2T = t_2 + t_3$

The time interval when switch $Q_1$and Q_2 are OFF $= \{T - (t_1 + t_2 + t_3)\} = t_4$

Time of Switching $= T = t_1 + t_2 + t_3 + t_4$

By solving equation (3-7) for output voltage we get

$$V_o = V_1 d_1 + V_2 d_2 \tag{3-8}$$

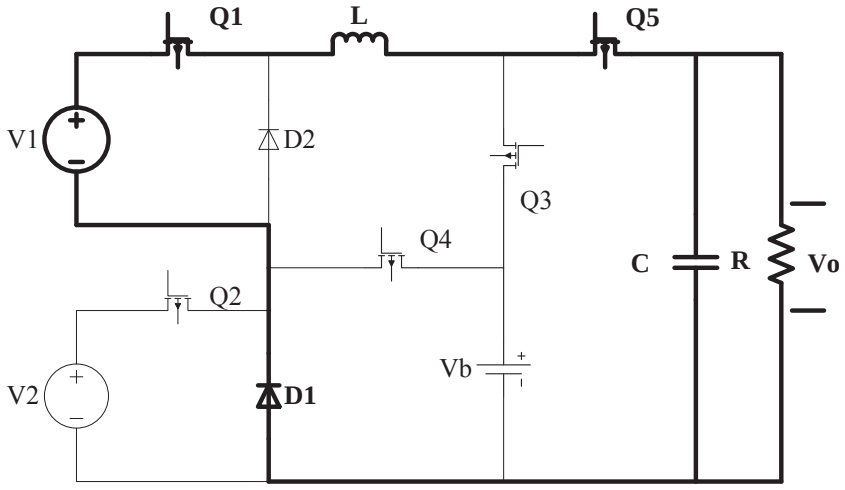

(a)

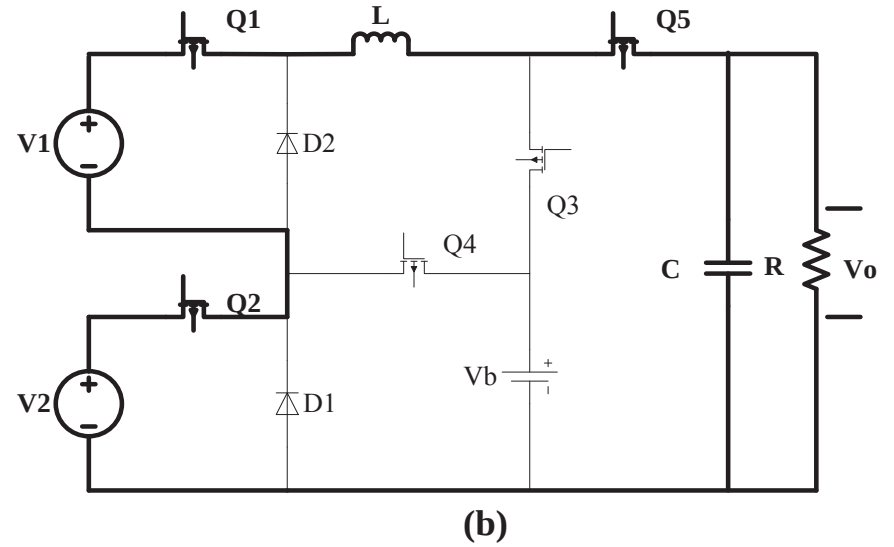

(b)

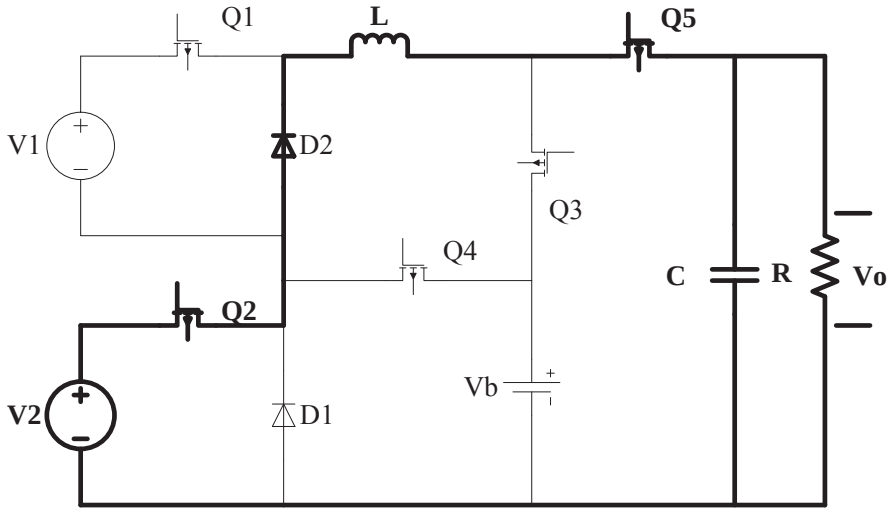

(c)

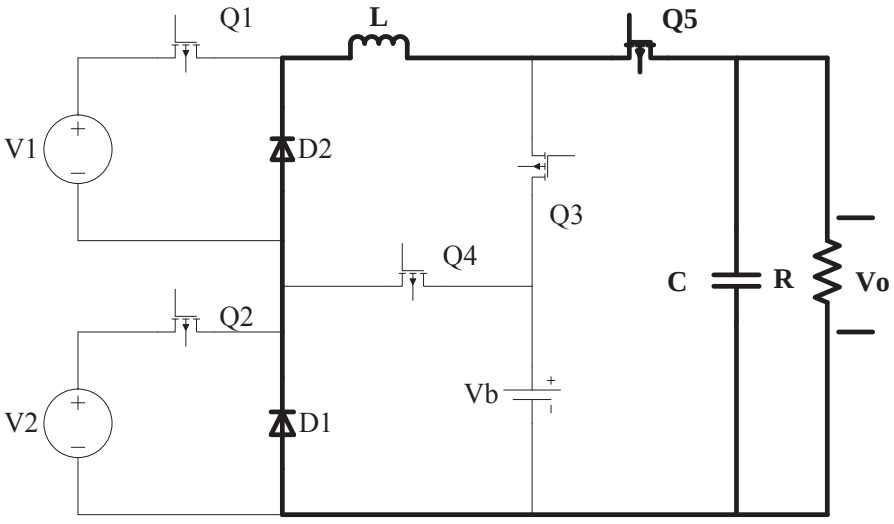

(d)

Figure 3-3 Equivalent Circuits for dual input sub mode 1 (a) Switching State 1 (b) Switching State 2 (c) Switching State 3 (d) Switching State 4

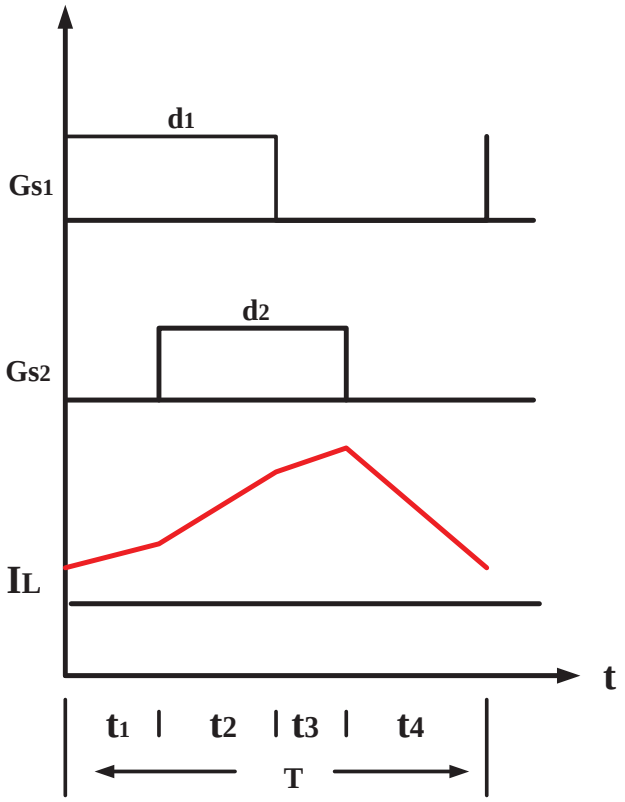

Figure 3-4 Gate signals and inductor current waveforms for dual input sub mode 1

3.2.1.2 Sub Mode 2 Voltage Source V_1 and V_b supplying the load

In this sub mode, the voltage source V_1 is available but voltage source V_2 is not available. If the load demand increases beyond the capacity of voltage source V_1, the additional load demand can be fulfilled with the battery so the battery acts as a second voltage source. The equivalent circuit is shown in Figure 3-5 and the waveforms for the gate signals and inductors current are Figure 3-6. The converter works as a dual input buck converter. As the battery discharges in this mode, therefore the switch Q_3 will remain OFF whereas Q_4 will remain ON for the period during which extra power is demanded form the battery. Switch Q_5 regulates the output voltage to reference value. Switch Q_1 will remain ON to extract maximum power from source one whereas Q_2 will remain OFF. Switching scheme as shown in Figure 3-3 (d) is adopted in this mode and depending on the duty cycle of the switches Q_1 and Q_4, in this scheme there are three states in one switching period.

3.2.1.2.1 Switching state 1

For time interval $t = t_1$ switch Q_1 is ON and Q_4 is OFF. See Figure 3-5(a) Output load demand is satisfied by V_1. The inductor current is given by

$$\frac{di_L(t_1)}{dt} = \frac{V_1 - V_o}{L} \tag{3-9}$$

3.2.1.2.2 Switching state 2

For time interval $t = t_2$, switch Q_4 is also turned ON. See Figure 3-5 (b). The load demand is satisfied by source one (V_1) and battery (V_b) simultaneously. Hence the voltage across inductor in this state is

$$\frac{di_L(t_2)}{dt} = \frac{(V_1 + V_b) - V_o}{L} \tag{3-10}$$

3.2.1.2.3 Switching state 3

For time interval $t = t_3$, both the switches Q_1 and Q_4 are OFF. See Figure 3-5 (c). The inductor current discharges through output capacitor and the voltage across the inductor is given by.

$$\frac{di_L(t_3)}{dt} = \frac{-V_o}{L} \tag{3-11}$$

Here V_1 = input voltage source 1

V_b = Battery voltage

V_o = output voltage

L = Inductance

The inductor voltage equation can be obtained by applying volt- second balance theorem for all the three states is given by.

$$(V_1 - V_o)(t_1) + [(V_1 + V_b) - V_o](t_2) - V_o(t_3) = 0 \tag{3-12}$$

The time interval when switch Q_1 is ON $= d_1T = t_1 + t_2$

The time interval when switch Q_4 is ON $= d_4T = t_2$

The time interval when switch $Q_1$and Q_2 are OFF $= \{T - (t_1 + t_2)\} = t_3$

Time of Switching $= T = t_1 + t_2 + t_3$

By solving equation (3-12) we get the expression for output voltage as

$$V_o = V_1 d_1 + V_b d_4 \tag{3-13}$$

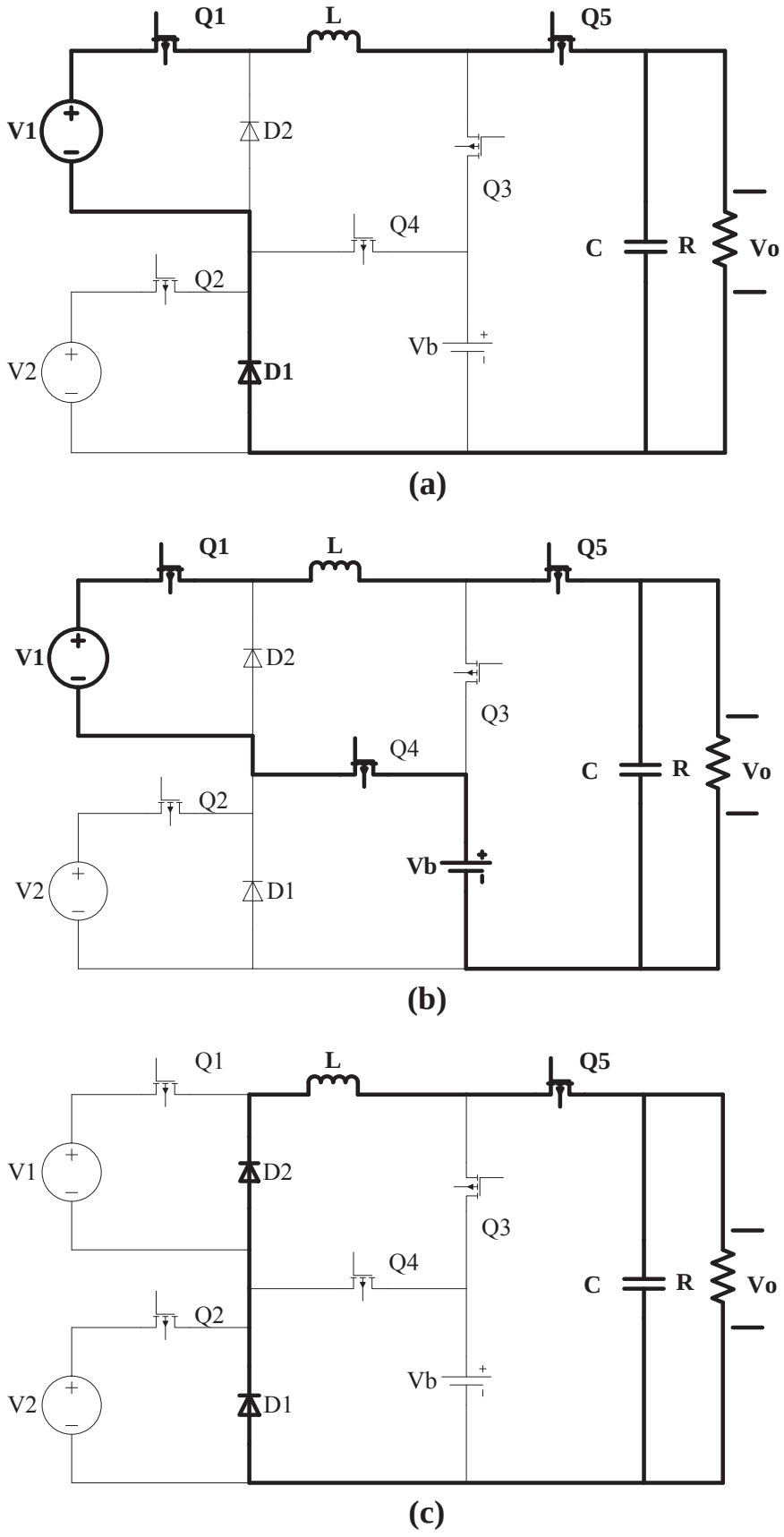

Figure 3-5 Equivalent Circuits for dual input sub mode 2 (a) Switching State 1 (b) Switching State 2 (c) Switching State 3

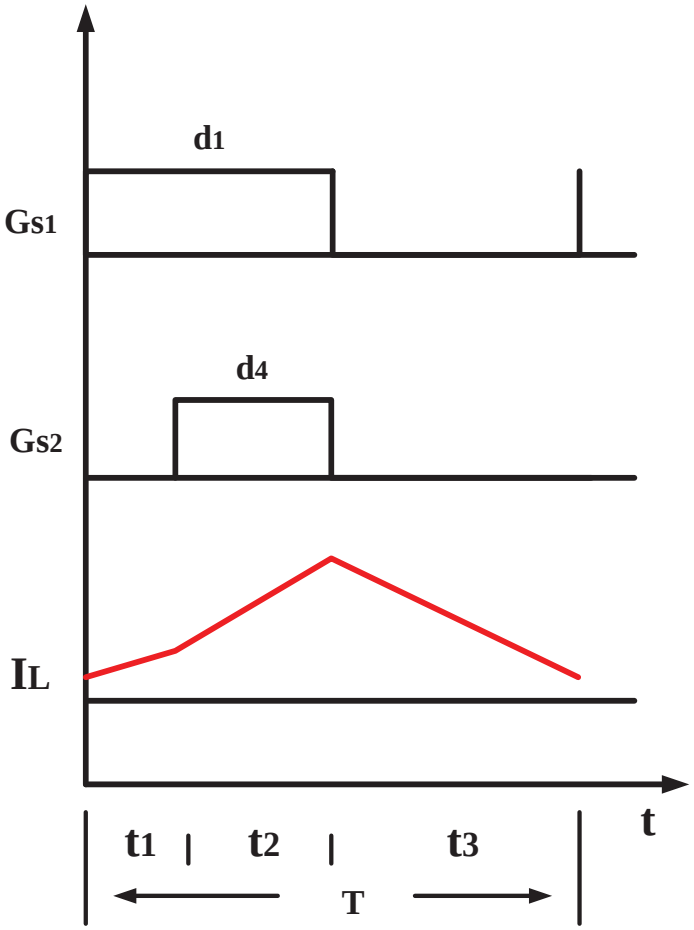

Figure 3-6 Waveforms for dual input sub mode 2

3.2.2 Dual input-Dual output mode

This mode of operation is applicable when both the renewable energy sources are available and maximum power can be harvested. In addition to power up the load, the surplus energy can be stored for later use. In dual output mode, the control switches Q_1 and Q_2 are utilized to track the maximum power point of renewable energy sources. As battery is charging in this mode and Q_3 will control the battery charging voltage and will turn OFF when the battery is fully charged or the input voltage falls below a certain predefined value where it cannot support dual output mode. The control switch Q_4 will remain OFF all the times. The output voltage for connected load will be regulated by control switch Q_5. Energy transfer from sources to loads depends on the control strategy adopted to generate the gate signals to control input and output switches depending upon the availability of input sources, load conditions and state of storage device (battery in this case).

Several input switching schemes have been discussed in the section 3.2.1. In this mode of operation, we will discuss about switching schemes for the output switches and steady state analysis will be done for different switching schemes. The output switching schemes discussed below are based on the input switching scheme as shown in Figure 3-2 (a) where duty cycles for both the input switches Q_1 and Q_2 are equal i.e. $d_1 = d_2$. In this case the duty cycle d_5 for the output switch Q_5 can be less than, greater than or equal to $d_1$and d_2. Whereas the switch Q_3 turns ON only when Q_5 is in OFF state. All the three cases are analysed as under. Equivalent circuit of dual output mode of the converter is shown in Figure 3-6, the waveforms are shown in Figure 3-7 (a, b & c) and switching scheme is shown in Table 3-2.

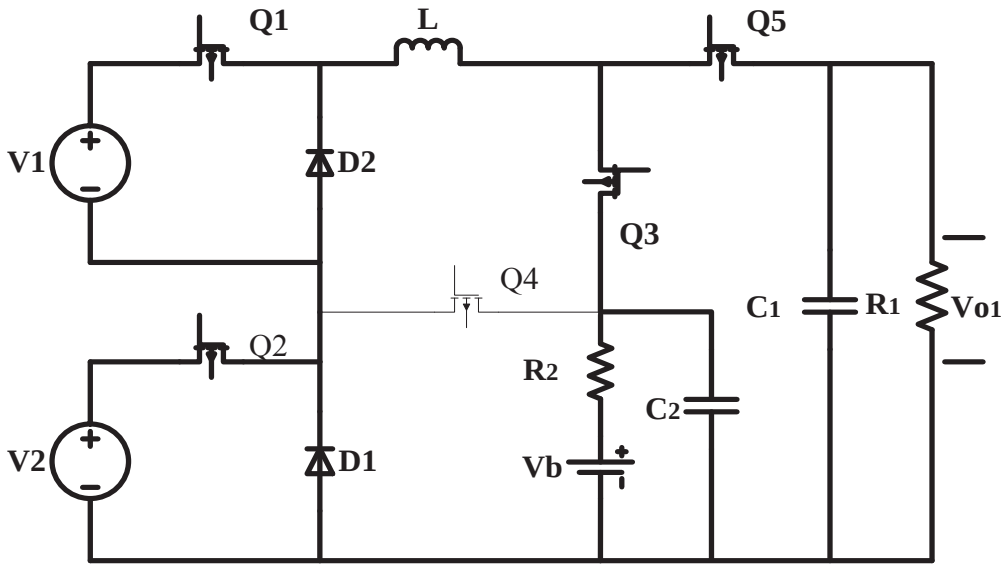

Figure 3-7 Equivalent Circuits for dual input-dual output mode

3.2.2.1 Case 1: $d_5 < (d_1 = d_2)$

This case has three switching states in one switching period. Equivalent circuit is shown in Figure 3-8 (a, b & c) and gate signals and inductor current waveforms are shown in Figure 3-9 (a)

3.2.2.1.1 Switching state 1

For the time interval $t = t_1$, switches Q_1, Q_2 and Q_5 are ON. The inductor is being charged and the voltage across inductor is given by

$$V_L = \frac{di_L(t_1)}{dt} = \frac{(V_1+V_2)- V_{o1}}{L} \qquad (3\text{-}14)$$

3.2.2.1.2 Switching state 2

For the time interval $t = t_2$, switches Q_1, Q_2 are ON whereas Q_5 is OFF, the inductor current ramps up and voltage across the inductor at this point is,

$$V_L = \frac{di_L(t_2)}{dt} = \frac{(V_1+V_2)-V_{o2}}{L} \tag{3-15}$$

3.2.2.1.3 Switching state 3

For the time interval $t = t_3$, switches Q_1, Q_2 and Q_5 are OFF, the inductor current in this state is discharges and the voltage becomes.

$$\frac{di_L(t_3)}{dt} = \frac{-V_{02}}{L} \tag{3-16}$$

In the above case, the inductor is charged in two states and is discharged in the last state.

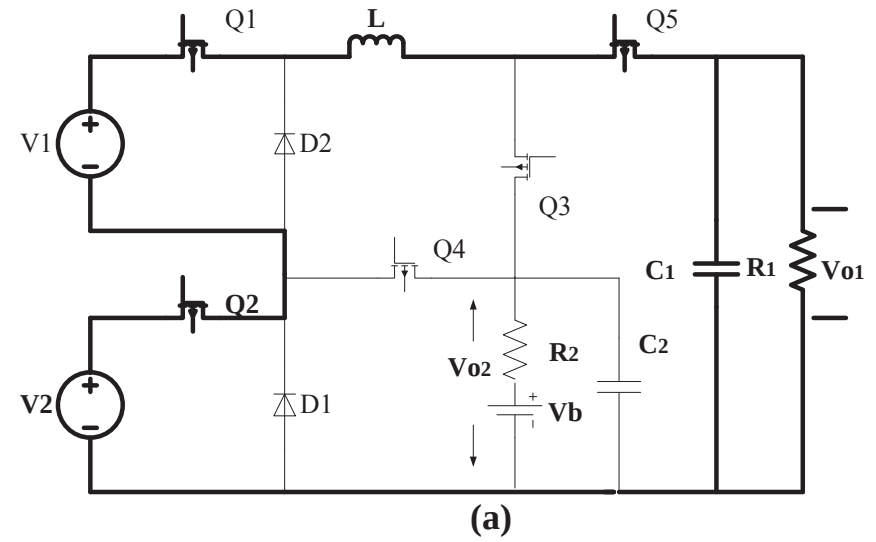

(a)

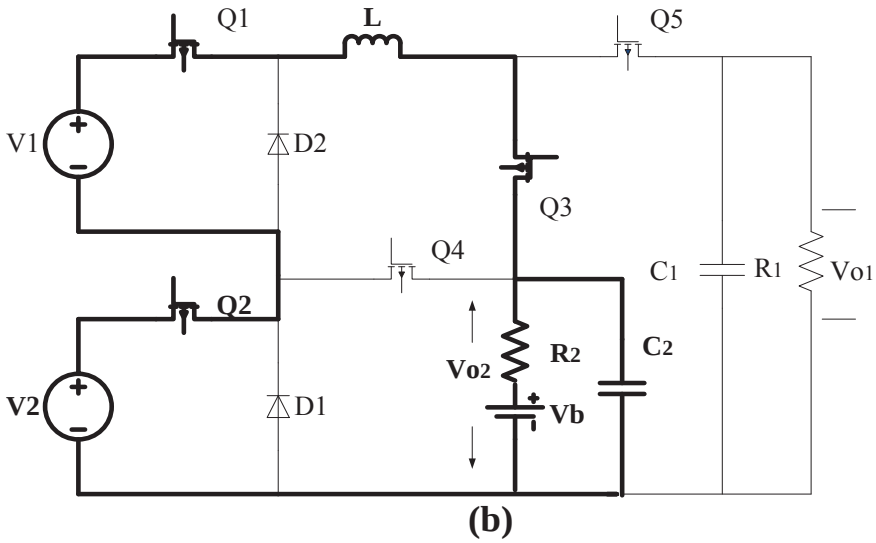

(b)

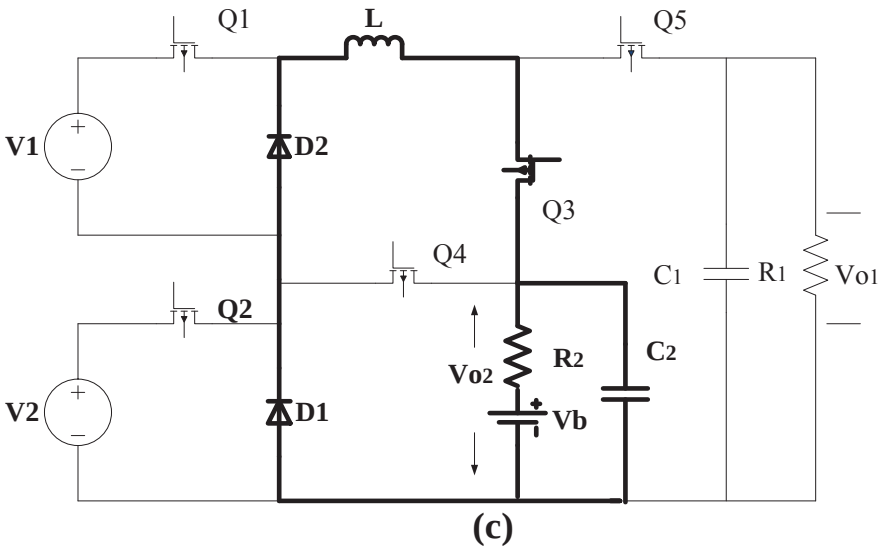

Figure 3-8 Equivalent Circuit DIDO mode: Case 1 (a) switching state 1 (b) Switching state 2 (c) Switching state 3

3.2.2.2 Case 2: $d_5 > (d_1 = d_2)$

This case has three states in one switching period as shown in Figure 3-9 (b)

3.2.2.2.1 Switching state 1

For the time interval $t = t_1$, switches Q_1, Q_2 and Q_5 are ON and the inductor is charged. The inductor voltage current is given by

$$\frac{di_L(t_1)}{dt} = \frac{(V_1+V_2)- V_{o1}}{L} \tag{3-17}$$

3.2.2.2.2 Switching state 2

For the time interval $t = t_2$, switches Q_1, Q_2 are OFF whereas Q_5 is still ON, the inductor current is discharged and the voltage across it at this stage is

$$\frac{di_L(t_2)}{dt} = \frac{-V_{o1}}{L} \tag{3-18}$$

3.2.2.2.3 Switching state 3

For the time interval $t = t_3$, switches Q_1, Q_2 & Q_5 are OFF, the inductor current in this state is discharges and the voltage across it is

$$\frac{di_L(t_3)}{dt} = \frac{-V_{o2}}{L} \tag{3-19}$$

In the above case, the inductor is charged in one state and is discharged in two states.

3.2.2.3 CASE 3: $d_5 = d_1 = d_2$

This case has two states in one switching period as shown in Figure 3-9 (c)

3.2.2.3.1 Switching state 1

For the time interval $t = t_1$, switches Q_1, Q_2 and Q_5 are ON and the inductor is charged hence the voltage across it is given as,

$$\frac{di_L(t_1)}{dt} = \frac{(V_1+V_2)- V_{o1}}{L} \tag{3-20}$$

3.2.2.3.2 Switching state 2

For the time interval $t = t_2$, switches Q_1, Q_2 and Q_5 are OFF and the inductor is discharges and the voltage is,

$$\frac{di_L(t_2)}{dt} = \frac{(V_1+V_2)- V_{o2}}{L} \tag{3-21}$$

The above described mode is summarized as, during the ON state of switches Q_1& Q_2, the energy is stored in the inductor and when these switches are in OFF state, the energy is distributed to one of the two outputs (V_{o2} & V_{o1}) depending on the state of switch Q_5.

V_1 = input voltage source 1
V_2 = input voltage source 1
V_{o2} = Output voltage to charge the battery
V_{o1} = output voltage for load
L = Inductance

By applying Volt-Second Balance Theorem on any of the above described cases to we get the equation for the voltage across inductor for one switching period. Considering case 1 as described above we get,

$$V_L = \frac{Ldi_L(T)}{dt} = [(V_1 + V_2) - V_{o1}](t_1) + [(V_1 + V_2)] - V_{O2}(t_2) - V_{O2}(t_3) = 0 \tag{3-22}$$

Here $t_1 = d_5$

$t_2 = (d_1 - d_5)$

$t_3 = d_3 - (d_1 - d_5)$

$$V_L = \left(V_1 d_1 + d_1 V_2\right) - V_{o1}(d_5) - V_{O2}(d_3) = 0 \tag{3-23}$$

As $d_1 = d_2$ so

$$V_L = \left(V_1 d_1 + d_2 V_2\right) - V_{o1}(d_5) - V_{O2}(d_3) = 0 \tag{3-24}$$

And by applying capacitor charge theorem we get

$$\frac{C_1 dv_{01}(T)}{dt} = I_L d_5 - \frac{V_{o1}}{R_1} = 0 \tag{3-25}$$

$$V_{o1} = I_L d_5 R_1 \tag{3-26}$$

$$\frac{C_2 dv_{02}(T)}{dt} = I_L d_3 - \frac{V_{o2}}{R_2} = 0 \tag{3-27}$$

$$V_{o2} = I_L d_5 R_2 \tag{3-28}$$

Putting V_{o1} and V_{o2} from (3-26) and (3-27) to (3-24) and solving for I_L gives the average inductor current

$$I_L = \frac{V_1 d_1 + V_2 d_2}{d_5^2 R_1 + d_3^2 R_2} \tag{3-29}$$

Putting I_L form (3-29) to equations (3-26) and (3-28) we get the expression for output voltages as

$$V_{o1} = d_5 R_1 \frac{(V_1 d_1 + V_2 d_2)}{d_5^2 R_1 + d_3^2 R_2} \tag{3-30}$$

$$V_{o2} = d_3 R_2 \frac{(V_1 d_1 + V_2 d_2)}{d_5^2 R_1 + d_3^2 R_2} \tag{3-31}$$

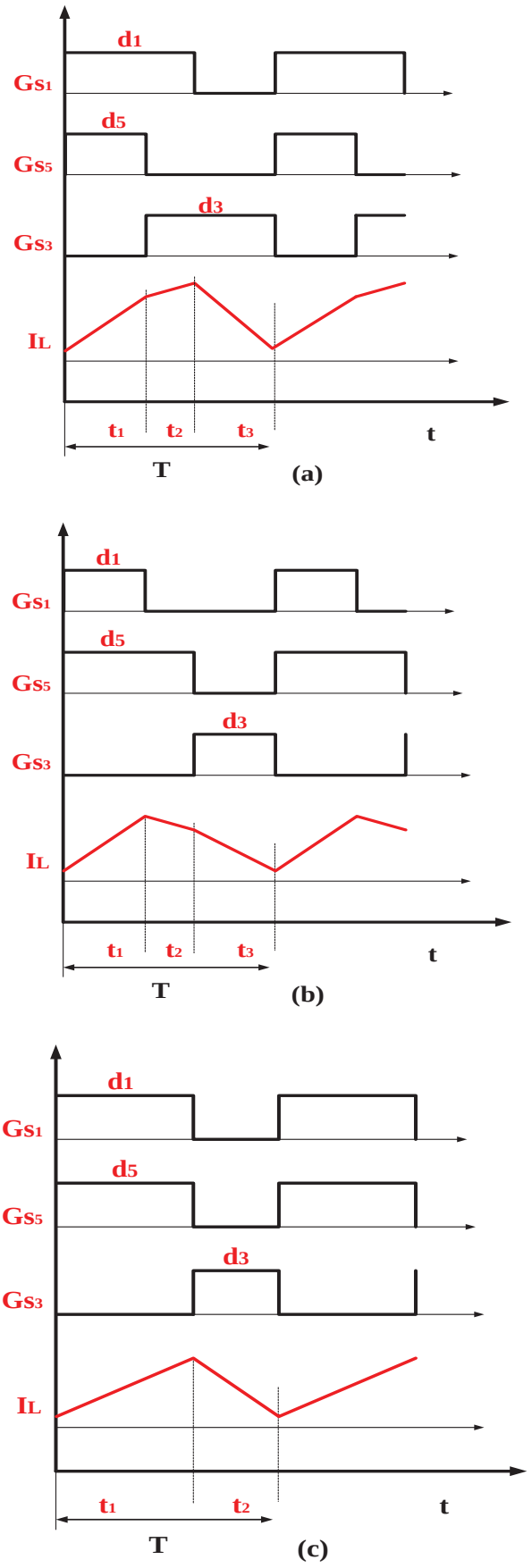

Figure 3-9 Waveforms for gate signals and inductor current (a) case 1 (b) case 2 (c) case 3

Table 3-2 Switching Schemes for Dual Input-Dual output mode

SWITCHING SCHEME FOR DUAL INPUT DUAL OUTPUT MODE								
Case	**Port**	**State**						**Description**
		t_1		t_2		t_3		
		ON	OFF	ON	OFF	ON	OFF	
(1)	Source switch	Q_1& Q_2		Q_1&Q_2			Q_1&Q_2	$d_5 < (d_1 = d_2)$. Output control switch Q_5 turns off before input control switches Q_1& Q_2
	Load switch	Q_5	Q_3	Q_3	Q_5	Q_3	Q_5	
(2)	Source switch	Q_1&Q_2			Q_1&Q_2		Q_1&Q_2	$d_5 > (d_1 = d_2)$. Output control switch Q_5 turns off after input control switches Q_1& Q_2
	Load switch	Q_5	Q_3	Q_5	Q_3	Q_3	Q_5	
(3)	Source switch	Q_1&Q_2			Q_1&Q_2	Not Applicable		$d_5 = d_1 = d_2$. Output control switch Q_5 and input control switches Q_1& Q_2 turn OFF at the same time
	Load switch	Q_5	Q_3	Q_3	Q_5			

3.2.3 Single input-Dual output mode

This mode is applicable when only one input source is available either source one or source two but the load demand is less therefore excess energy can be stored. In single input-dual output mode the control switch Q_1 is utilized to track the maximum power point of available renewable energy source. The control switch Q_4 will remain OFF all the times as battery is charging in this mode and Q_3 will remain ON till the battery is fully charged or the input voltage falls below a certain predefined value. The output voltage for connected load will be regulated by control switch Q_5. All the switching schemes described in the section (3-2-2) are also applicable in this mode. Equivalent circuit with voltage source one powering the load and charging the battery is shown in Figure 3-10.

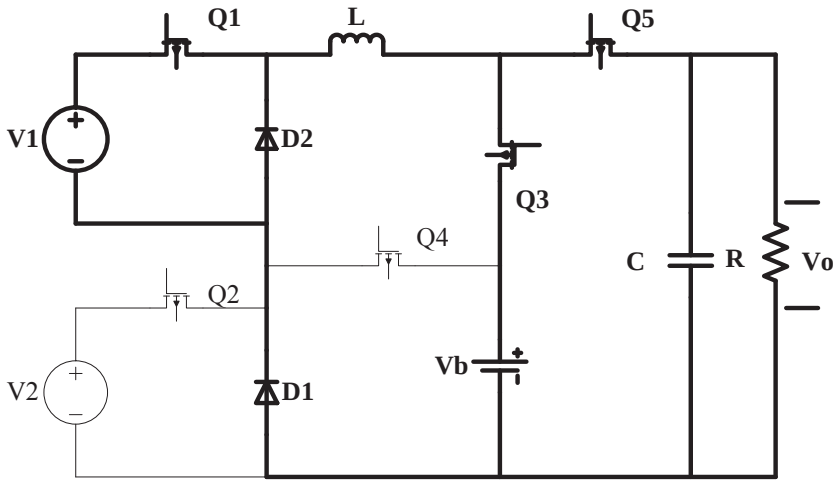

Figure 3-10 Equivalent Circuits for single input-single output mode

3.2.4 Single Input-Single output mode

This mode is applicable when only one of the two input sources is available and the obtainable energy is just enough to power up the load. Any of two connected sources can power up the load individually and if both the sources are not available, then battery can take up and fulfill load demand. In this mode, the control switches $(Q_1 \& Q_2)$ associated with sources will keep the sources as maximum power point and control switch Q_5 will regulate the output voltage to reference point. In case of battery powering the load control switch Q_4 regulates the output voltage, switch Q_5 remains ON for entire mode of operation and the switch Q_3 remains OFF all the times. Figure 3-11 shows only one source energizing the connected load (a) source two energizing (b) source one energizing (c) battery energizing.

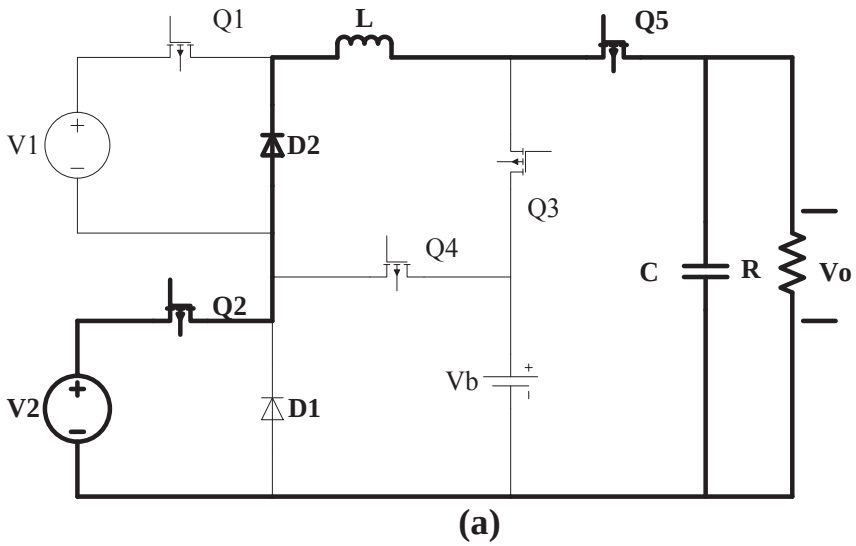

(a)

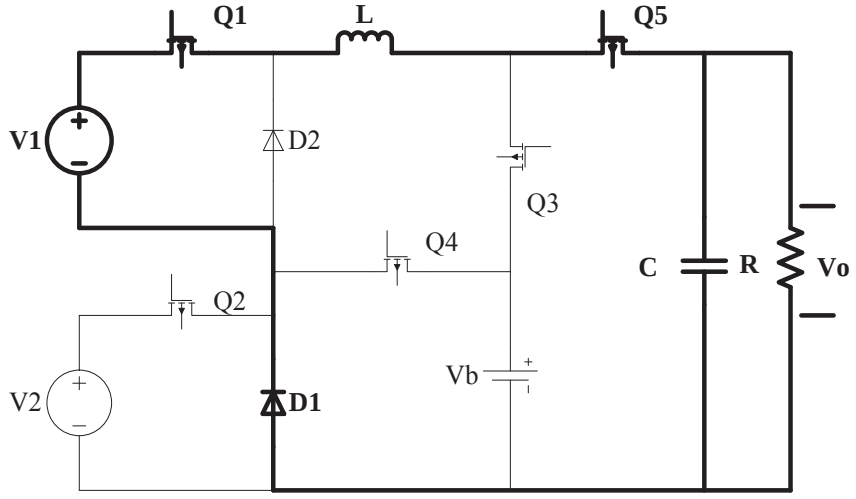

(b)

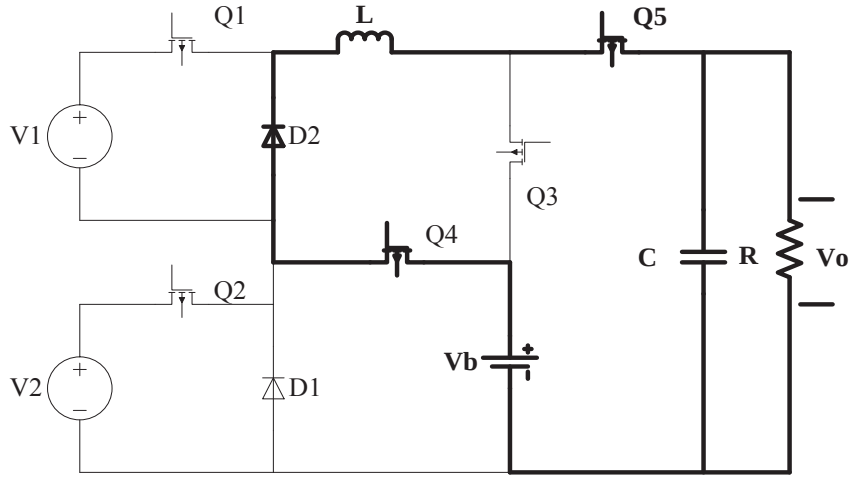

(c)

Figure 3-11 Equivalent Circuit (a) source two energizing (b) source one energizing (c) battery energizing

3.3 Design of Components

The section provides the design and selection guidelines to develop the new converter topology for steady state operation in continuous conduction mode.

3.3.1 Inductor Rating

Determining the inductor rating is the most critical step in designing of multiport converter since inductor has a huge impact on converter's efficiency and line and load transient response. Furthermore, it also determines the maximum value of output current the converter can handle and deliver [140]. Saturation in the inductor is determined by the peak current passing through it which intern is used to determine the size of the inductor. The inductor peak current can be determined by the following equation

$$I_{peak} = I_{o,max} + \frac{\Delta I_L}{2} \tag{3-32}$$

Whereas the current ripple ΔI_L can be found as

$$\Delta I_L = \frac{1}{f_{sw}L}\left(V_{in,max} - V_o\right)\frac{V_o}{V_{in,max}} \tag{3-33}$$

Here f_{sw} is the switching frequency, L is the inductance of the inductor, V_o is the output voltage. Writing ΔI_L in terms of current ripple ratio "ŕ" evaluated at maximum load current, $I_{o,max}$ gives

$$\acute{r} = \Delta I_L / I_{o,max} \tag{3-34}$$

Now from equation 3-33 and 3-34 we can get the minimum inductance value of inductor.

$$L = \frac{1}{I_{o,max}\,\acute{r} f_{sw}}\left(V_{in,max} - V_o\right)\frac{V_o}{V_{in,max}} \tag{3-35}$$

The above equation gives the value of inductor for a single output buck converter operating at switching frequency f_{sw}. In case of multiple output buck converter, the inductor is shared between the outputs therefore the value of inductor needs to be selected so that the ripple current of the largest output does not increase [104]. So, the value of inductor can be determined as,

$$L = \left(\frac{1}{I_{o,max}\,\acute{r} f_{sw}}\left(V_{in,max} - V_{o,j}\right)\frac{V_{o,j}}{V_{in,max}}\right) \tag{3-36}$$

(j = 1,2…..n)

3.3.2 Output Capacitor Rating

Output capacitor plays an important role in converter by reducing the output voltage overshoot and ripple. Insufficient output capacitance causes large voltage overshoots and large ripples. The designed capacitor should be large enough to prevent the inductor's stored energy to surpass the output voltage beyond the specified maximum value when the load is instantly removed [141]. The max value of output voltage overshoot is specified at the time of design and can be calculated by the following equation.

$$\Delta V = \left[\sqrt{V_o^2 \frac{L(I_{o,max}+{\Delta I_L}/{2})^2}{C_o}}\right] - V_o \tag{3-37}$$

Rearranging equation (3-37) for the value of capacitor C_o we get

$$C_o = \frac{L\left(I_{o,max}+{\Delta I_L}/{2}\right)^2}{(\Delta V+V_o)^2 - V_o^2} \tag{3-38}$$

The minimum value of the output Capacitor can be found by equation (3-38) by specifying the design value of ΔV.

3.3.3 Diode Rating

Selecting suitable diodes is another important factor in designing of multiport converters. The important parameters that must be taken into account while selecting a diode for a multiport converter are [142].

- The value of reverse breakdown voltage of the diode must be greater than the output voltage of the converter.
- The diode must be able to operate with the forward current injected by the inductor
- The forward voltage should be as small as possible to minimize power loss.
- diode must have a short reverse-recovery time

Power dissipation is a limiting factor in selection of a diode. The average power can be calculated as

$$P_D = \left[1 - \frac{V_{out,max}}{V_{in,max}}\right] * I_o V_D \quad (3\text{-}39)$$

Here P_D is Diode Power dissipation and V_D is the voltage drop across the diode.

3.3.4 MOSFET Rating

MOSFET is the most important part of the converter and it must be able to withstand the drain-to-source voltage that occurs when the inductor is discharging through the diode. The rated value of drain current of MOSFET needs to be greater than the peak inductor current [142]. Power dissipation in MOSFET is caused by switching losses and 'ON' resistance ($R_{DS(ON)}$). The power dissipation ($P_{R_{ON}}$) can be calculated as

$$P_{R\_ON} = \frac{V_{out,max}}{V_{in,min}} * I_{o,max}^2 * R_{DS(ON)} \quad (3\text{-}40)$$

Although switching losses constitute a relatively smaller portion of total power dissipated in the MOSFET, yet these must be considered while designing a converter. A MOSFET with low gate-to-source and drain-to-source capacitances will exhibit minimal switching losses. Switching losses can be calculated as

$$P_{Sw} = (V_{in} - V_o) * (\frac{I_{o,max}}{2}) * T_{(ON)} + T_{(OFF)} * f_{sw} + (C_{oss} * (V_{in} - V_o)^2 * f_{sw} \quad (3\text{-}41)$$

3.4 Conclusion

In this chapter, basic architecture and analysis of a newly proposed non-isolated Dual input-Dual output dc-dc buck converter, is presented. This converter has two input ports to assimilate two input renewable sources which can power up the load independently and simultaneously, one bidirectional port for controlled storage and backup power and a fully controlled output port. Smooth transition of power from input to output is controlled by independent duty cycles. It utilizes single inductor which makes the size compact and easy to control. The converter can operate in Dual input-Dual output, Single input-Dual output, Dual input-Single output mode and Single input-Single output mode. Steady state analysis of the proposed converter for all the modes has been presented in continuous conduction mode. In section 3.3, design guidelines for the selection of different components are presented.

Chapter 4

4 Control of Novel Multiport Converter Topology

4.1 Introduction

low power electronic equipment like digital cameras, mobile phones, wireless sensor networks and other hand held portable measuring instruments require multiple and independent voltage levels for different operations to minimize the overall power consumption as explained in chapter 2. Several single input multiple output methods have been adopted to fulfil this requirement [112],[143] however single inductor multiple output converters have gained more popularity to quench this necessity due to the advantages like small size, less components and good power conversion efficiency [105],[144]. Despite of all these advantages, a major drawback of these SIMO converters is the interdependency of the various outputs and due to cross coupling thereby variation in any of the parameter may have an effect on other parameters especially output voltages [117],[145]. Hence there is a dire need to develop a control strategy to minimize this cross-regulation issue for proper operation of SIMO converters. Several control techniques have been presented in the literature. A predictive digital current mode controller is proposed in [146], in this technique duty cycle value for every switch in the converter is determined based on the reference value of the current and the estimated inductor current. Although the result is reduction of cross-regulation but implementation needs high calculations. A time multiplexing control scheme is adopted to convert the SIMO converter to multiplexed SISO converters while operating in discontinuous conduction operation [147]. Another control scheme in Pseudo-continuous conduction mode is adopted by adding an extra freewheeling switch parallel to the inductor [148]. Although both of these control techniques have minimized the cross-regulation problem but only in discontinuous conduction mode and at the cost of ripple, increased size and power dissipation. To reduce the ripple, a duty ratio based current estimation method is used in [117]. An integrated solutions to minimize the cross-regulation is presented in [149] however, the control system is complex and requires accuracy. A digital control methodology based on independent regulation of differential mode and common mode voltages is presented [150],[151]. Phase sequence Interchange method is

applied and digitally implemented to suppress the cross-regulation problem. Another control scheme is adopted for converter operating in continuous conduction mode where reference current determines the duty ratio of each output [152] however load variation still affects the output. A multivariable control scheme for voltage mode control of dual output converter is implemented in [153]. A small signal model technique based on inductor current ripple and with a specified operating point pole zero placement is proposed in [154]. As this technique is designed for specific operating point therefore input voltage variations may reduce its utility. A model predictive voltage control scheme is adopted in [155]. Although the cross- regulation problem is minimized however these control scheme involves complex calculations and its implementation is a tedious process. A power-multiplexed control scheme is presented in [156]. By operating the output switches at a lower frequency than the power stage switches, each output is independently regulated when the corresponding output switch is turned on. However, needs synchronization of output and input switches.

In this work, a decentralized control of a Dual input-Dual output DC-DC buck converter is adopted. The decentralized control system is based on decoupling technique in which a feedback controller is augmented with a decoupling block with the intention to mathematically eliminate the effect of coupling or interaction. Thus, this decoupling block transforms the controller from a full block matrix to a diagonal matrix. The advantage of this control technique its design and implementation simplicity and results in substantial reduction of cross regulation [133]. In contrast with the control schemes presented in the literature which only deal with the single input multi output systems, the proposed control scheme deals with the multi input multi output systems.

4.2 Control Objectives for Multiport Buck Converter

As explained in chapter 3, the two output voltages of the new multiport buck converter are required to be regulated at a reference value in response to variations/disturbances in the input voltages and output load. The output voltage regulation is achieved through an appropriate feedback controller and Pulse Width Modulation (PWM) of the duty cycles of control switches. In this topology, the output switches Q_3 & Q_5 are responsible to control the output voltages through the duty cycles d_3 & d_5 (as shown

in Figure 3-7). As in case of practical electronics circuits there are many causes of disturbances like fluctuation in input voltages, dynamic loading conditions and changes in circuit parameters therefore it is not possible to permanently set the output duty cycle values to achieve constant output values under all conditions. Therefore, the controller in the circuit is required to automatically adjust the duty cycle values to obtain the constant output voltages at desired values despite of all the variations in source voltages and output loads. To achieve this goal an appropriate feedback controller is required to regulate the output voltages V_{o1} & V_{o2} to their reference value by automatically adjusting the duty cycle d_3 & d_5 values and to further achieve the following objectives

- Fast response to variations in input voltages and output load
- Low overshoot
- Zero steady state error and low noise susceptibility

In feedback control system as shown in Figure 4-1, the output voltage V_{out} is compared with a reference value V_{ref} and an error signal V_{err} is generated which is fed to the controller. The controller produces control voltage signal V_{Gs} which acts as an input voltage to the Pulse Width Modulation (PWM) block. The PWM block then produces a switching signal (d) to control switch and to regulate the output voltage. If the feedback control system works properly the error signal V_{err} should ideally be zero however this is not the case in practical conditions. The error signal is usually a nonzero term therefore a compensator is added in a system to minimize the error term and to bring the output voltage close to reference value. In this way, the system imperfections are compensated by modifying the feedback chain through a well-designed compensator.

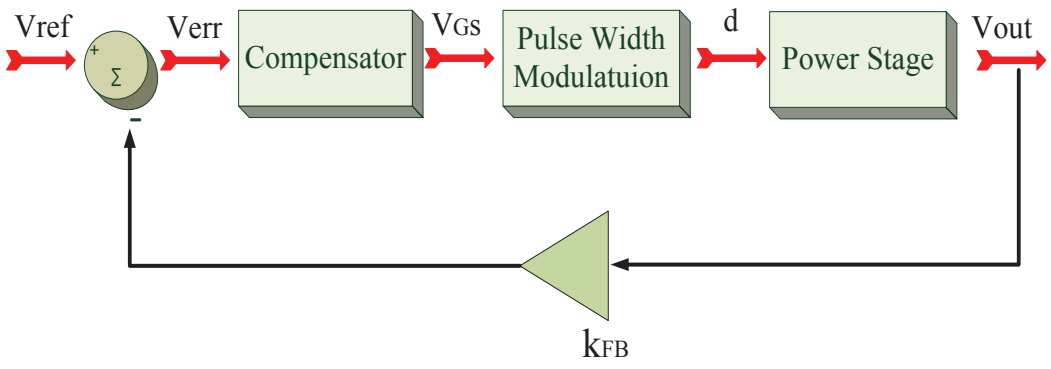

Figure 4-1 Feedback Control System

To understand the effects of source and load variations on the output voltages, a dynamic model of the circuit is required. Therefore, the steady state model developed in chapter 3 is required to be extended to a dynamic model. The presented topology is a time variant nonlinear system therefore to design and analyse the control system the converter model must be transformed to an average small signal model so that the conventional linear control theories can be applied around its steady state operating points and to design a proper feedback controller and compensation network. To develop a small signal model, average representation of the converter in continuous conduction mode is done to ascertain its dynamic characters. Several averaging techniques have been presented in the literature however State Space Averaging (SSA) technique is used in this work to develop an average model of the presented topology.

4.3 Dynamic Representation of New Topology

To dynamically represent the characteristics of the presented topology in continuous conduction mode State Space Averaging Technique is used in this work. SSA is a well-known Technique to approximate the switching converters as a continuous linear system [157]. To determine the state space representation, the state variables vectors xt, the input vectors ut and the output vectors yt for each mode of converters operation are defined first and the state equations are then obtained.

When the converter is operating in Dual input-Single output mode, the objective is to regulate the input power and output voltage V_{o2} hence the plant's outputs are I_L and V_{o1}which are also the state variables of the system for this mode whereas the control variables are d_1 and d_5. The state equations in this mode are

$$\begin{cases} \frac{Ldi_L}{dt} = d_1V_1 + d_2V_2 - d_5\,V_{o1} \\ \frac{C_2dv_{o1}}{dt} = d_5i_L - \frac{v_{o1}}{R_1} \\ p_{in} = d_1V_{in}i_L \end{cases} \tag{4-1}$$

Similarly, in Dual input-Dual output mode the control variables d_1,d_3 and d_5 are used to control the state variables are I_L, V_{o1} and V_{o2}. The state equations in this mode can be written as

$$\begin{cases} \frac{Ldi_L}{dt} = d_1V_1 + d_2V_2 - d_5\,V_{o1} - d_3\,V_{o2} \\ \frac{Cdv_{o1}}{dt} = d_5 i_L - \frac{v_{o1}}{R_1} \\ \frac{Cdv_{o2}}{dt} = d_3 i_L - \frac{v_{o2}}{R_2} \end{cases} \quad (4\text{-}2)$$

And for Single input-Dual output mode

$$\begin{cases} \frac{Ldi_L}{dt} = d_1V_1 - d_5\,V_{o1} - d_3\,V_{o2} \\ \frac{Cdv_{o1}}{dt} = d_5 i_L - \frac{v_{o1}}{R_1} \\ \frac{Cdv_{o2}}{dt} = d_3 i_L - \frac{v_{o2}}{R_2} \end{cases} \quad (4\text{-}3)$$

By considering the state space descriptions in equations (4-1) to (4-3), it can be easily deduced that the system is time variant as it includes the switching functions. The time variant function is converted to time invariant model by applying state space averaging technique. As per SSA the average of the product of plant's variable (xt) and plant's inputs (switching function dt) can be approximated by product of their averages as

$$\langle d(t)x(t)\rangle_{T_s} = \langle d(t)\rangle_{T_s}\langle x(t)\rangle_{T_s} = d(t)\langle x(t)\rangle_{T_s} \quad (4\text{-}4)$$

Applying SSA to equation 4-2 gives

$$\begin{cases} \frac{L\langle di_L\rangle_{T_S}}{dt} = d_1\langle V_1\rangle_{T_s} + d_2\langle V_2\rangle_{T_s} - d_5\langle V_{o1}\rangle_{T_s} - d_3\langle V_{o2}\rangle_{T_s} \\ \frac{C\langle dV_{o1}\rangle_{T_S}}{dt} = d_5\langle i_L\rangle_{T_s} - \frac{\langle V_{o1}\rangle_{T_S}}{R_1} \\ \frac{C\langle dV_{o2}\rangle_{T_S}}{dt} = d_3\langle i_L\rangle_{T_s} - \frac{\langle V_{o2}\rangle_{T_S}}{R_2} \end{cases} \quad (4\text{-}5)$$

The converter model described by equation 4-5 is a time invariant model but the model is still nonlinear due to the presence of different signals multiplications. In order to obtain a linear time invariant model, equation 4-5 needs to be linearized around its equilibrium point. The equilibrium point can be obtained by setting the derivatives terms in 4-5 to zero and solving equation to find the values of output voltages V_{o1}, V_{o2} and inductor current I_L as

$$V_{o1} = I_L d_5 R_1 \quad (4\text{-}6)$$

$$V_{o2} = I_L d_5 R_2 \quad (4\text{-}7)$$

$$I_L = \frac{V_1 d_1 + V_2 d_2}{d_5^2 R_1 + d_3^2 R_2} \tag{4-8}$$

By putting the value of I_L from (4-8) to (4-6) and (4-7) we get

$$V_{o1} = d_5 R_1 \frac{(V_1 d_1 + V_2 d_2)}{d_5^2 R_1 + d_3^2 R_2} \tag{4-9}$$

$$V_{o2} = d_3 R_2 \frac{(V_1 d_1 + V_2 d_2)}{d_5^2 R_1 + d_3^2 R_2} \tag{4-10}$$

4.4 Small Signal Modelling

The average model as described in equation (4-5) can be linearized by considering perturbations around its equilibrium position. Each of the state and source variable in equation (4-5) is comprised of two terms. An equilibrium or DC term and a perturbation or AC term [157]. Hence the duty cycles input voltage and state variables have two components i.e. the DC values and perturbations therefore we have

$$\begin{cases} \langle x \rangle = \mathrm{X} + \hat{x} \\ \langle d \rangle = \mathrm{D} + \hat{d} \\ \langle v \rangle = \mathrm{V} + \hat{v} \end{cases} \tag{4-11}$$

Here X, D and V are the equilibrium values and $\hat{x}$, $\hat{d}$ and $\hat{v}$ are the small signal perturbations. It is assumed that the perturbations are very small and their products are negligible therefore they do not change significantly in a switching period. Therefore, the small signal model in the matrix form can be represented as

$$\dot{x} = \mathrm{A}\, x + \mathrm{Bu}$$
$$\mathrm{y} = \mathrm{C}\, x + \mathrm{Du} \tag{4-12}$$

The matrix formation of dual input single output mode is shown in equations (4-13) and (4-14) whereas dual input-dual output mode is represented by equations (4-15) and (4-16).

$$\frac{d}{dt}\begin{bmatrix} i_L \\ v_{02} \end{bmatrix} = \underbrace{\begin{bmatrix} 0 & \frac{-d_3}{L} \\ \frac{d_3}{c_2} & -\frac{1}{R_2 C_2} \end{bmatrix}}_{A} \underbrace{\begin{bmatrix} i_L \\ v_{02} \end{bmatrix}}_{x} + \underbrace{\begin{bmatrix} \frac{v_1}{L} & -\frac{v_{02}}{L} \\ 0 & \frac{i_L}{C_2} \end{bmatrix}}_{B} \underbrace{\begin{bmatrix} d_1 \\ d_3 \end{bmatrix}}_{u} \tag{4-13}$$

$$\begin{bmatrix} p_{in} \\ v_{02} \end{bmatrix} = \underbrace{\begin{bmatrix} d_1 V_{in} & 0 \\ 0 & 1 \end{bmatrix}}_{C} \underbrace{\begin{bmatrix} i_L \\ v_{02} \end{bmatrix}}_{x} + \underbrace{\begin{bmatrix} i_L V_{in} & 0 \\ 0 & 0 \end{bmatrix}}_{D} \underbrace{\begin{bmatrix} d_1 \\ d_3 \end{bmatrix}}_{u} \tag{4-14}$$

$$\frac{d}{dt}\begin{bmatrix} i_L \\ v_{01} \\ v_{02} \end{bmatrix} = \begin{bmatrix} 0 & \frac{-d_5}{L} & \frac{-d_3}{L} \\ \frac{d_5}{C_1} & -\frac{1}{R_1 C_1} & 0 \\ \frac{d_3}{C_2} & 0 & -\frac{1}{R_2 C_2} \end{bmatrix}\begin{bmatrix} i_L \\ v_{01} \\ v_{02} \end{bmatrix} + \begin{bmatrix} \frac{(v_1+v_2)}{L} & -\frac{v_{01}}{L} & -\frac{v_{02}}{L} \\ 0 & -\frac{i_L}{C_1} & 0 \\ 0 & 0 & -\frac{i_L}{C_2} \end{bmatrix}\begin{bmatrix} d_1 \\ d_5 \\ d_3 \end{bmatrix} \quad (4\text{-}15)$$

$$\begin{bmatrix} p_{in} \\ v_{01} \\ v_{02} \end{bmatrix} = \begin{bmatrix} d_1 V_{in} & 0 & 0 \\ 0 & 1 & 0 \\ 0 & 0 & 1 \end{bmatrix}\begin{bmatrix} i_L \\ v_{01} \\ v_{02} \end{bmatrix} + \begin{bmatrix} i_L V_{in} & 0 & 0 \\ 0 & 0 & 0 \\ 0 & 0 & 0 \end{bmatrix}\begin{bmatrix} d_1 \\ d_5 \\ d_3 \end{bmatrix} \quad (4\text{-}16)$$

A small signal for the converter can now be developed from the above stated equations to demonstrate the dynamic behavior of the converter and to get the input to output transfer functions. In Figure 4-2 the small signal model of the converter is shown. The independent voltage and current sources are shown in circles whereas the squares represent the dependent sources. The dependent sources terms are combined and modelled as an ideal transformer. Hence the final equivalent small signal circuit demonstrating the behavior of the new topology is shown in Figure 4-3. Small signal analysis has been explained in detail in [158].

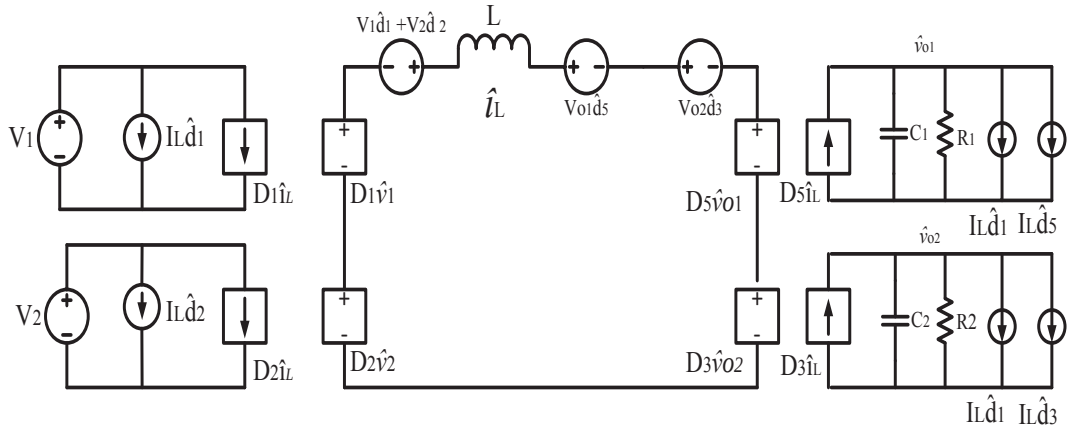

Figure 4-2 Small Signal Model of dual input-dual output Converter

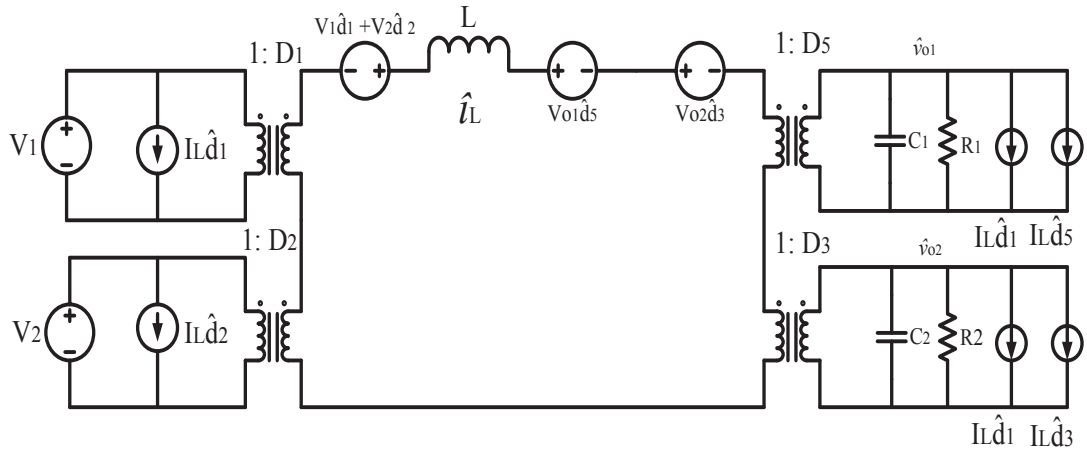

Figure 4-3 Equivalent Small Signal Model of dual input-dual output Converter

After obtaining the small signal model the feedback control system as shown in Figure 4-1 can be represented as the Figure 4-4. As shown in the Figure 4-1, KFB is the sensing circuit gain, G_{PWM} is the transfer function of pulse width modulator, G_{PS} is the transfer function of power stage of the converter and G_C is the transfer function of controller. The loop transfer function or loop gain from Point A to B can be represented as the product of small signal gains in the forward and feedback path of the feedback loop [159] as represented in (4-17)

$$G_L(s) = G_C(s)G_{PWM}(s)G_{PS}(s)k_{FB} \tag{4-17}$$

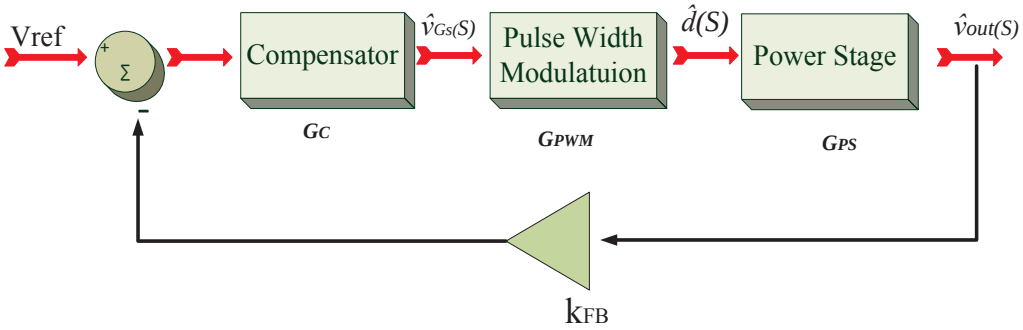

Figure 4-4 Feedback loop block diagram

4.5 Power Stage Transfer Functions

In the presented topology, the inputs and out puts of the plant are identified as follows and shown in Figure 4-5. Plant's inputs are (a) source or input voltages V_1 and V_2 (b) Input duty cycles d_1 and d_2 and (c) Output duty cycles d_3 and d_5. Plant's outputs are the output voltages V_{o1} and V_{o2}.

Depending on inputs and outputs of the plant, three types of transfer function can readily be identified

(A) Input to Output Transfer Function G_{Vin}

This transfer function plays an important role in designing of output voltage regulator as it determines the effect of variations in the input voltages on the system's output voltages. This transfer function is obtained by setting the duty cycle variations to zero and solving the transfer function from $\hat{v}_0$(s) to $\hat{v}_{in}$(s).

(B) Input duty cycle to output voltage G_{din}

This transfer function describes the influence of input duty cycle over output voltage. This transfer function is obtained by setting the input voltage variations to zero and solving the circuit model for $\hat{v}_0$(s) as a function of $\hat{d}_{in}$

(C) Output duty cycle to output voltage G_{dout}

This transfer function describes the influence of output duty cycles over output voltages. This transfer function is obtained by setting the input voltage variations to zero and solving the circuit model for $\hat{v}_0(s)$ as a function of $\hat{d}_{out}$

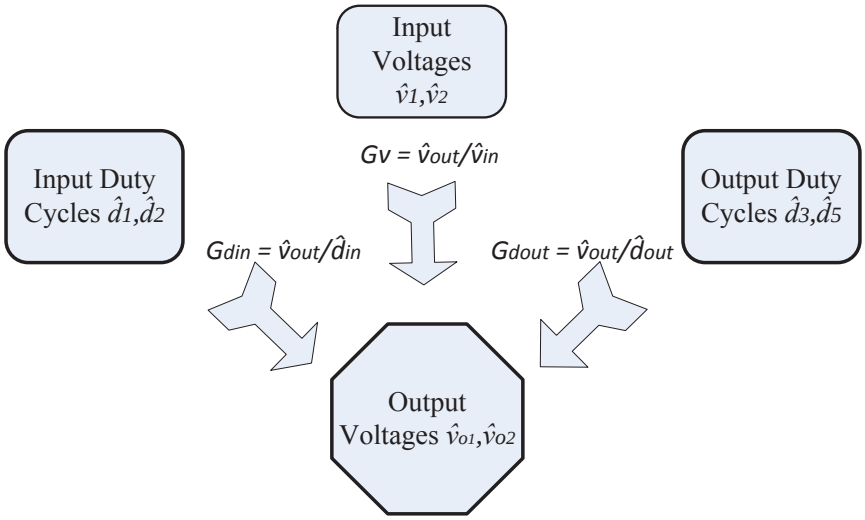

Figure 4-5 Inputs, Outputs and Transfer Function of the converter

Based on the small signal model different transfer functions can be obtained as

(A) $\boldsymbol{G_{Vin}}$

$$G_{v1}(s) = \frac{\hat{v}_{o1}}{\hat{v}_{in}} = \frac{d_1 d_5 Z_{eq1}(s)}{\delta(s)} \tag{4-18}$$

Here $\hat{v}_{in} = \hat{v}_1 + \hat{v}_2$ and $D_1 = D_2$

similarly

$$G_{v2}(s) = \frac{\hat{v}_{o2}}{\hat{v}_{in}} = \frac{d_1 d_3 Z_{eq2}(s)}{\delta(s)} \tag{4-19}$$

(B) $\boldsymbol{G_{din}}$

$$G_{d1}(s) = \frac{\hat{v}_{o1}}{\hat{d}_1} = \frac{V_{in} d_5 Z_{eq1}(s)}{\delta(s)} \tag{4-20}$$

$$G_{d2}(s) = \frac{\hat{v}_{o2}}{\hat{d}_1} = \frac{V_{in} d_3 Z_{eq1}(s)}{\delta(s)} \tag{4-21}$$

(C) G_{dout}

$$G_{d15}(s) = \frac{\hat{v}_{o1}}{\hat{d}_5} = \frac{I_L Z_{eq1}(s)\left[(d_3)Z_{eq2}(s)+s.L+r_L\right]+d_5 Z_{eq1}(s)\,(V_{o2}-V_{o1})}{\delta(s)} \quad (4\text{-}22)$$

$$G_{d25}(s) = \frac{\hat{v}_{o2}}{\hat{d}_5} = \frac{-[I_L Z_{eq2}(s)\left[(d_5)Z_{eq1}(s)+s.L+r_L\right]+d_3 Z_{eq2}(s)\,(V_{o1}-V_{o2})}{\delta(s)} \quad (4\text{-}23)$$

$$G_{d13}(s) = \frac{\hat{v}_{o1}}{\hat{d}_3} = \frac{-[I_L Z_{eq1}(s)\left[(D_3)Z_{eq1}(s)+s.L+r_L\right]+D_5 Z_{eq1}(s)\,(V_{o1}-V_{o2})}{\delta(s)} \quad (4\text{-}24)$$

$$G_{d23}(s) = \frac{\hat{v}_{o2}}{\hat{d}_3} = \frac{[I_L Z_{eq2}(s)\left[(D_5)Z_{eq1}(s)+s.L+r_L\right]+D_3 Z_{eq2}(s)\,(V_{o2}-V_{o1})}{\delta(s)} \quad (4\text{-}25)$$

Here

$$Z_{eq1}(s) = R_1 // \left(\frac{1}{s.C_1} + r_{C1}\right) \quad (4\text{-}26)$$

$$Z_{eq1}(s) = \frac{R_1.(1+s.C_1.r_{c1})}{[1+s.C_1.(R_1+r_{c1})]} \quad (4\text{-}27)$$

$$Z_{eq2}(s) = R_2 // \left(\frac{1}{s.C_2} + r_{C2}\right) \quad (4\text{-}28)$$

$$Z_{eq2}(s) = \frac{R_2.(1+s.C_2.r_{c2})}{[1+s.C_2.(R_2+r_{c2})]} \quad (4\text{-}29)$$

$$\delta(s) = D_5^2 Z_{eq1}(s) + D_3^2.Z_{eq2}(s) + s.L + r_L \quad (4\text{-}30)$$

$$I_{o1} = \frac{V_{o1}}{R_1} \quad (4\text{-}31)$$

$$I_{o2} = \frac{V_{o2}}{R_2} \quad (4\text{-}32)$$

$$I_L = I_{o1} + I_{o2} \quad (4\text{-}33)$$

4.6 Design of Compensator

As discussed earlier the aim of designing a control system for the presented converter topology is to reject the disturbances, to ensure stability and transient response. Each

of these requirements enforces a constraint on loop gain therefore a compensator is added in the system to modify the loop gain and to compensate for system disturbances as shown in Figure 4-4. Several strategies for design of a compensator have been presented in the literature. A Proportional, Integral, Derivative (PID) compensation is widely used in switching converters. The same compensation is utilized in the present work.

4.6.1 Review of PID Control

The term PID stands for Proportional, Integral, and Derivative. These three terms are the basic elements of the PID controller. Each of these three performs a different function and has a different effect on the performance of overall system. In this section a brief review of PID controller is presented.

(A) The Proportional (P) Term

The proportional term links the amplitude of control voltage *VGs* to the difference of system reference and feedback voltage which is called the error signal. If the difference is large, then the control voltage signal is increased and on the contrary the control voltage signal is reduced. This relationship is established with the help of a gain introduced in the chain of feedback system which is called proportional gain denoted by term K_p. The control voltage in terms of error signal and proportional gain can be expressed as

$$V_{Gs}(t) = K_p V_{err}(t) \tag{4-34}$$

The error signal is scaled up by a factor K_p as shown in equation (4-34) and Figure 4-6. The main objective of proportional controller is to reduce the steady state error of the plant. If K_p is set high, the result is the fast response but with the risk of an overshoot on the other hand if K_p is very small, the overshoot is reduced but the system has sluggish response.

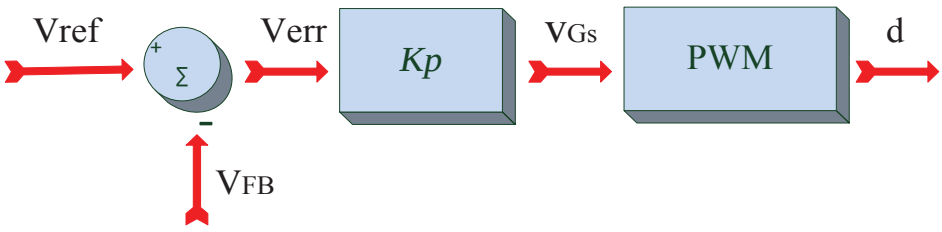

Figure 4-6 Inclusion of Proportional Term in feedback path

(B) The Derivative (d) Term

The slope of error signal determines whether a small driving signal is required or the larger one. This slope of the error signal is assessed by introducing the derivative coefficient K_d. as shown in Figure 6-7. Hence the control voltage becomes

$$V_{Gs}(t) = K_d \frac{dV_{err}(t)}{dt} \quad (4\text{-}35)$$

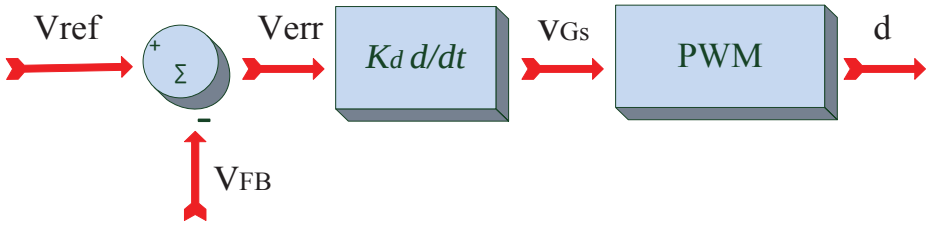

Figure 4-7 Inclusion of Derivative Term in feedback path

Equation (6-35) shows that in case of a fast change, the control voltage will quickly react to impose the fast change in the output because of the presence of derivate term. The presence of derivative term limits the output voltage overshoot. The negative point of the derivative term is that it slows down the system.

(C) The Integral (I) Term

The integral term in the feedback path ensures the least error between reference point and error signal by integrating the error signal over time. Hence the integral term maintains precision over time. The contribution of integral term can be adjusted by the parameter K_i and is used to cancel the error between the set point and the output. The control voltage in terms of integral term is shown in equation (4-36) and Figure 4-8.

$$V_{Gs}(t) = K_i \int V_{err}(t)\, dt \quad (4\text{-}36)$$

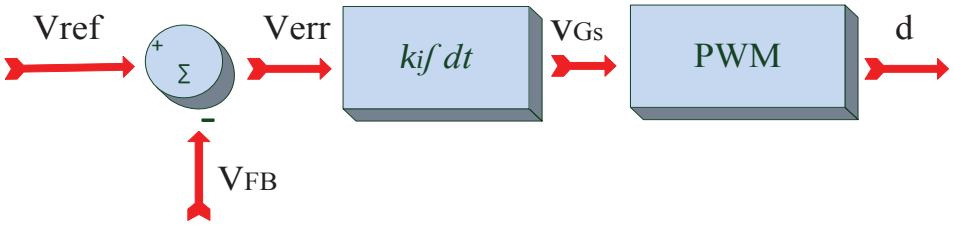

Figure 4-8 Inclusion of Integral Term in feedback path

To design a control system which reacts quickly to perturbations and exhibits small steady state error, a combination of all the functions of PID block could be utilized. The coefficients K_i, K_p and K_d are tweaked individually to obtain the desired performance of the converter. The combination of all the blocks is shown in Figure 4-9 and the control signal V_{Gs} can easily be obtained by the sum of all the blocks as shown in equation (4-37).

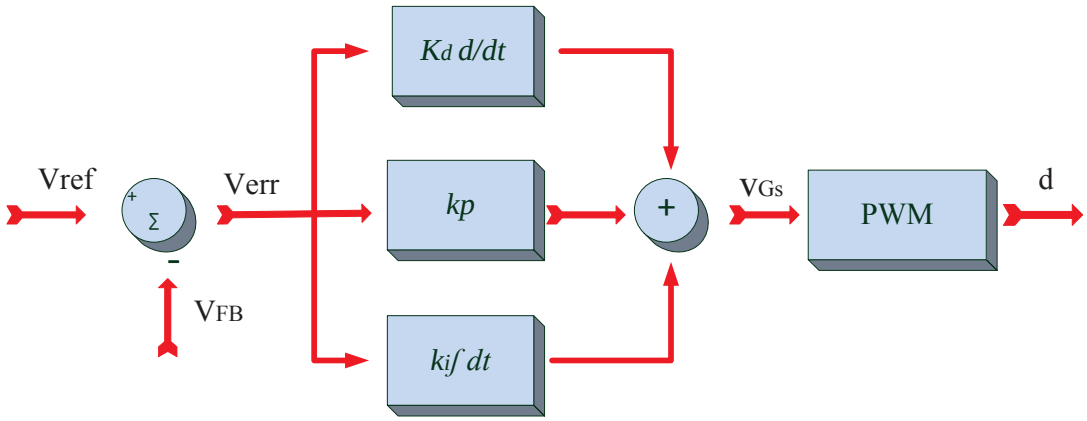

Figure 4-9 PID System combining all the three coefficients

$$V_{Gs}(t) = K_p V_{err}(t) + K_i \int V_{err}(t)\, dt + K_d \frac{dV_{err}(t)}{dt} \tag{4-37}$$

4.7 Multi-Input Multi Output System

The converter operates in different modes of operation i.e. Single input-Single output, Single input-Dual output, Dual input-Single output, and Dual input-Dual output therefore it is realized as a Multi input-Multi output (MIMO) system. The most challenging aspect in the control of these MIMO systems is the interaction or coupling of different outputs. In MIMO systems every input influences every output as well as the outputs will have effect on each other. Because of the interaction or coupling between the outputs, design of compensators for close loop system becomes a difficult process.

4.8 Decoupling Control

The open loop control to output transfer function matrix of the converter can be represented as a 2*2 MIMO system at i_{th} operating point and is given as

$$\begin{bmatrix} v_{01}(s) \\ v_{02}(s) \end{bmatrix} = \begin{bmatrix} G_{i11}(s) & G_{i12}(s) \\ G_{i21}(s) & G_{i22}(s) \end{bmatrix} \begin{bmatrix} d_5 \\ d_3 \end{bmatrix} \tag{4-38}$$

In the transfer function matrix of this 2*2 MIMO system there are of non-zero off-diagonal terms which introduce coupling between the outputs.

A MIMO transfer function matrix G(s) is obtained from state space model [160] and is represented by

$$G(s) = C(sI - A)^{-1}B + D \tag{4-39}$$

For the presented converter, the transfer matrices with the plant inputs and outputs can be shown as

For 2x2 System $y = G_{2*2}u$

$$\begin{bmatrix} y_1 \\ y_2 \end{bmatrix} = \begin{bmatrix} g_{11} & g_{12} \\ g_{21} & g_{22} \end{bmatrix} \begin{bmatrix} u_1 \\ u_2 \end{bmatrix} \tag{4-40}$$

And for 3x3 system $y = G_{3*3}u$

$$\begin{bmatrix} y_1 \\ y_2 \\ y_3 \end{bmatrix} = \begin{bmatrix} g_{11} & g_{12} & g_{13} \\ g_{21} & g_{22} & g_{23} \\ g_{31} & g_{32} & g_{33} \end{bmatrix} \begin{bmatrix} u_1 \\ u_2 \\ u_3 \end{bmatrix} \tag{4-41}$$

In order to overcome the cross-regulation problem, the MIMO system is modified so that decentralized control can be adopted. This modification is done by adding a pre-compensator to make resultant system transfer function matrix to a diagonal matrix. By this modification, the MIMO system is transformed into a dynamically decoupled system where every single output depends on single input. Hence the problem is reduced to single input-single output (SISO) system so that the compensators can be designed as a SISO with separate control loops [160].

In decoupling network for MIMO system a state vector matrix x can be represented as, x = G u *. Here u* is a modified input vector representing plant inputs or duty cycles u. So, u* = T u which implies x = TG u. To control one output by one input seperatly, the TG must be a diagonal matrix.

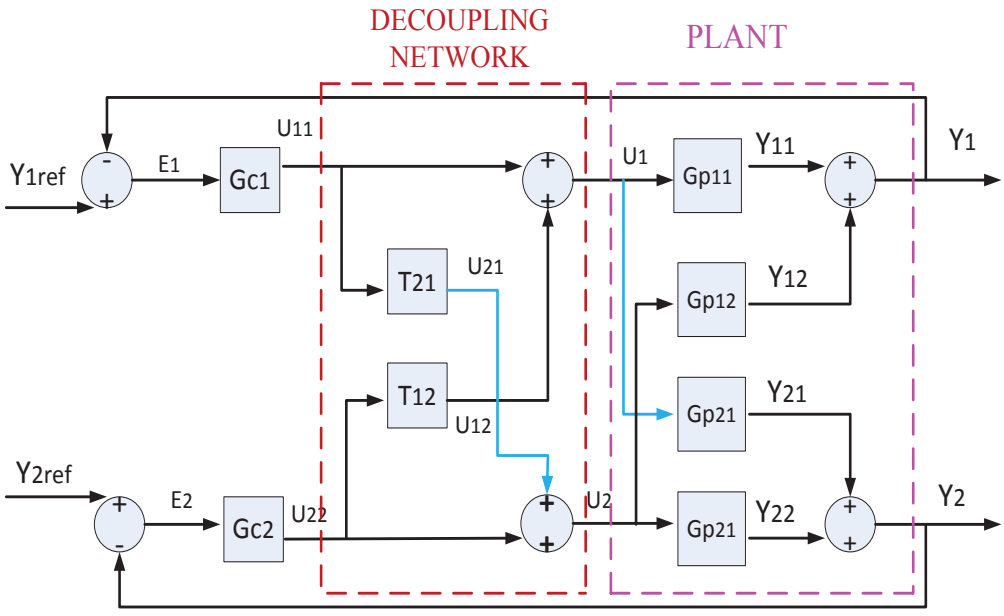

Figure 4-10 2x2 Decoupling control system

In Figure 4-10 above a decoupled controller for Dual input-Dual output system is shown. Here the objective is to cancel the effect of second input (U_2) on First output (Y_1). The cancellation will only occur if the output of the decoupler T_{21} satisfies the equation.

$$G_{p21}U_{11} + G_{p22}U_{21} = 0 \tag{4-42}$$

$$U_{21} = T_{21}U_{11} \tag{4-43}$$

$$U_{11}(G_{p21} + G_{p22}T_{21}) = 0 \tag{4-44}$$

As U_{11} is not equal to zero therefore an ideal decoupler is given by

$$T_{21} = -\frac{G_{p21}}{G_{p22}} \tag{4-45}$$

Similarly effect of U_1 on Y_2 also needs to be cancelled therefore

$$G_{p12}U_{22} + G_{p11}U_{12} = 0 \tag{4-46}$$

$$T_{12} = -\frac{G_{p12}}{G_{p11}} \tag{4-47}$$

The decoupling matrix T then can be written as
For Two input-Two output system

$$T_{2x2} = \begin{bmatrix} 1 & -g_{12}/g_{11} \\ -g_{21}/g_{22} & 1 \end{bmatrix}$$

And For Three input-Three output system

$$T_{3x3} = \begin{bmatrix} 1 & \frac{g_{13}.g_{32}-g_{12}.g_{33}}{g_{11}.g_{33}-g_{13}.g_{31}} & \frac{g_{12}.g_{23}-g_{13}.g_{22}}{g_{11}.g_{22}-g_{12}.g_{21}} \\ \frac{g_{23}.g_{31}-g_{21}.g_{33}}{g_{22}.g_{33}-g_{23}.g_{32}} & 1 & \frac{g_{13}.g_{21}-g_{11}.g_{23}}{g_{11}.g_{22}-g_{12}.g_{21}} \\ \frac{g_{21}.g_{32}-g_{22}.g_{31}}{g_{22}.g_{33}-g_{23}.g_{32}} & \frac{g_{12}.g_{31}-g_{11}.g_{32}}{g_{11}.g_{33}-g_{13}.g_{31}} & 1 \end{bmatrix}$$

For the pairing of inputs and outputs in decentralized control scheme Relative Gain Array (RGA) method is used. The RGA method provides a quantitative approach to analyse the interactions between the controls and the output, and thus provides a technique for pairing manipulated and controlled variables to generate a control scheme. Further details can be found in [160]

The decoupling network T_{2x2} transforms a two-loop cross-coupled system G_{2x2} to two independent single loop control systems in the form of equation,

$$\frac{y_1}{u_1} = g_{11} - g_{12}\frac{g_{21}}{g_{22}} \tag{4-48}$$

$$\frac{y_2}{u_2} = -g_{12}\frac{g_{21}}{g_{11}} + g_{22} \tag{4-49}$$

Likewise, for the systems where three independent outputs are to be determined, three independent decoupled single loop control systems can be achieved as follows

$$\frac{y_1}{u_1} g_{11} + g_{12}\frac{g_{13}.g_{32}-g_{12}.g_{33}}{g_{11}.g_{33}-g_{13}.g_{31}} + g_{13}\frac{g_{12}.g_{23}-g_{13}.g_{22}}{g_{11}.g_{22}-g_{12}.g_{21}} \tag{4-50}$$

$$\frac{y_2}{u_2} = g_{21}\frac{g_{23}.g_{31}-g_{21}.g_{33}}{g_{22}.g_{33}-g_{23}.g_{32}} + g_{22} + g_{23}\frac{g_{13}.g_{21}-g_{11}.g_{23}}{g_{11}.g_{22}-g_{12}.g_{21}} \tag{4-51}$$

$$\frac{y_3}{u_3} = g_{31}\frac{g_{21}.g_{32}-g_{22}.g_{31}}{g_{22}.g_{33}-g_{23}.g_{32}} + g_{32}\frac{g_{12}.g_{31}-g_{11}.g_{32}}{g_{11}.g_{33}-g_{13}.g_{31}} + g_{33} \tag{4-52}$$

The above equations can now be used to obtain the transfer function of the system which in now decoupled. Furthermore, the close loop compensators can now be independently designed considering the system as single input-single output by adopting SISO design techniques.

In the succeeding chapter, simulation model is built for control of Dual Input-Dual output converter model to verify the effectiveness of presented control scheme and analysis and discussion is presented in chapter 7.

4.9 Conclusion

In this chapter, different control schemes adopted in multiport converters have been studied. A decentralized control scheme for multi input-multi output systems has been studied and presented for the proposed new topology. The decentralized control scheme has been found suitable to minimize the cross-regulation problem in a Dual input-Dual output converter operating in continuous conduction mode. The control scheme is based on decoupling control method in which Multi input Multi output (MIMO) systems are modified by adding a pre- compensator to make the resultant transfer function to a nearly diagonal matrix hence making the decentralized control scheme feasible for MIMO systems. The advantage of the proposed control scheme is its design and implementation simplicity and results in substantial reduction of cross regulation problems associated with single inductor multiport converters and provide the satisfactory dynamic performance of the converter in Continuous Conduction mode.

Chapter 5

5 Simulation Setup

Based on the converter model discussed in Chapter 3, a simulation system platform for the presented Multi input-Multi output DC-DC converter has been developed in MATLAB/Simscape. The simulation model is used to test the developed converter under different operating conditions and to verify the analytical results obtained in chapter 3. The parameters used for simulation studies are defined first and are shown in Table 5-1. The input voltages correspond to the voltage level of small renewable energy sources like solar panel, fuel cell and small wind turbines. The output voltage V_{o1} is designed to power up low power electronics devices and the output voltage V_{o2} is designed to charge a 6V battery. The values of elements like inductor and capacitor are obtained as per equations (3-36) and (3-38) as presented in chapter 3. The performance of the converter under different operating conditions in open loop and closed loop systems is evaluated and discussed in this chapter.

Table 5-1 System Parameters for simulation studies

Design Parameter	Value
Input Voltage Vin_1	0-9V
Input Voltage Vin_2	0-6V
Battery Voltage V_b	6V
Output voltage Vo_1	3.3V
Battery Charging Voltage Vo_2	6.8V
Inductance	150µH
Capacitance	1000µF
Switches	MOSFETS
Switching Frequency	100 KHZ
Output Voltage ripple	136mV
Inductor ripple current	0.435A

5.1 Open Loop Simulation model

Simulation model for a Dual input-Dual output converter is shown in Figure 5-2. In this model, both the input sources are present therefore in addition to powering up the load, the additional power is stored in the battery. As the model represents an open

loop system therefore input and output duty cycles are fixed to a constant value as shown in Table 5-2 and it is assumed that there is no variation in input voltages and load current. A constant voltage equivalent to 3.3 V is obtained at one of the output ports to power up the load whereas the other output port is used to charge the battery at a constant voltage 6.8V. Inductor Current and Duty Cycles are shown in Figure 5-1. Output voltages and are shown in Figures 5-3 and 5-4 and inductor current is shown in Figure 5-5.

Table 5-2 Duty Cycle and Output Voltage for open loop Converter

Parameter	Value
Duty Cycle d_1	52%
Duty Cycle d_2	52%
Duty Cycle d_3	99%
Duty Cycle d_5	25%
Output Voltage Vo_1	3.3V
Output Voltage Vo_2	6.8V

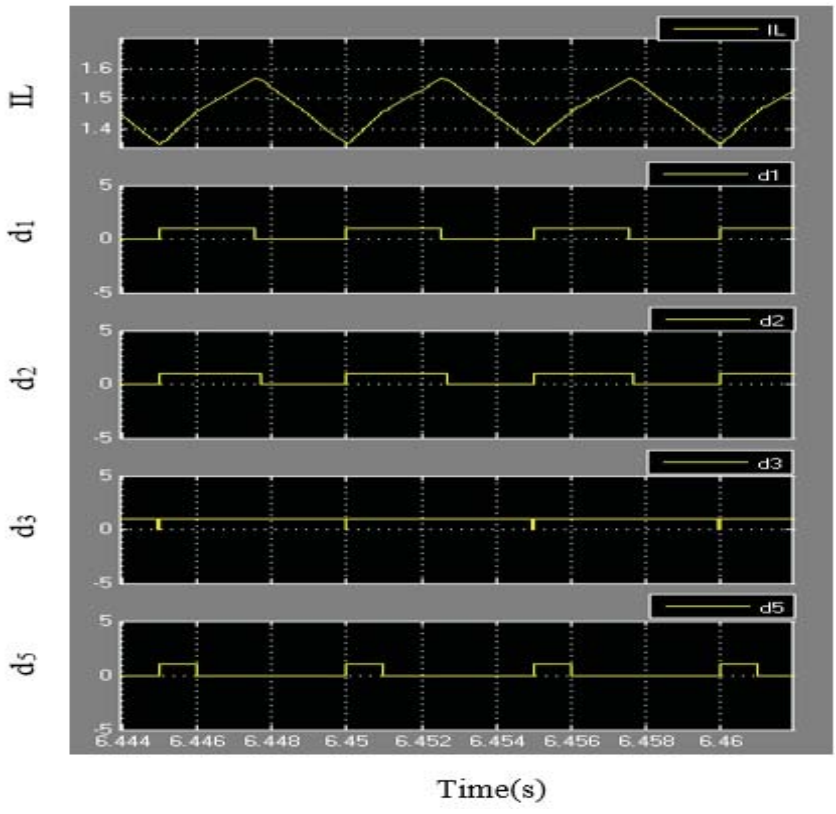

Figure 5-1 Inductor Current and Duty Cycles

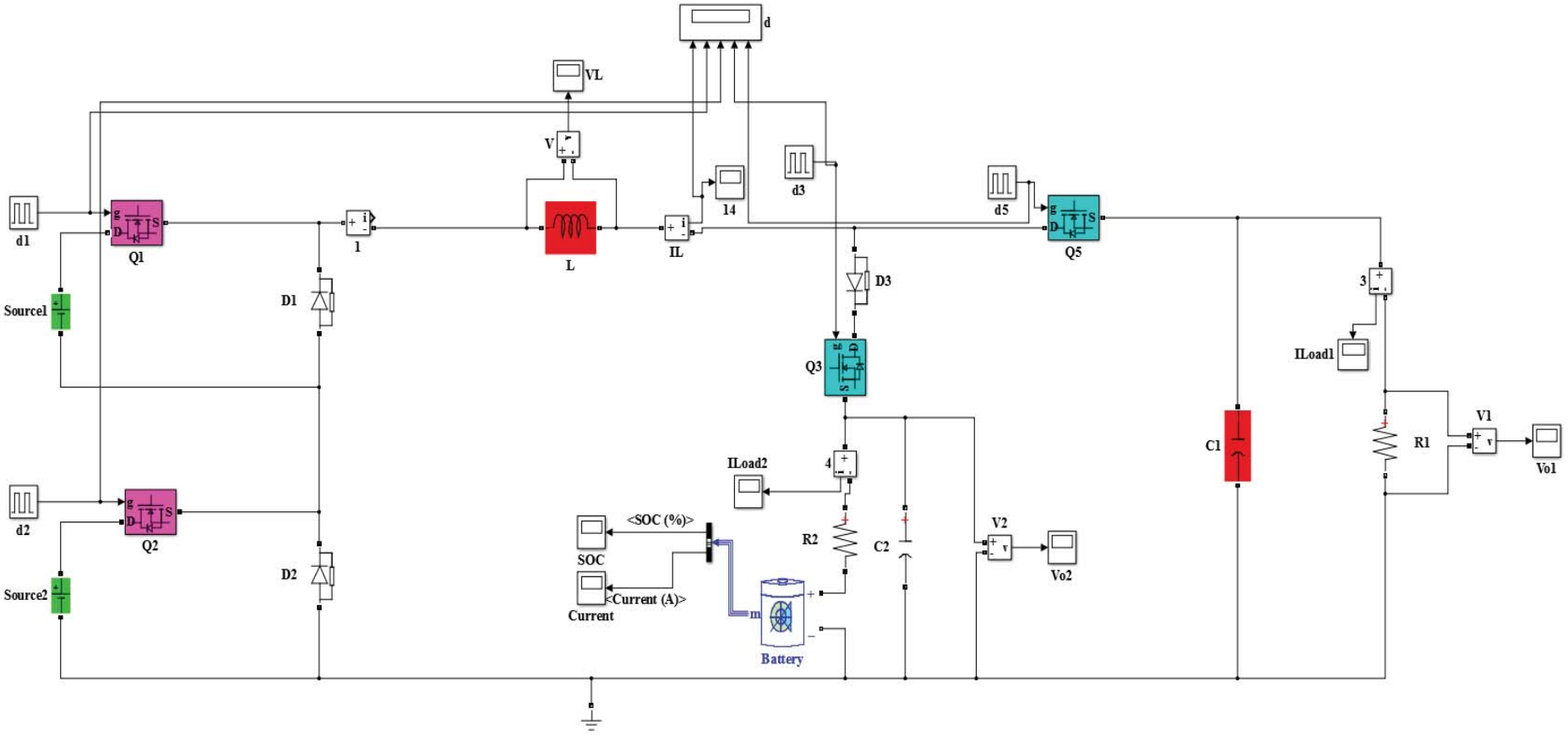

Figure 5-2 Open Loop Simulation model for Dual Input Dual Output Converter

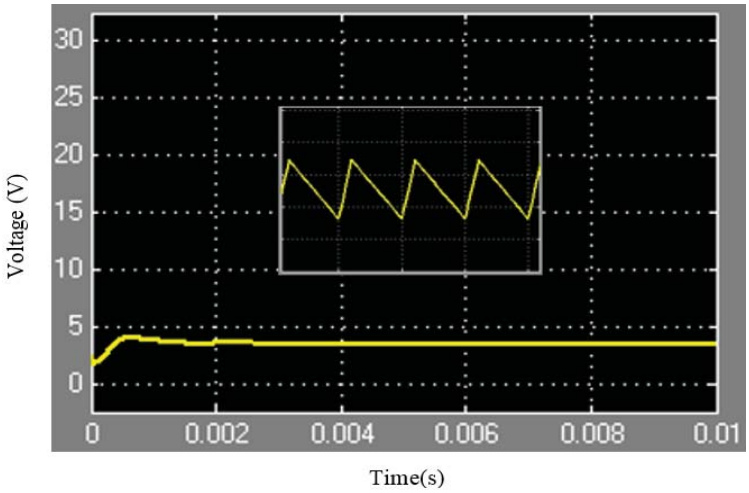

Figure 5-3 Open loop Output Voltage V_{o1} in Dual input-Dual output mode

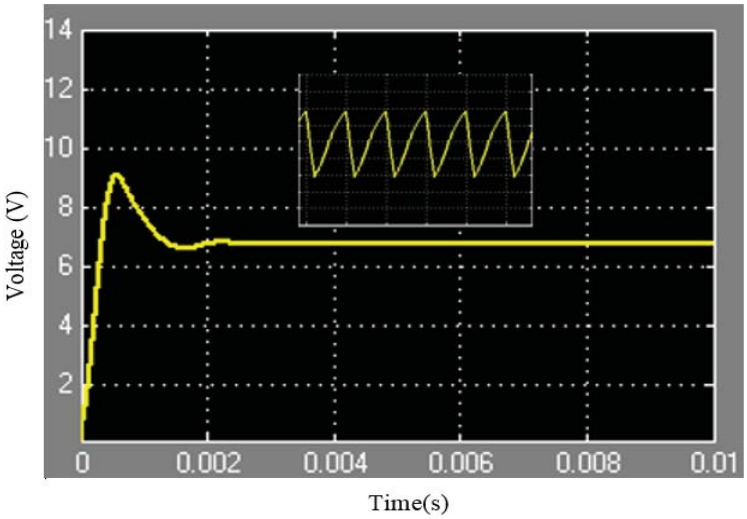

Figure 5-4 Open loop Output Voltage V_{o2} in Dual input-Dual output mode

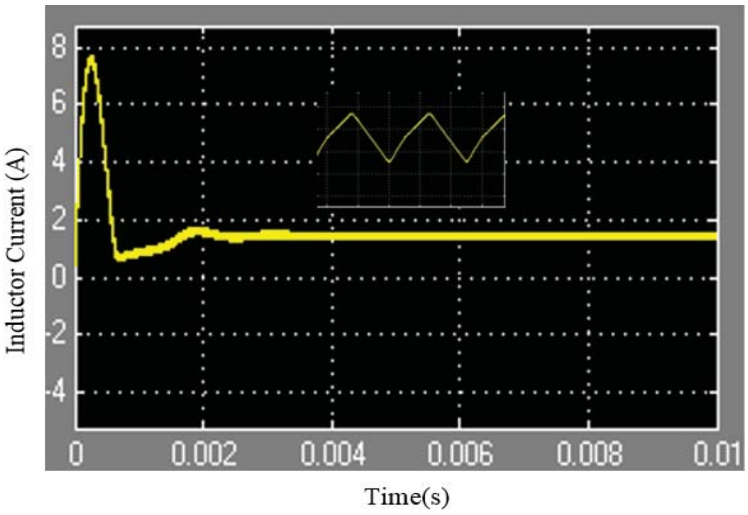

Figure 5-5 Inductor Current

When both the input sources are available (the switches Q_1 and Q_2 are close) they charge the inductor and power up the load. When there is no load requirement i.e. the switch Q_5 is open, both the sources charge the battery. Likewise, when switches Q_1 and Q_2 are OFF, the inductor is discharged through battery. This Situation is illustrated in Figure 5-1. The open loop simulation results demonstrate the presented converter can assimilate two different sources at the input ports and can power up two different loads with different voltage levels connected at the output ports. As no controller or compensation block is added therefore the overshoots and undershoots are quite noticeable. In the following section simulation results with closed loop by adding a controller will be presented.

5.2 Close loop Simulation Model

Close loop control or the feedback control is essential to keep the output voltages close to the desired values despite all the variations and perturbations in the input voltages and load current. Close loop simulation model of the converter is shown in Figure 5-6. In this model, the output voltages are compared with a reference value and error signal is generated. A compensator is added in the system to modify the loop gain and to compensate for the system perturbations. A PI controller is used in this study to resolve the oscillatory, sluggish response and overshoot problems. The manipulated error signal is now fed to PWM block to generate duty cycle to regulate the output voltages. In this model, there are two closed loop systems. One of the loops is used to regulate the load voltage while the other maintains constant voltage for charging the battery. The input duty cycles d_1 and d_2 can be utilized to track maximum power from the input sources however, in this study, constant DC sources replicate the renewable energy sources therefore the values of d_1 and d_2 are fixed. The duty cycles d_3 and d_5 are utilized to regulate the output voltages V_{o2} and V_{o1} respectively.

In the simulation model shown in Figure 5-6, the converter operates in different modes. Mode detection circuitry as shown in Figure 5-6 (block A) selects converter's mode of operation. This circuitry works as per the flow chart shown in Figure 5-7. Based on the availability of input sources, output load requirements and state of battery, the following modes of operation are discussed

- Dual Input-Dual output mode (DIDO)
- Dual input-Single Output mode (DISO)
- Single Input-dual output mode (SIDO)
- Single input-Single output mode (SISO)

When both the input sources are available and the combined voltage (V_{in}) of both the sources is equal to or greater than 9 volts and the nominal voltage of the battery is less than 6 volts, the converter operates in Dual Input-Dual output (DIDO) mode. In this mode, in addition to power up the load, excess available energy is stored in the battery. When the battery is fully charged and/or the input voltage (V_{in}) is less than 9 volts i.e. excess energy is not available from the input sources then the converter shifts to Dual input-Single output (DISO) mode where both the sources are utilized to power up the load. In case of light load conditions and/or the input voltage from source one is equal to or greater than 9 volts i.e. enough power is available from source one, the converter operates in Single input-Dual output (SIDO) mode. Here only one source is used to power up the load and to charge the battery. In the scenario when only one of the input sources is available, the converter operates in single input Single output (SISO) mode. If none of the input sources is available, the battery is utilized to energize the load (SISO2).

5.2.1 Line Regulation

The purpose of the presented converter is to integrate renewable energy sources and to provide regulated voltage to the load despite of all the variations in the input supply voltage. To demonstrate that the converter can serve the intended purpose, simulation studies are conducted. Two different scenarios are considered. In the first scenario, the behavior of the converter is observed while there is a reduction in the voltage of one of the input sources whereas the in the second situation, observations are made when one of the input sources is completely vanished. Therefore, in addition to the observations on converter's response to the input perturbations, behavior of the converter is also examined during the transition of its mode of operation. For this simulation studies voltage of source, one is 9V and that of source two is taken as 6V at the maximum power point of respective renewable energy sources. Source one can vary from zero to nine volts and source two can vary from zero to six volts. Under any particular mode of operation, the converter responds to any variation in the input

voltages within their defined operating range as stated in table 5-1. A 6V battery is used to store the surplus energy and act as a backup source. The output voltage to the load is desired to be kept at 3.3V and voltage to charge the battery is required to be maintained at 6.8V.

5.2.1.1 Input Perturbations

At the start, both the sources are available therefore in addition to powering up the load, extra power must be stored in the battery. Control switches Q_3 and Q_5 are both ON and the duty cycles $d_3$and d_5 regulate the output voltages. The converter responds to any change in the input voltage of source one or source two independently and/or change in voltage of both the sources concurrently. The output voltages are regulated to desired values despite the variation, increase or decrease in input voltage level of the sources within the operating range as defined above in table 5-1. For an instance at time t = 0.03s, input perturbation is initiated in the form of reduction of voltage for source one from 9V to 7V as shown if in Figure 5-8. Due to change in the input voltage, a slight change in the output voltages is observed. Figure 5-10 shows the regulation of output voltages, as no compensator is added in the system therefore there is a slight decrease in the output voltages. Figure 5-11 shows regulation of output voltages after a PI controller is added in the system. A slight dip in the output voltages is observed as the input voltage changes, however the controller quickly responds and brings the voltages back to the desired values. Inductor current for this mode is shown in Figure 5-9.

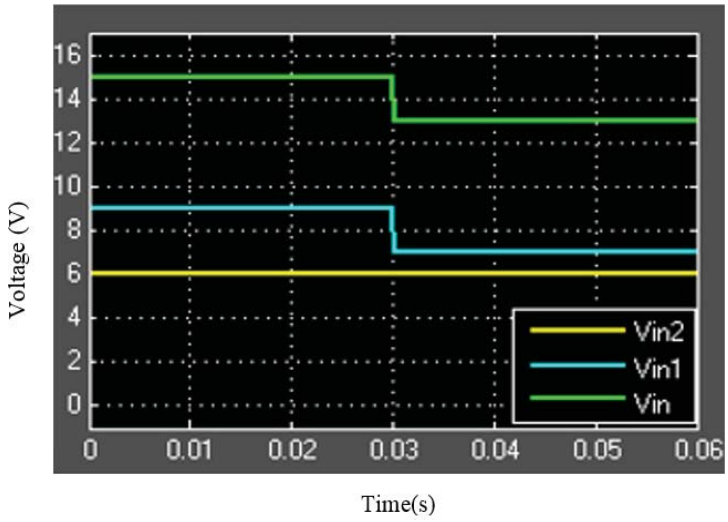

Figure 5-6 Variation in Input Voltage

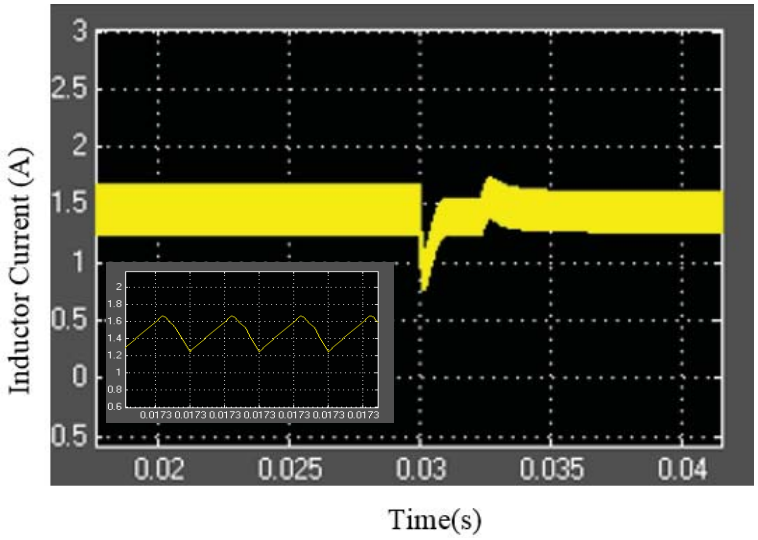

Figure 5-7 Inductor current

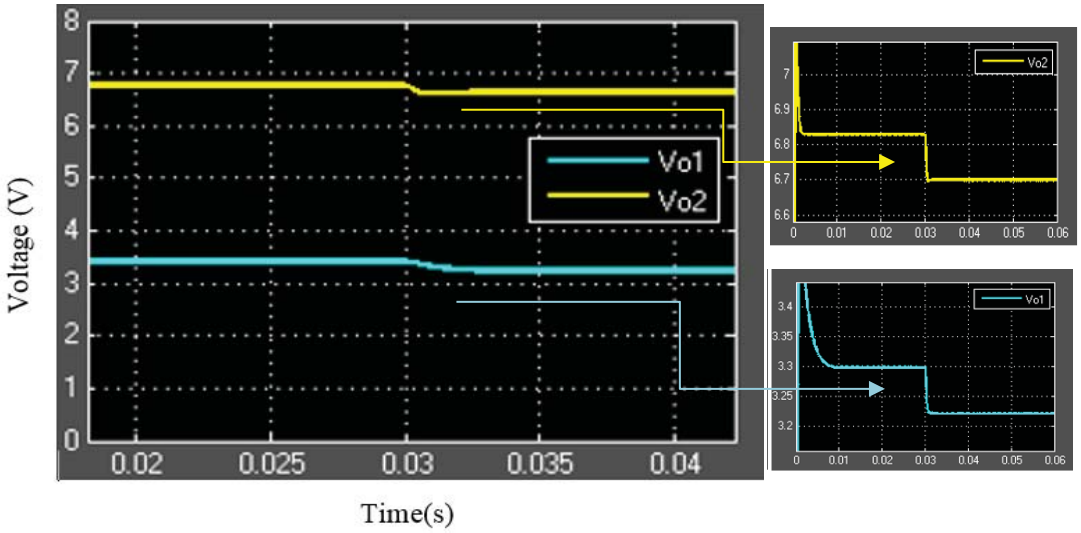

Figure 5-8 Output voltage Regulation without compensation

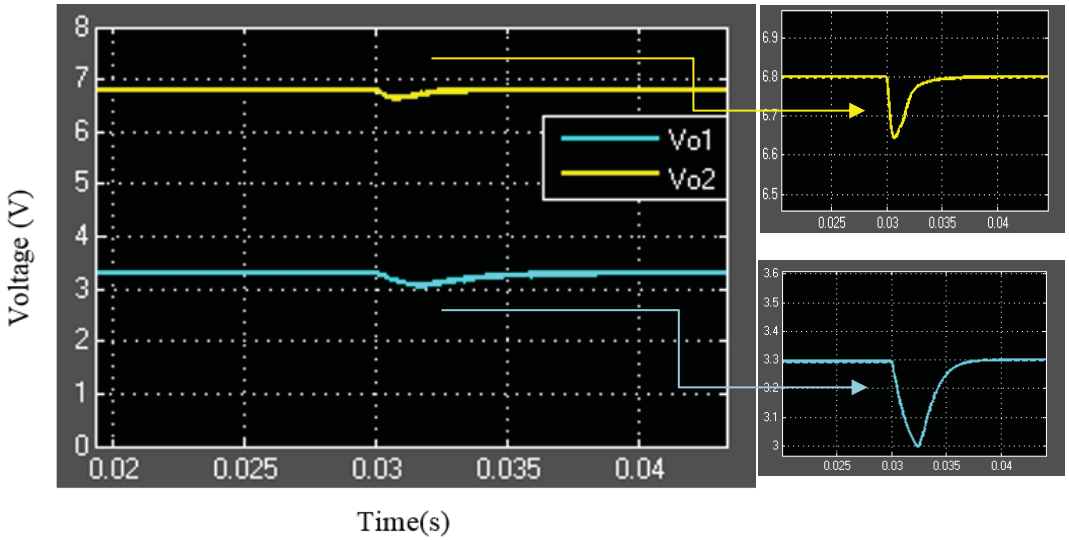

Figure 5-9 Output voltage Regulation with compensation

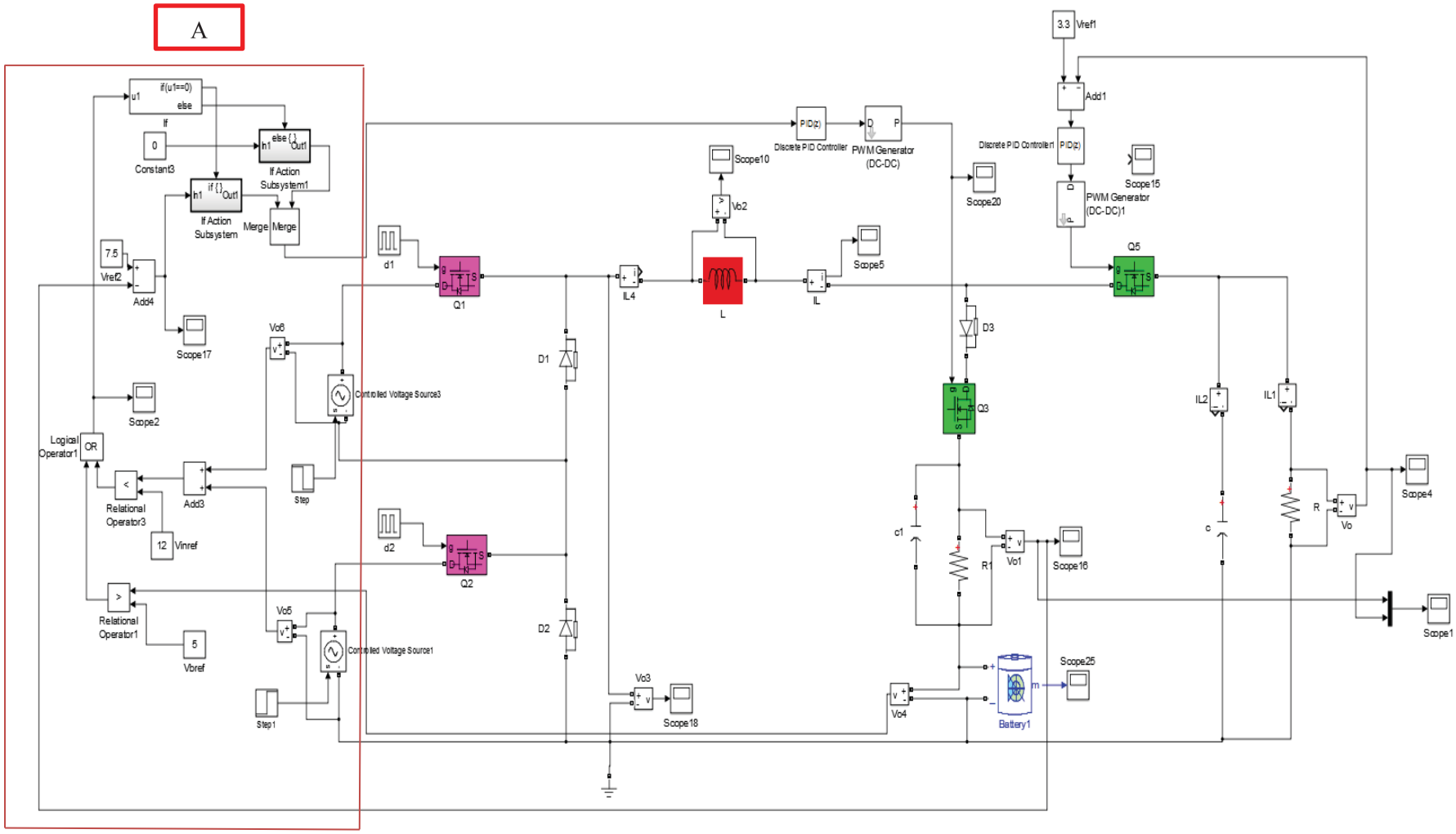

Figure 5-10 Close loop Simulation model for Dual Input Dual Output Converter

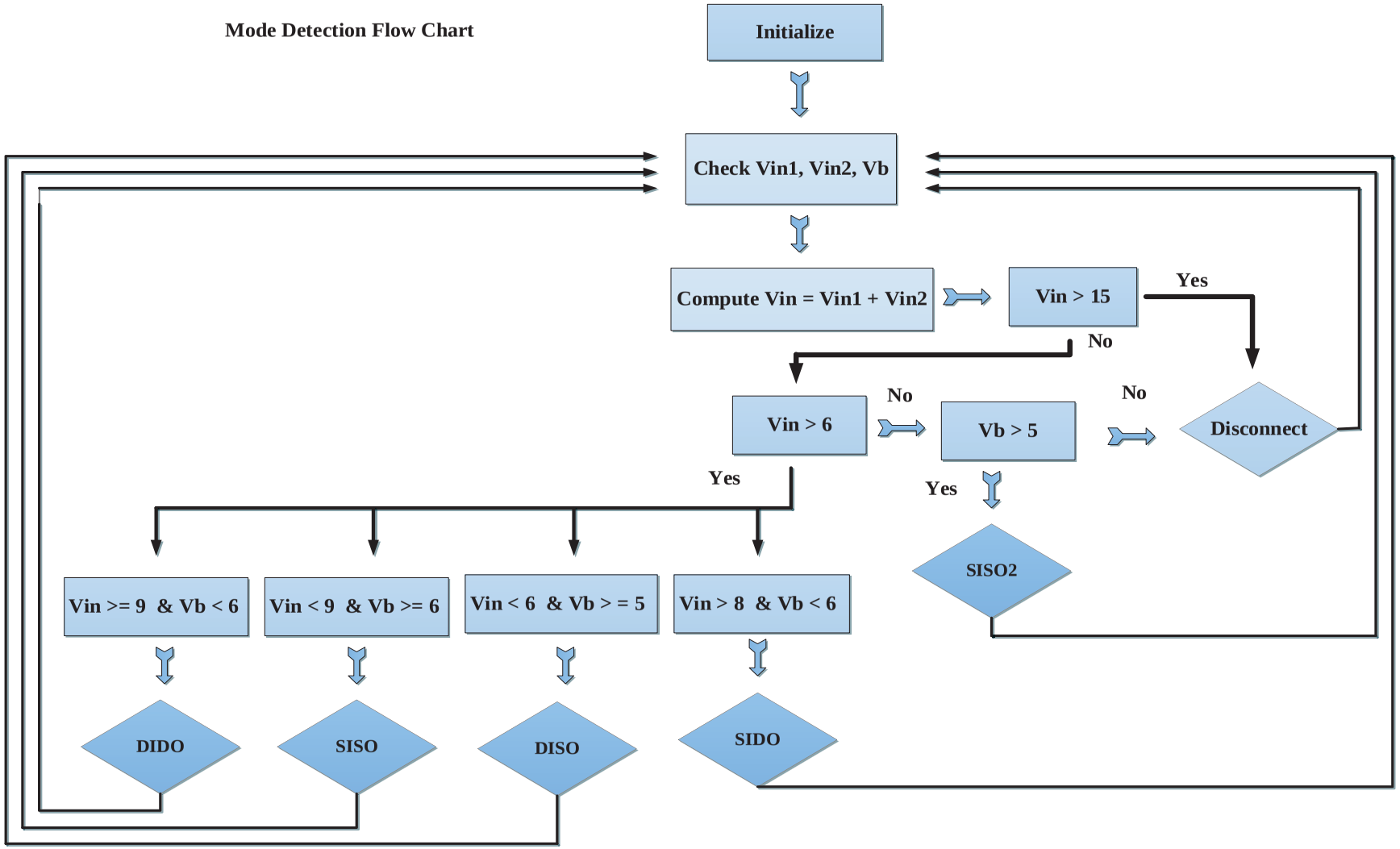

Figure 5-11 Flow chart for detection of mode of operation

5.2.1.2 Transition in mode of operation

At the start, both the sources are available therefore in addition to powering up the load, extra power must be stored in the battery. Control switches Q_3 and Q_5 are both ON and the duty cycles d_3 and d_5 regulate the output voltages. At time t = 0.03s, source two diminishes therefore battery charging is disconnected and only load demand is fulfilled. The converter shifts from Dual input-Dual output mode to Single input-Single output mode. Since the input power is decreased, the duty cycle d_5 increases to keep the output voltage V_{o1} to desired value. On the other hand, duty cycle d_3 goes to zero as the switch Q_3 turns OFF at this stage. Variation in Input voltage is shown in Figure 5-12. Output voltages are shown in Figure 5-13. Regulation of Output Voltage V_{o1} during mode transition is shown in Figure 5-14. Simulation results show smooth transition of converter's mode from dual input dual output to single input single output mode and prove that despite of variation in input voltages the output voltage is strictly regulated. Change in duty cycles value is shown in Figure 5-15. As load two i.e. battery is disconnected therefore the inductor current decreases as shown in Figure 5-16.

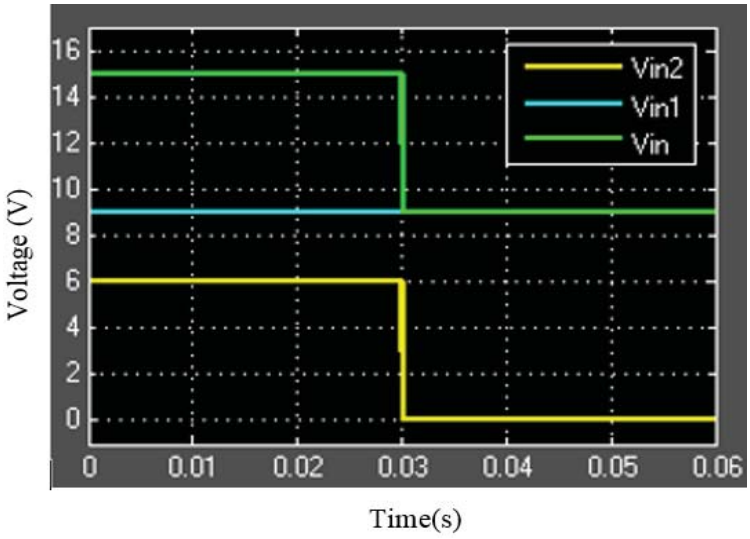

Figure 5-12 Variation in Input Voltages

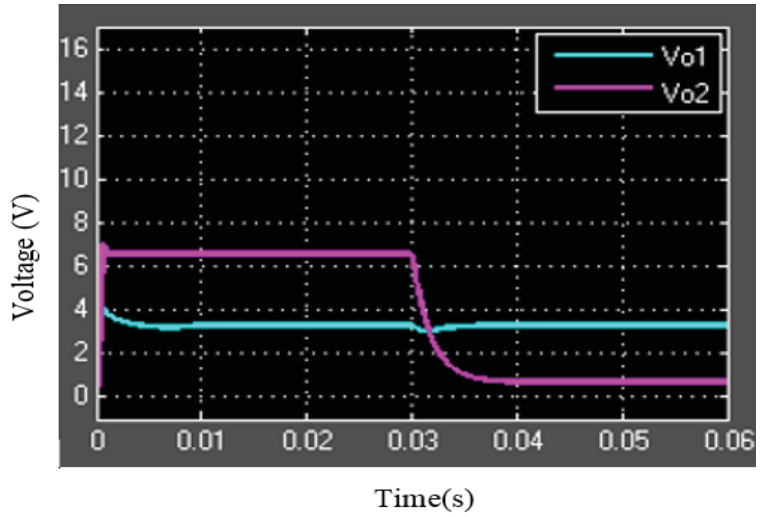

Figure 5-13 Change in Output Voltages V_{o1} and V_{o2}

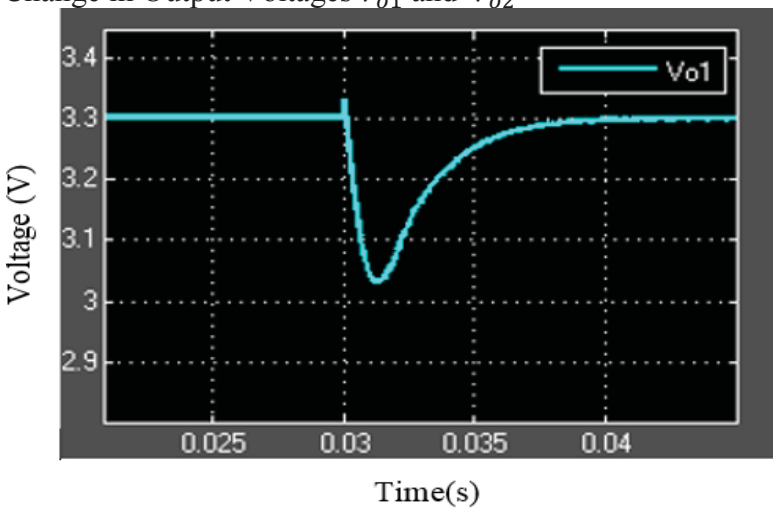

Figure 5-14 Regulation of Output Voltage V_{o1}during mode transition

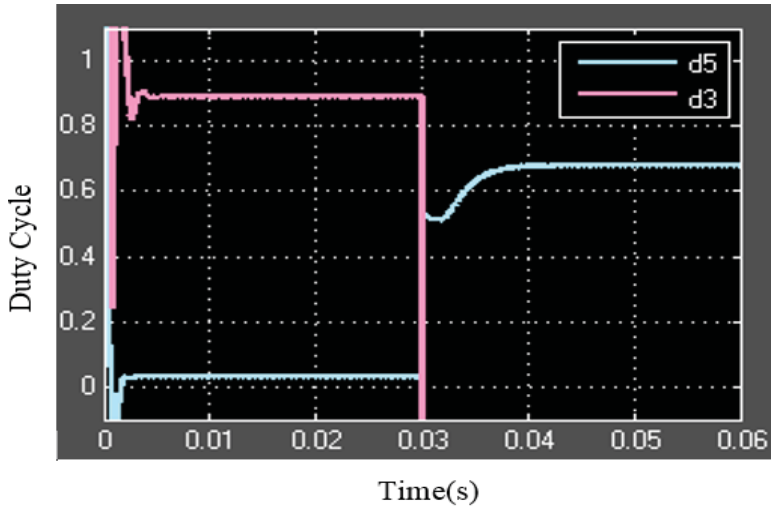

Figure 5-15 Change in Duty Cycles d_3 and d_5

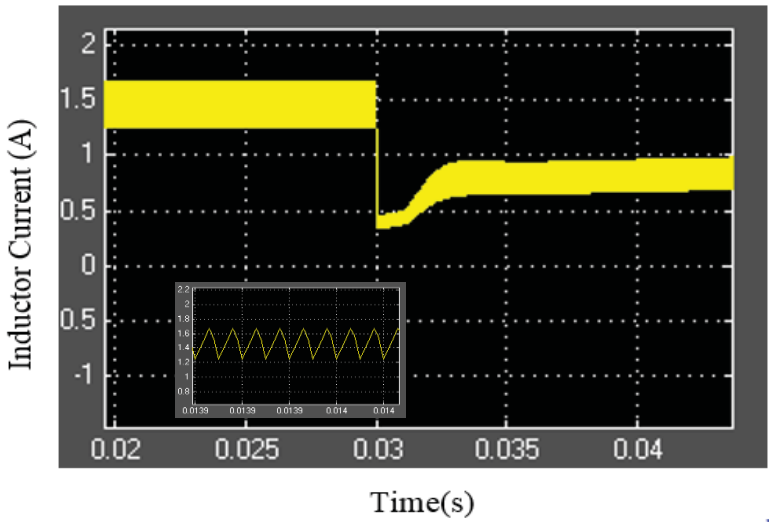

Figure 5-16 Decrease in Inductor Current due to decrease in load

5.2.2 Load Regulation

The simulation studies are extended further to study the effect of load variation on the performance of the converter. At time t = 0.03s, there is an increase in the load current from 0.65A to 0.8A as shown in Figure 5-17 and 5-18. But despite of change in the load current, the output voltages remains constant at the desired level as shown in Figure 5-19 and 5-20. However due to change in load current, the inductor current increases as shown in Figure 5-21. The simulation results show that the converter responds to input voltage and load variations and provides regulated voltage to the load.

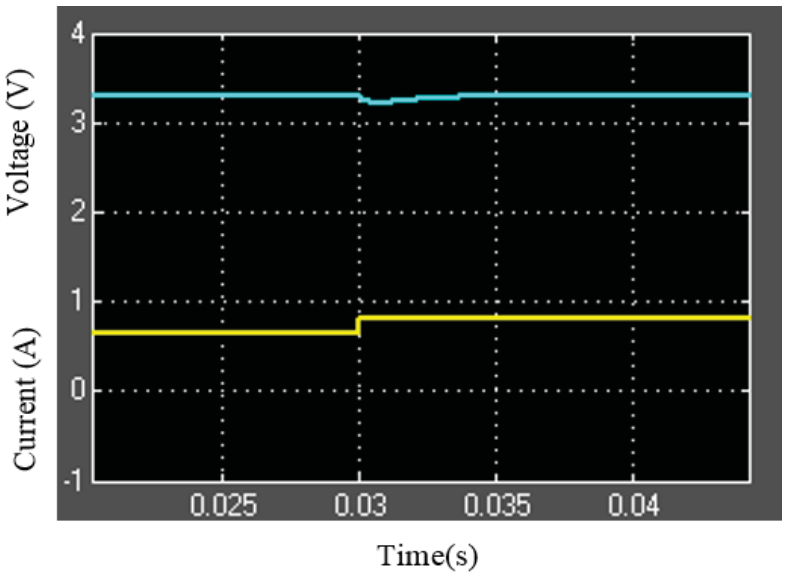

Figure 5-17 Regulated output voltage (V_{o1}) after increase in load current

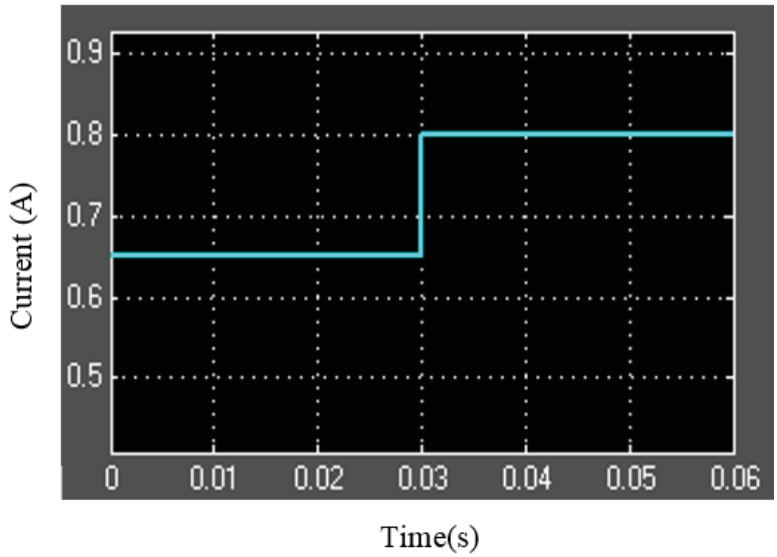

Figure 5-18 Increase in Load current from 0.65 A to 0.8 A

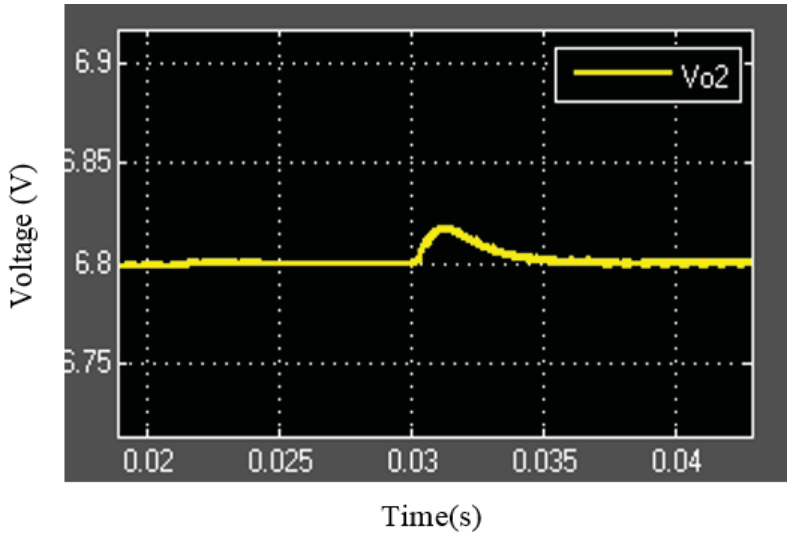

Figure 5-19 Output Voltage (Vo2) Regulation after increase in load current

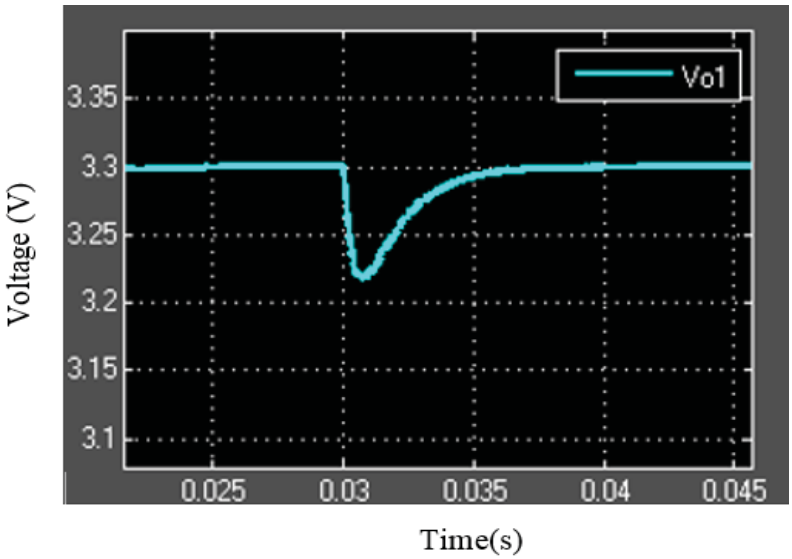

Figure 5-20 Output Voltage (Vo1) Regulation after increase in load current

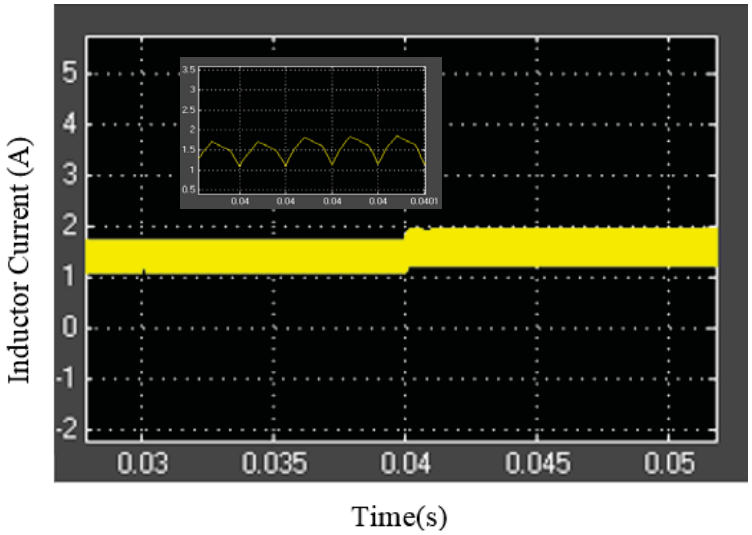

Figure 5-21 Increase in Inductor Current due to increase in load current

5.2.3 Cross Regulation

Despite of all the advantages, a major drawback of Single Inductor Multi Output (SIMO) converters is the interdependency of the various outputs and due to cross coupling thereby variation in any of the parameter may influence other parameters especially output voltages. To minimize this cross-regulation issue Multi Input Multi Output control strategy with decoupling control is used as explained in chapter 4 Section 4.7. Due to employment of decoupling control scheme, the cross-regulation problem has been minimized. Results in Figure 5-10, 5-13, 5-19 and 5-20 confirm that the variation in one of the output voltage due to change in input voltage or load current has a minimal effect on the other output voltage and furthermore the controller can quickly compensate and regulate the output voltages regardless of all the source and load perturbations.

5.3 Conclusion

In this chapter, simulation model of new multiport converter topology is built in MATLAB/SIMSCAPE. The model is developed to test and verify the analytical results obtained in chapter 3 and to test the control strategy developed in chapter 4. The behaviour of the converter is observed in different modes of operation. Simulation studies have been conducted observe the phenomenon like line, load and cross regulation.

In section 5.1, the response of the converter is observed under constant input voltage and load conditions. The obtained results show the proposed topology successfully integrated two energy sources and powered up the two loads with different voltage levels.

In section 5.2, the converter is examined under variable source and load conditions. Observations have been made for variable input voltage. The results show that converter provides regulated output voltages regardless of the variations in the source voltage. The studies are further extended to variable load conditions and it is found that converter with the adopted control strategy, responds quickly to the load variations and provides regulated output voltages. Results prove that the presented multiport converter topology serves the intended purpose of integrating the multiple energy sources and power up multiple loads under variable source and load conditions.

Chapter 6

6 Experimental Verification

To verify the analytical and simulation results presented in chapter 3 and chapter 5 respectively, a low voltage prototype model of the presented converter is developed. The prototype model for the presented converter is used to test the converter under different operating conditions and behavior of the converter is observed and analyzed for variations in input voltage and load current. Several modes of operations are studied and results are presented. The experimental setup is shown in Figure 6-1.

The parameters used for experimental studies are defined first and are shown in Table 6-1. Just like the simulation setup, the input voltages correspond to the voltage level of small renewable energy sources like solar panel, fuel cell and small wind turbines. The output voltage V_{o1} is designed to power up low power electronics devices and the output voltage V_{o2} is designed to charge a 6V battery. The minimum values of elements like inductor and capacitor are calculated as per equations (3-36) and (3-38) as presented in chapter 3. After calculations, the values of capacitor and inductor are chosen keeping in view the parameters like operating voltages, current, ripple voltage, ripple current, ESR value for capacitors and DC resistance for inductor. The components and their design value is shown in Table 6-2. For experimental setup, the input voltage sources are taken as a DC voltage source. Digital control scheme with Proportional and Integral control is implemented by Microcontroller Microchip dsPIC30F2020. The code is presented in Appendix B.

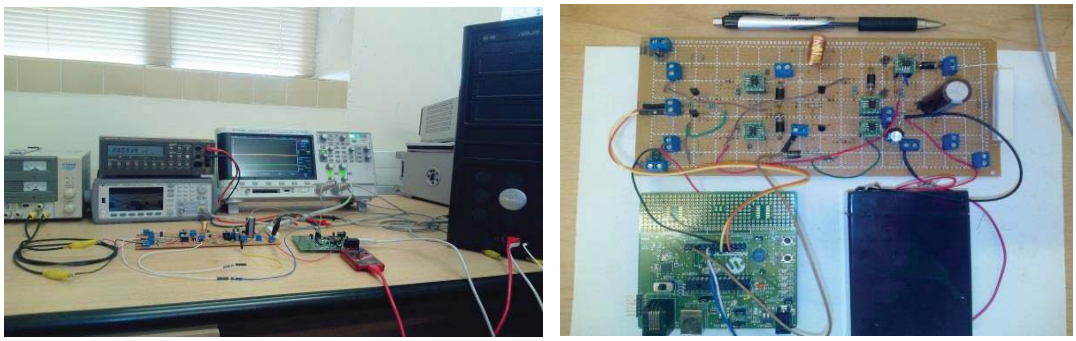

Figure 6-1 Experimental setup for Prototype Converter

Table 6-1 Design Parameters for Experimental Setup

Design Parameter	Value	Unit
Input Voltage V_1	0-9	V
Input Voltage V_2	0-6	V
Battery Voltage V_b	6	V
Max. Input Voltage $V_{in,max}$	15	V
Output Voltage V_{o1}	3.3	V
Output Voltage V_{o2}	6.8	V
Output Current I_{o1}	0.55	A
Output Current I_{o2}	0.85	A
Switching Frequency	100	kHz

Table 6-2 Components Value for Experimental setup

Component	Design Parameters						
	Value	**Unit**	**ESR**	**ESL**	**R_{DC}**	**$R_{DS(ON)}$**	**Type**
Inductor	150	µH	-	-	0.045 Ω		Toroidal
Capacitor C1	1000	µF	0.11Ω	0			Electrolytic
Capacitor C2	1000	µF	0.11 Ω	0			Electrolytic
Switches	30	V	-	-	-	50m Ω	MOSFET P-Type
Diodes	-	-	-	-	-	-	Schotkey
Controller							Michrochip dsPIC 30F2020

In the succeeding sections, converter's behaviour under different conditions and several modes of operation is examined and results are presented.

6.1.1 Dual input-Dual output mode (DIDO)

In Dual input-Dual output mode, input voltages are set at constant values of 5.0V and 4.6V respectively. The output voltage $V_{o1}$is desired to be kept at 3.3V and the output voltage V_{o2} is desired to be kept at 6.8V to charge the battery at 0.85A current. Duty Cycles d_1 and d_2, meant to achieve the maximum power point of solar and wind energy source, are set at predefined fixed value as the renewable energy sources are

replaced by constant power sources whereas duty cycles d_3 and d_5 control the output voltages V_{o2} and V_{o1} respectively. In this mode, source one is not able to independently power up the load and charge the battery therefore is complemented by source two. The equivalent circuit of the converter in DIDO mode is shown in Figure 6-2. The values of Duty cycle d_1 and d_2 is shown in Table 6-3 and Figure 6-3. Similarly values of duty cycles d_3 and d_5 to regulate the output voltages are also shown in Table 6-3 and Figure 6-4.

Table 6-3 Measured values for DIDO mode

Parameter	**Value**	**Unit**
Input Voltage V_1	5	V
Input Voltage V_2	4.6	V
Output Voltage V_{o1}	3.3	V
Output Voltage V_{o2}	6.8	V
Output Current I_{o1}	0.55	A
Output Current I_{o2}	0.85	A
Duty Cycle d_1	75	%
Duty Cycle d_2	65	%
Duty Cycle d_5	35	%
Duty Cycle d_3	76	%

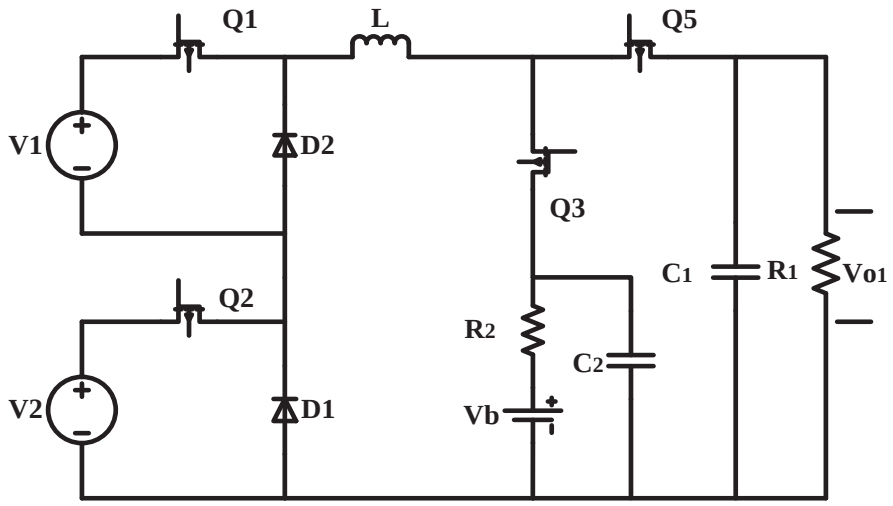

Figure 6-2 Equivalent Circuits for Dual input-Dual output mode

In one switching period, when the switches Q_1, Q_2 and Q_5 are ON, both the sources charge the inductor and energize the load. When the switch Q_5 turns OFF to regulate the output voltage V_{o1}, the switch Q_3 turns ON thus the sources charge the inductor and charge the battery. When the switch Q_2 turns OFF, the inductor and battery are still being charged by source one. The inductor discharges its current through battery when the switch Q_1 is also turned OFF. The inductor current is shown in Figure 6-5. The output voltages kept at desired values are shown in Figure 6-6.

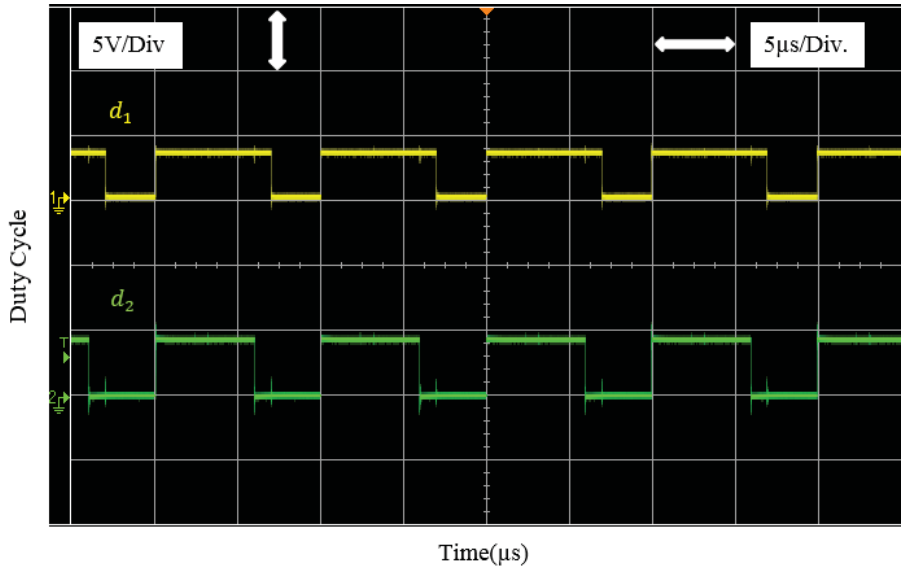

Figure 6-3 Input Duty Cycles d_1 and d_2 in DIDO mode

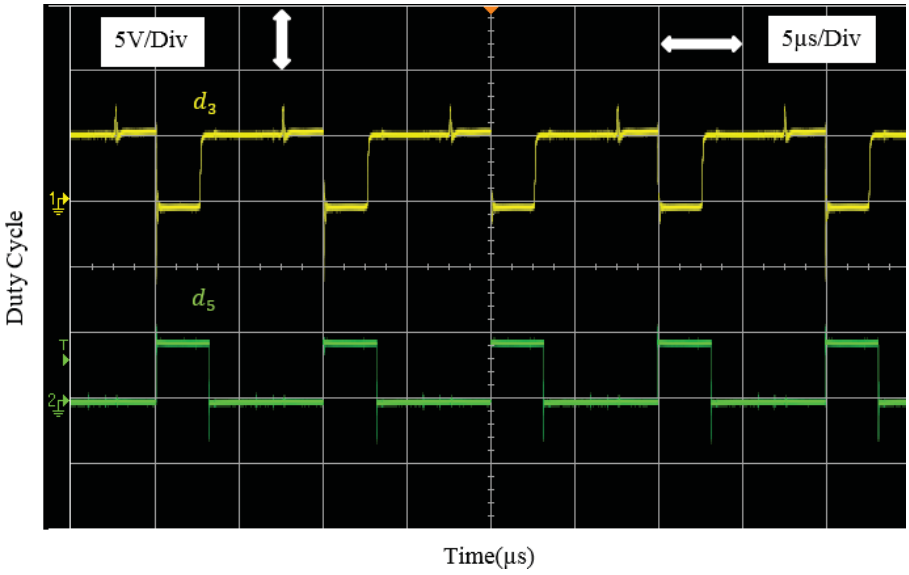

Figure 6-4 Output Duty Cycles d_3 and d_5 in DIDO mode

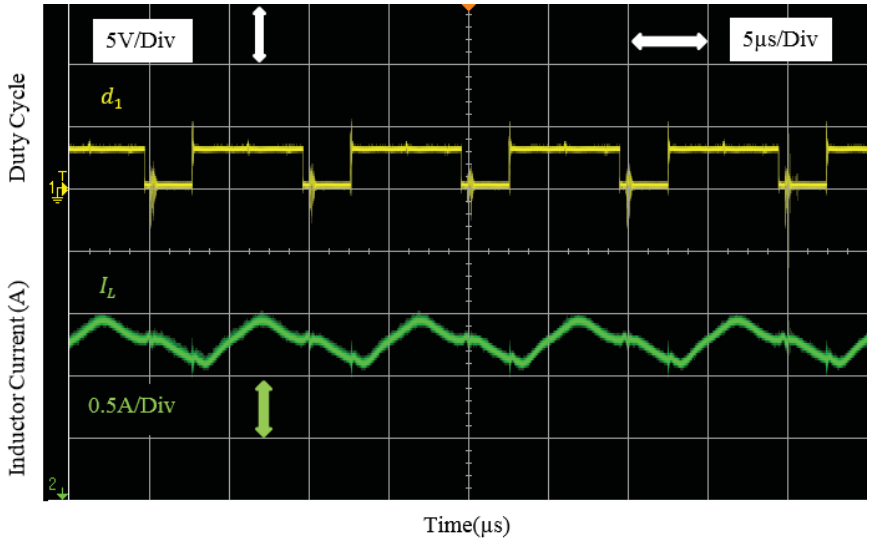

Figure 6-5 Duty Cycle d_1 and Inductor Current I_L in DIDO mode

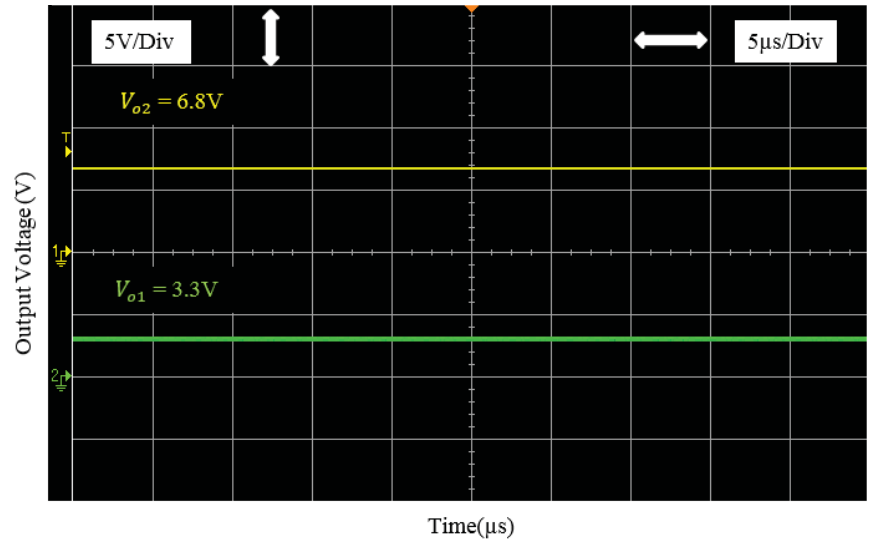

Figure 6-6 Regulated Output Voltages in DIDO mode

6.1.2 Dual input-Single output mode (DISO)

In this mode when the available power from the sources is not enough to support both the outputs i.e. to energize the load and to charge the battery, the battery charging circuit is disconnected and both the sources are utilized to power up the load. The equivalent circuit is shown in Figure 6-7. As the battery charging circuit is disconnected therefore switch Q_3 remains OFF. Whereas the switch Q_5 remains ON. The duty cycle d_1 regulates the output voltage. Table 6-4 summarizes the values of duty cycle, input, and output voltages.

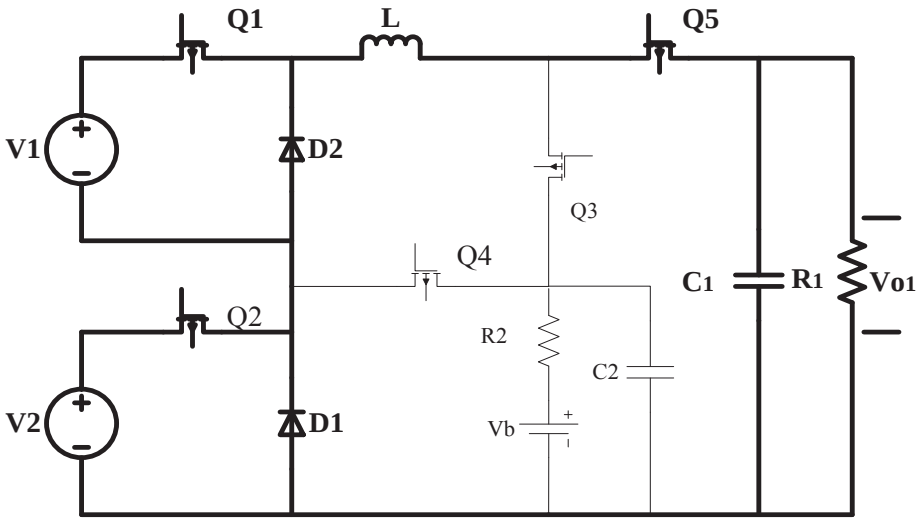

Figure 6-7 Equivalent Circuits for Dual input-Single output mode

Table 6-4 Measured values for DISO mode

Parameter	Value	Unit
Input Voltage V_1	4.0	V
Input Voltage V_2	3.0	V
Output Voltage V_{o1}	3.3	V
Output Current I_{o1}	0.55	A
Duty Cycle d_1	65	%
Duty Cycle d_2	65	%
Duty Cycle d_5	100	%
Duty Cycle d_3	0	%

In one switching period, when the switches Q_1 and Q_2 are ON, the sources charge the inductor and power up the load. When the switches are OFF, the inductor current discharges through load. Duty cycles d_1 and d_2 are shown in Figure 6-8. Similarly, the inductor current is shown in Figure 6-9 and duty cycles d_1 and d_5 are shown in Figure 6-10 whereas the Figures 6-11 represents output voltages. In this mode, if the source two is not available to supplement the source one, the extra required energy to power up the load can be taken from the battery which acts as a second source. The switch Q_4 is turned ON in this case.

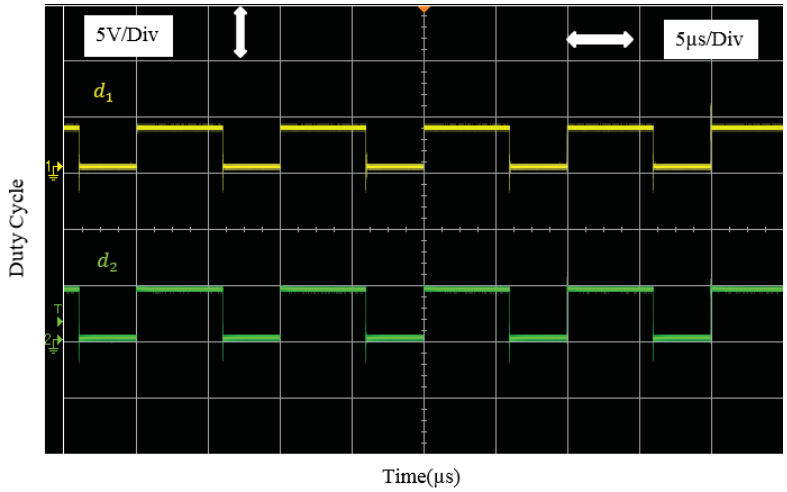

Figure 6-8 Duty Cycles d_1 and d_2 in DISO mode

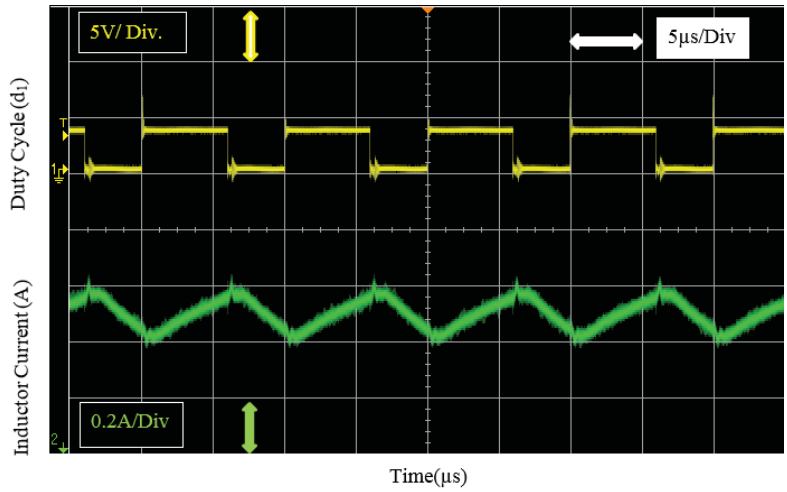

Figure 6-9 Duty Cycle d_1 and Inductor Current I_L in DISO mode

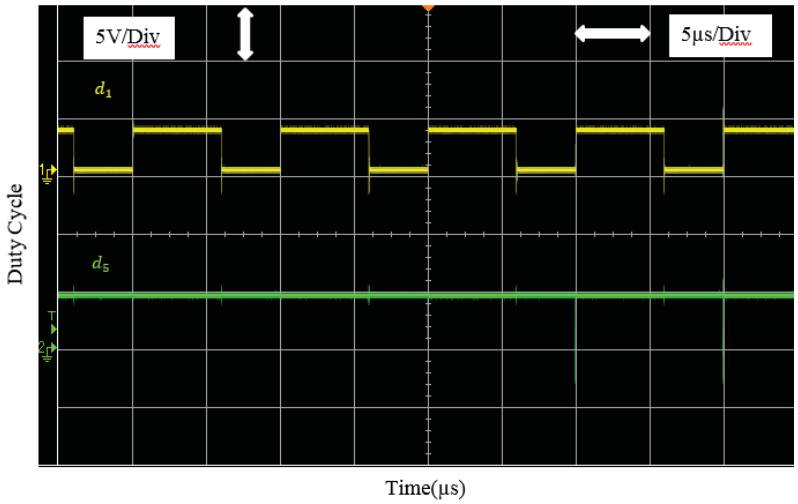

Figure 6-10 Duty Cycles d_1 and d_5 in DISO mode

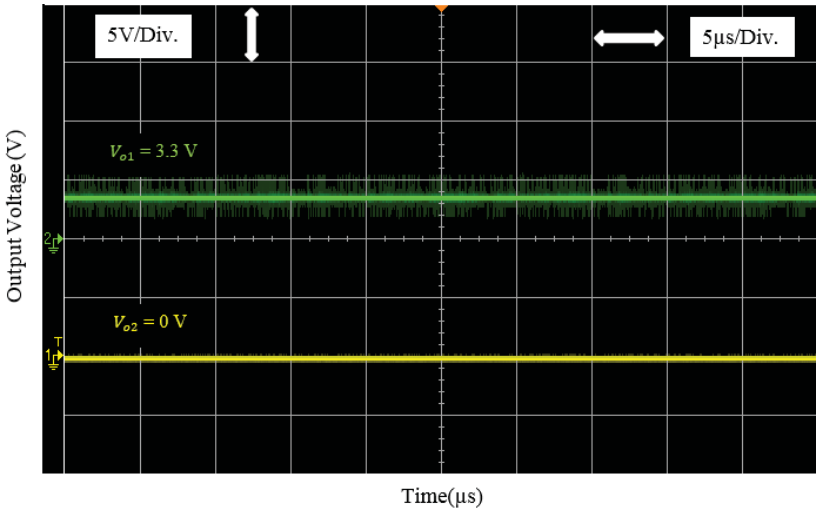

Figure 6-11 Regulated Output Voltage in DISO mode

6.1.3 Single input-Dual output mode (SIDO)

In this mode, only one power source is present. However, the available energy from this source is more than the requirement of the load therefore the excess energy can be used to charge the battery. The parameters values for this mode are shown in Table 6-5 and the equivalent circuit is shown in Figure 6-12. In one switching period, when the switches Q_1 and Q_5 are ON, the inductor is charged and the load is energized however when the switch Q_5 turns OFF, the switch Q_3 is still ON, therefore the energy is used to charge the battery. When the switch Q_1 turns OFF, the inductor current is discharged to the battery through switch Q_3. Duty Cycle d_1 and inductor current I_L are shown in Figure 6-13. Whereas the Figure 6-14 shown the output duty cycles d_3 and d_5. The regulated output voltages are shown in Figure 6-15.

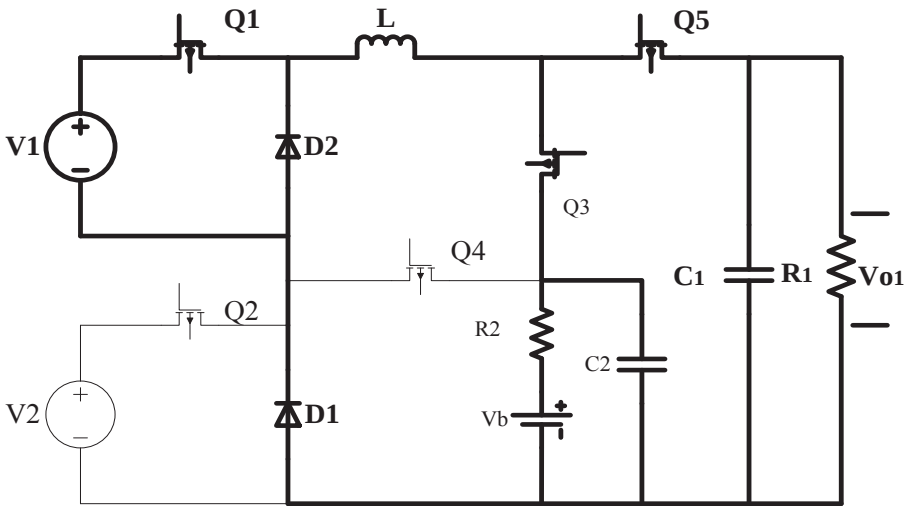

Figure 6-12 Equivalent Circuits for Single input-Dual output mode

Table 6-5 Measured values for SIDO mode

Parameter	Value	Unit
Input Voltage V_1	9.0	V
Output Voltage V_{o1}	3.3	V
Output Voltage V_{o2}	6.8	V
Output Current I_{o1}	0.55	A
Output Current I_{o2}	0.85	A
Duty Cycle d_1	80	%
Duty Cycle d_5	35	%
Duty Cycle d_3	81	%

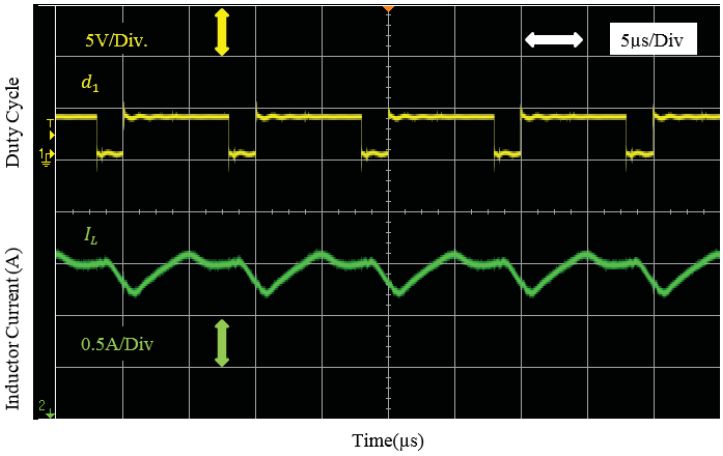

Figure 6-13 Duty Cycle d_1 and Inductor Current I_L in SIDO mode

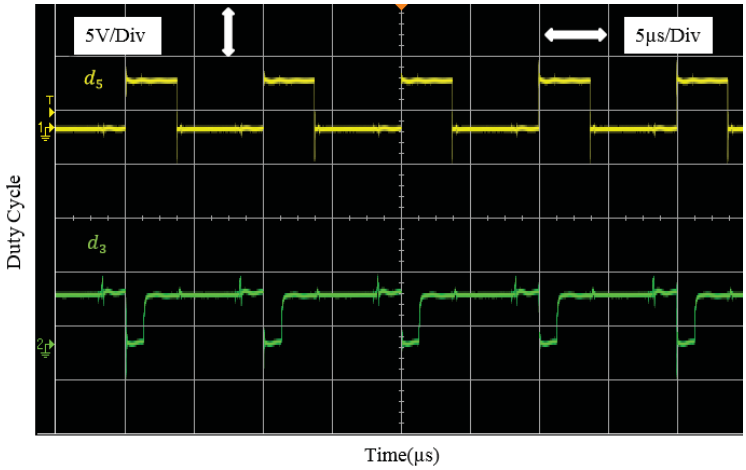

Figure 6-14 Duty Cycles d_1 and d_5 in SIDO mode

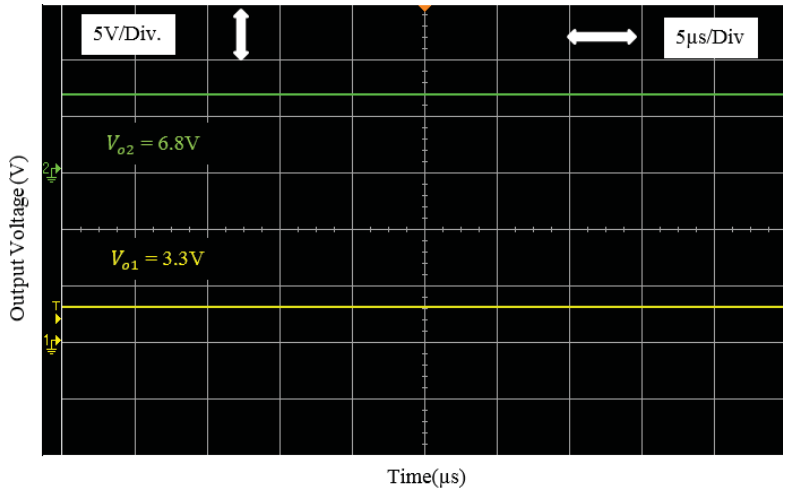

Figure 6-15 Regulated Output Voltages in SIDO mode

6.1.4 Single input-Single output Mode (SISO)

The presented converter can act as an ordinary single input single output buck converter. In this mode, any of the input sources can independently power up the load. If both the sources are not available, battery can act as source and can individually power up the load. In this case the switch Q_4 will remain ON and regulate the output voltage through duty cycle d_4. Whereas the switch Q_5 will remain ON for the entire period. Duty Cycles d_4 and d_5 are shown in Figure 6-15. Inductor current I_L and duty cycle d_4 are presented in Figure 6-16 whereas regulated output voltage is shown in Figure 6-17.

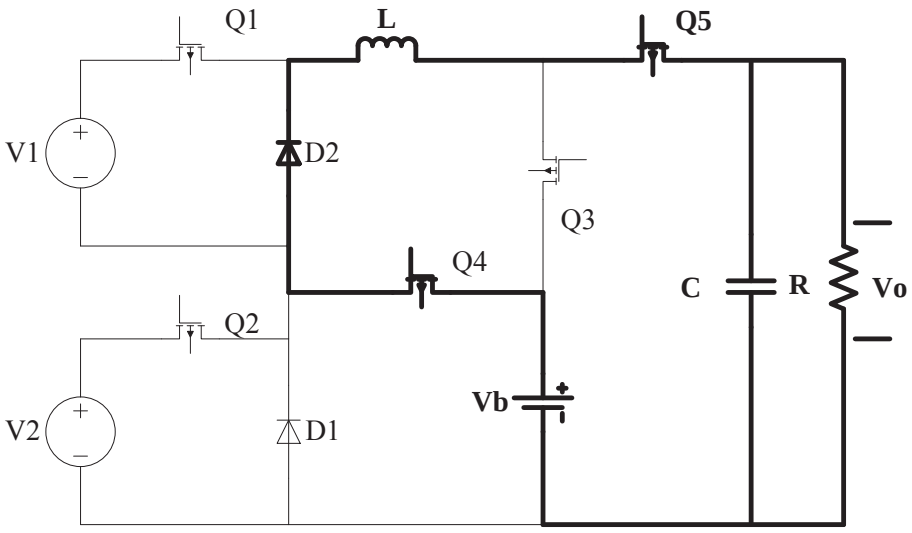

Figure 6-16 Equivalent Circuits for Single input-Single output mode

Table 6-6 Measured values for SISO mode

Parameter	Value	Unit
Input Voltage V_b	6.0	V
Output Voltage V_{o1}	3.3	V
Output Current I_{o1}	0.55	A
Duty Cycle d_4	65	%
Duty Cycle d_5	100	%

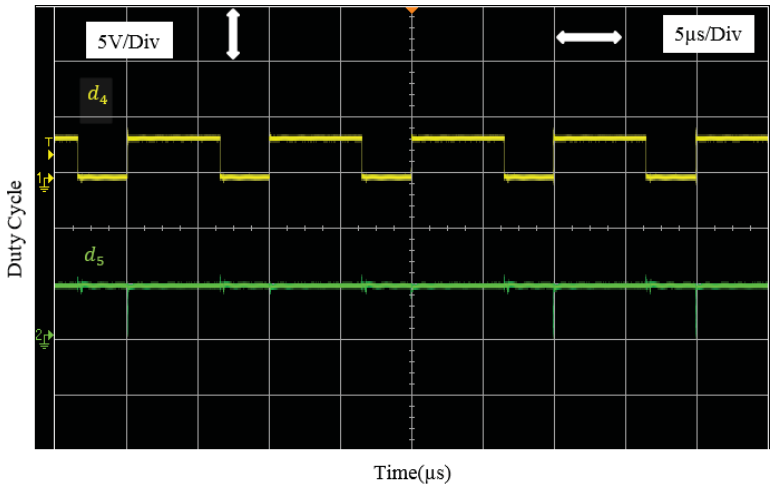

Figure 6-17 Duty Cycles d_4 and d_5 in SISO mode

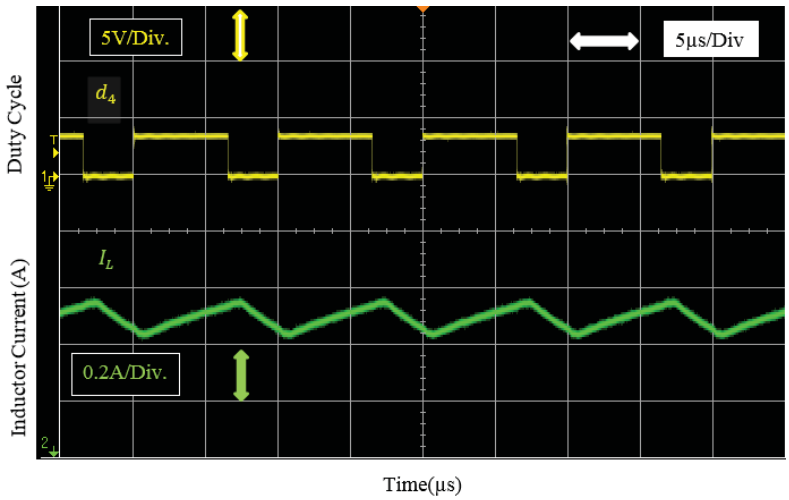

Figure 6-18 Duty Cycle d_4 and Inductor Current I_L in SISO mode

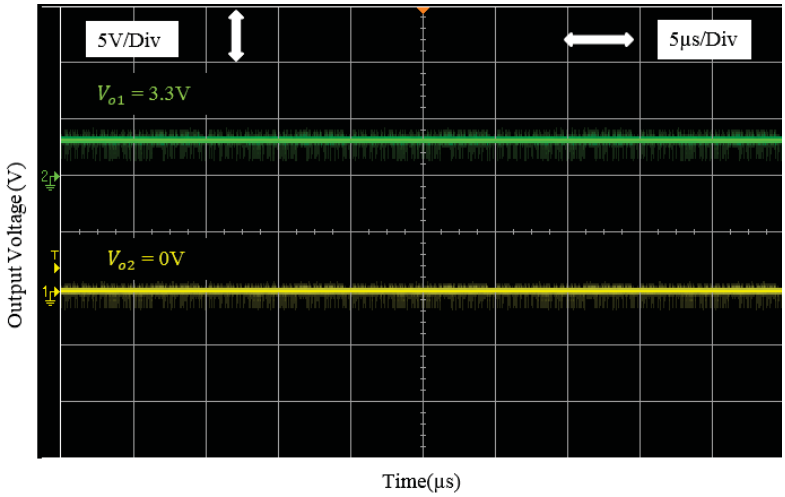

Figure 6-19 Regulated Output Voltage in SISO mode

6.2 Conclusion

To validate the analytical and simulation results obtained in chapter 3 and chapter 5 respectively, a low voltage/power prototype model of multiport converter is built. The parameters used for experimental studies are defined and the minimum values of elements like inductor and capacitor are calculated. The presented converter topology is tested under different operating conditions and behavior of the converter is observed and analyzed. Experimental results for several modes of operation are presented. The obtained results prove that the developed converter can accommodate two input sources and the sources can power up two different loads individually and simultaneously. Although the connected loads have different voltage and current requirements even then the converter has successfully provided regulated voltage to both the loads. In case of absence of both the input sources, the uninterrupted power supply to the load is ensured and battery energizes the load. In this chapter the experimental results are presented for constant source voltage and load current. The experimental results for variable source voltage and load current are presented in chapter 7.

.

Chapter 7

7 Results Analysis and Discussion

The presented multiport topology has been examined from different aspects. Chapter 3 presents mathematical modelling and analysis. Chapter 5 presents simulation results and experimental results are presented in Chapter 6. The results obtained in the mentioned chapters demonstrate that the converter can respond to the perturbations in input voltage and load current and is able to provide regulated output voltage to energize the load and to charge the battery. In this chapter, the presented multiport topology will be further examined in terms of its efficiency, reliability and stability under different modes of operation.

7.1 Efficiency Analysis

In order to calculate the overall efficiency of the converter, the power loss in all the components is calculated first and then the efficiency of the converter is calculated by the following equation.

$$\text{Efficiency} = \eta = \frac{V_{out} * I_{out}}{(V_{out} * I_{out}) + P_{Ci} + P_{co} + P_{DCR} + P_{Dsw} + P_{DsON} + P_{Diode}} * 100 \quad (7\text{-}1)$$

Here V_{out} & I_{out} are DC Values

$V_{out} * I_{out}$ = Output power = $(V_{out1} * I_{out1} + V_{out2} * I_{out2})$

P_{Ci} = Power Dissipated in input capacitor

P_{co} = Power Dissipated in output capacitor

P_{DCR} = Power Dissipated due to DC resistance of the inductor

P_{Diode} = Power Dissipated diode

P_{DsON} = Power dissipation due to ON- resistance of switch

P_{Dsw} = MOSFET switching losses

The parameters used for efficiency calculation are shown in Table 7-1

Table 7-1 Parameters used for efficiency calculation

Parameter	Value	Unit
Input Voltage for DIDO & SIDO	10	V
Input Voltage for DISO & SISO	6	V
Output Voltage V_{o1}	3.3	V
Output Voltage V_{o2}	6.8	V
Output Current I_{o1}	0.55	A
Output Current I_{o2}	0.85	A
Current Ripple ΔI_L	0.42	A
Capacitor ESR	0.11	Ω
Reverse transfer Capacitance	70	pF
Voltage drop across schottky diode	0.47	V
R_DsON for P-type MOSFET	50	mΩ
R_DsON for N-type MOSFET	25	mΩ
Switching Frequency	100	kHz

7.1.1 Power Dissipation in Diode

Diode contributes majority of power loss in the switching converters. The average power dissipated by at full load current is calculated as,

$$P_{Diode} = \left\{1 - \frac{V_{out}}{V_{in,max}}\right\} * I_{out,max} * V_D \quad (7\text{-}2)$$

Here V_{out} = 6.8V

$V_{in,max}$ = 10V

$I_{out,max}$ = 1.4A

V_D = 0.47 V (Voltage drop across schottky diode)

By putting values is equation (7-2) we get power dissipation in diode

$$P_{Diode} = 0.211\text{W}$$

7.1.2 Power Dissipation in MOSFET

There are two type of losses in the MOSFETS. One is switching loss and other is conduction loss. The conduction loss in MOSFET is due to its ON-resistance and is calculated as

$$P_{DsON} = \left\{\frac{V_{out}}{V_{in,max}}\right\} * I^2_{out,max} * R_DsON \quad (7\text{-}3)$$

Here R_DsON for P-type MOSFET = 50mΩ

Here R_DsON for N-type MOSFET = 25mΩ

By putting values in equation 7-3 we get

$P_{DsON(P)}$ = 0.0666W

$P_{DsON(N)}$ = 0.0333W

Although switching losses constitute only a smaller portion of MOSFET'S power dissipation, yet these are considered. Switching losses can be calculated as

$$P_{Dsw} = V_{inmax} * \frac{I_{outmax}}{2} * (T_{rise} + T_{fall}) * F_{sw} + C_{RSS} * V^2_{in\,max} * F_{sw} \quad (7\text{-}4)$$

Here C_{RSS} = Reverse transfer Capacitance = 70pF

Assume max $(T_{rise} + T_{fall})$ = 100nsec

F_{sw} = 100kHz

By putting values, we get

P_{Dsw} = 0.0715

Total power dissipation in MOSFET (P-Type) = 0.1381W

Total power dissipation in MOSFET (N-Type) = 0.1048W

7.1.3 Power Dissipation in Inductor

Power dissipation in Inductor due to its DC-Resistance can be calculated as

$$P_{DCR} = \left(I_{outmax} + \Delta I_L * \sqrt{2}\right)^2 * DCR \quad 7\text{-}5$$

Here DCR = 0.045Ω

ΔI_L = 0.42A

Putting Values in 7-5 we get,

$$P_{DCR} = 0.178$$

7.1.4 Power Loss in Capacitor

$$P_{co} = (\Delta I_L)^2 * ESR_{Co}$$

By Putting Values, we get $P_{co} = 0.0194W$

For input capacitor Assume $\Delta I = I_{out,max}/2 = 1.4/2 = 0.7$

$$P_{cin} = (\Delta I_L)^2 * ESR_{Cin}$$

By Putting Values, we get $P_{cin} = 0.05W$

7.1.5 Efficiency of Converter in DIDO mode

In dual input, dual output mode, four switches are in the state of conduction. Two diodes conduct when the switches are OFF and two capacitors are used to smooth the output voltage. The power loss in this mode is shown in Table 7-2. The efficiency of the converter in this mode can be calculates as

Output Power

$P_{out1} = V_{o1} * I_{o1} = 3.3 * 0.55 = 1.815W$

$P_{out1} = V_{o2} * I_{o2} = 6.8 * 0.85 = 5.78W$

$P_{outT} = 7.595W$

Table 7-2 Power loss in DIDO mode

Losses(Watts)	
P_{Ci} = Power Dissipated in input capacitor	0.053
P_{co} = Power Dissipated in output capacitor	0.038
P_{DCR} = Power Dissipated due to DC resistance of the inductor	0.178
P_{Diode} = Power Dissipated diodes	0.421
P_{DsON} = Power dissipation in MOSFETs	0.3227
Total Losses	**1.0144W**

$$\text{Efficiency} = \eta = \frac{V_{out} * I_{out}}{(V_{out} * I_{out}) + Losses} * 100\% = \frac{7.595}{8.609} * 100 = 88.2\%$$

If Diodes are replaced by MOSFETS as shown in Figure 7-1 then the losses are reduced and efficiency is increased as shown below

$$\eta = \frac{7.595}{8.403} * 100 = 90.38\%$$

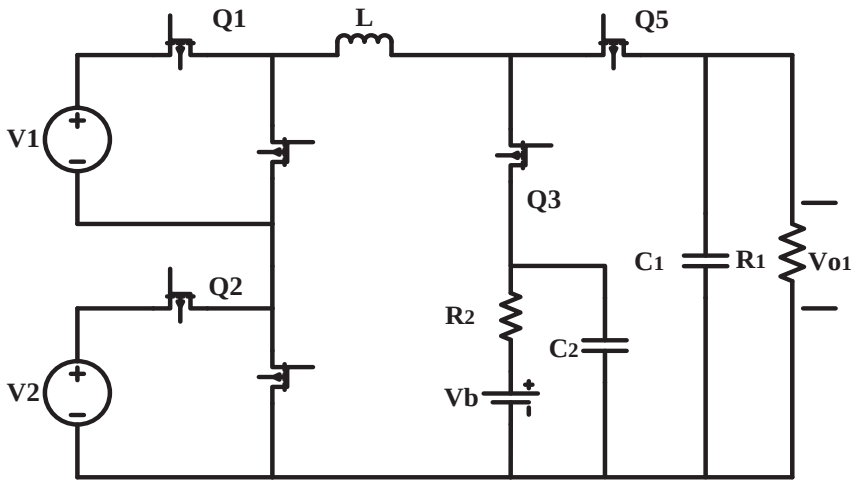

Figure 7-1 Equivalent circuit of DIDO converter in synchronous mode

Figure 7-2 presents the pie chart of all the losses in the components of the converter in Dual Input-Dual output mode under full load conditions. It is evident from the chart that majority of the power (43%) is lost in two freewheeling diodes. The second biggest contributor to the power loss is MOSFETs. As there are four active switches in this mode therefore there is a noticeable power loss. However, the overall efficiency of the converter under full load condition is excellent, considering the converter accommodates multiple input sources and energizes multiple loads. Furthermore, the overall efficiency of the converter can be improved by replacing the freewheeling diodes with the switches.

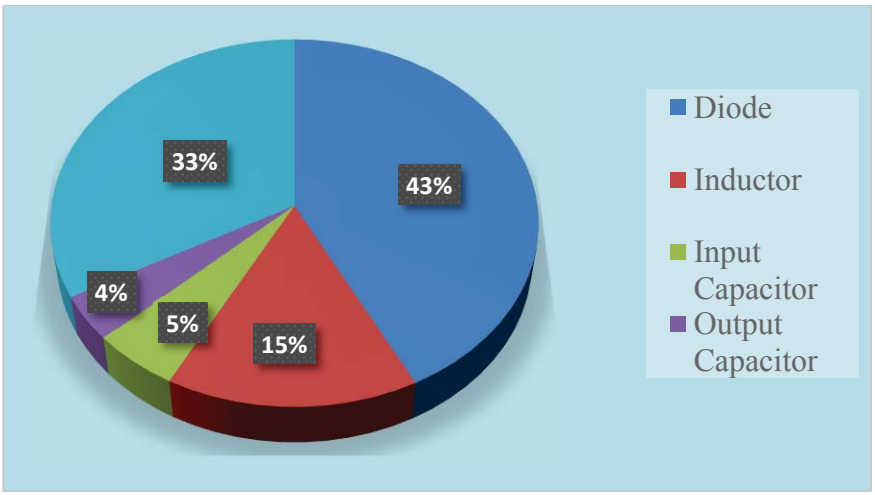

Figure 7-2 Power loss Pie Chart in DIDO mode under full load

7.1.6 Efficiency of Converter in SIDO mode

In single input, dual output mode, three switches are in operation. Two diodes conduct when the switches are OFF and two capacitors are used to smooth the output voltage.

Losses in this mode are shown in Table 7-3. The efficiency of the converter in this mode can be calculated as

Output Power

$P_{out1} = V_{o1} * I_{o1} = 3.3 * 0.55 = 1.815W$

$P_{out1} = V_{o2} * I_{o2} = 6.8 * 0.85 = 5.78W$

$P_{outT} = 7.595W$

Table 7-3 Power loss in SIDO mode

Losses(Watts)	
P_{Ci} = Power Dissipated in input capacitor	0.054
P_{co} = Power Dissipated in output capacitor	0.058
P_{DCR} = Power Dissipated due to DC resistance of the inductor	0.178
P_{Diode} = Power Dissipated diodes	0.3216
P_{DsON} = Power dissipation in MOSFETs	0.231
Total Losses	0.8428

$$\text{Efficiency} = \eta = \frac{V_{out} * I_{out}}{(V_{out} * I_{out}) + Losses} * 100\% = \frac{7.595}{8.438} * 100 = 90\%$$

If Diodes are replaced by MOSFETS then the efficiency becomes

$$\eta = \frac{7.595}{8.22} * 100 = 92.39\%$$

7.1.7 Efficiency of Converter in DISO mode

In Dual input, Single output mode, three switches are in operation. Two diodes conduct when the switches are OFF and one output capacitor is used to smooth the output voltage. Losses in this mode are shown in Table 7-4. The efficiency of the converter in this mode can be calculated as

Output Power $P_{outT} = V_{o1} * I_{o1} = 3.3 * 0.55 = 1.815W$

Table 7-4 Power loss in DISO mode

Losses(Watts)	
P_{Ci} = Power Dissipated in input capacitor	0.0083
P_{co} = Power Dissipated in output capacitor	0.00299
P_{DCR} = Power Dissipated due to DC resistance of the inductor	0.027
P_{Diode} = Power Dissipated diode	0.232
P_{DsON} = Power dissipation in MOSFET	0.069
Total Losses	0.339

$$\text{Efficiency} = \eta = \frac{V_{out} * I_{out}}{(V_{out} * I_{out}) + Losses} * 100\% = \frac{1.815}{2.154} * 100 = 84.22\%$$

If Diodes are replaced by MOSFETS then the efficiency is $\eta = \frac{1.815}{1.964} * 100 = 92.4\%$

7.1.8 Efficiency of Converter in SISO mode

In single input, single output mode, two switches are in operation. Two diodes conduct when the switches are OFF and one output capacitors is used to smooth the output voltage. Losses in this mode are shown in Table 7-5. The efficiency of the converter in this mode can be calculated as

Output Power $P_{outT} = V_{o1} * I_{o1} = 3.3 * 0.55 = 1.815W$

Table 7-5 Power loss in SISO mode

Losses(Watts)	
P_{Ci} = Power Dissipated in input capacitor	0.0083
P_{co} = Power Dissipated in output capacitor	0.00299
P_{DCR} = Power Dissipated due to DC resistance of the inductor	0.027
P_{Diode} = Power Dissipated diode	0.232
P_{DsON} = Power dissipation in MOSFET	0.0455
Total Losses	0.3157

$$\text{Efficiency} = \eta = \frac{V_{out} * I_{out}}{(V_{out} * I_{out}) + Losses} * 100\% = \frac{1.815}{2.13} * 100 = 85.17\%$$

If Diodes are replaced by MOSFETS then the efficiency is $\eta = \frac{1.815}{1.8916} * 100 = 93.5\%$

Figure 7-3 presents the summery of converter's efficiency in all the modes of operation. Red line in the chart represents the converter used in asynchronous mode and diodes are used as freewheeling device whereas the purple line represents when switches replace diodes and converter operates in synchronous mode. It is evident that the efficiency of the converter increases considerably when the converter is used in synchronous mode. The efficiency of the converter in Single Input-Single output (SISO) mode appears to be a bit lower than anticipated value in SISO buck converters. The reason being an additional diode in the freewheeling path and the two diodes are responsible for most of the power dissipation under light load conditions as shown in pie chart represented by Figure 7-4. This drawback can be removed by replacing the diodes with power MOSFETS with a low ON-resistance. When these two freewheeling diodes are replaced by the power MOSFETS, an immense improvement in the efficiency is observed and 94% efficiency is achieved. Similar situation can be observed in Dual Input-Single output mode.

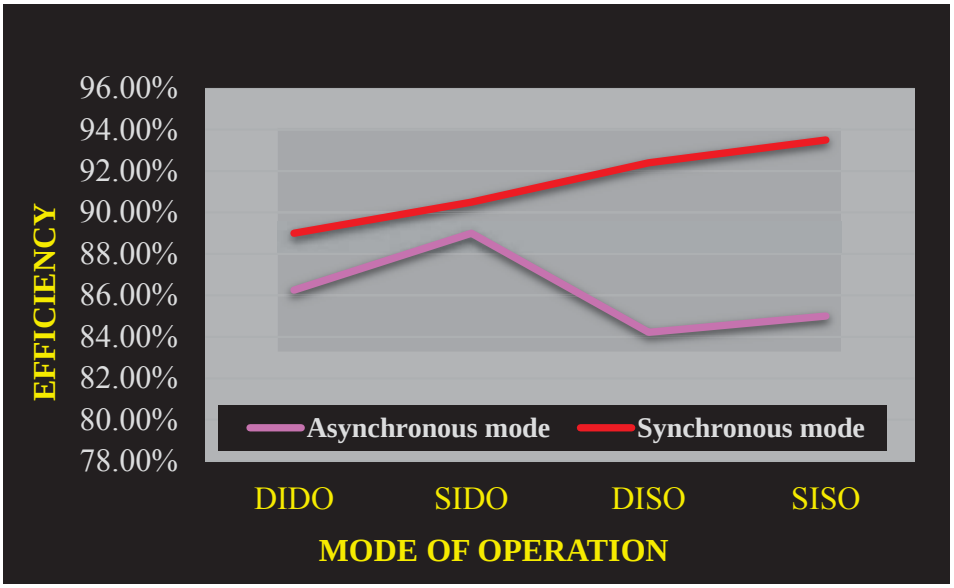

Figure 7-3 Efficiency of the converter in different modes of operation.

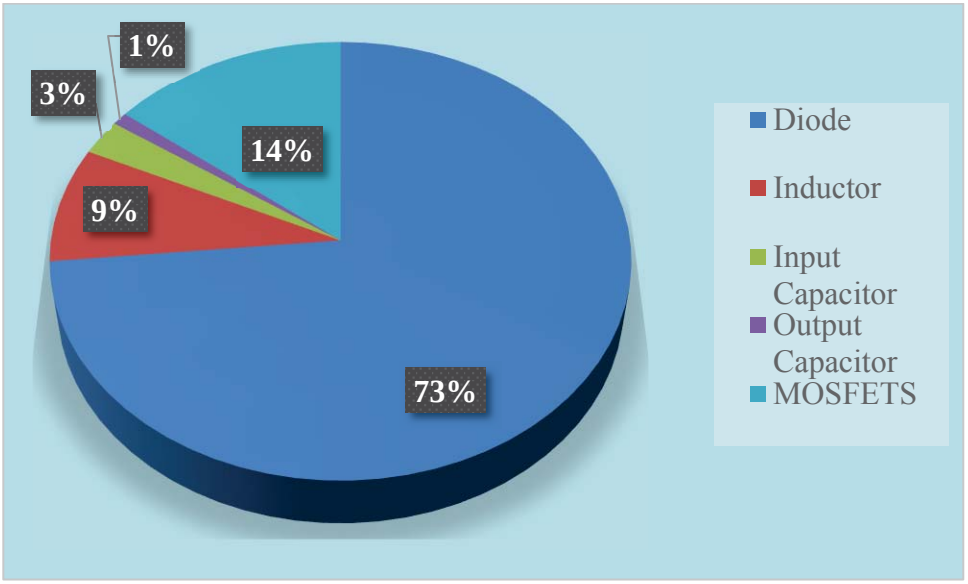

Figure 7-4 Power loss Pie Chart in SISO mode

Figure 7-5 represents the efficiency of the converter in Dual Input-Dual Output mode with different loading conditions. It is evident that as the load current decreases, the efficiency of the converter increases and an efficiency of over 92% is achieved when the total load current is 1.0A. A further improvement in the efficiency is observed when converter is operated in synchronous mode the freewheeling diodes are replaced by the power MOSFETS where the overall efficiency reaches over 95%.

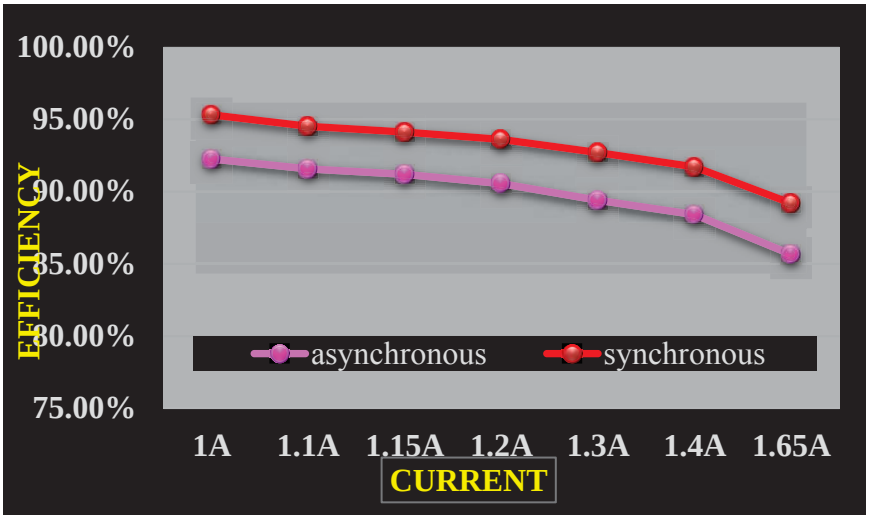

Figure 7-5 Efficiency of the converter in DIDO mode with different load current

A comparison of efficiency obtained by calculation, simulation and experimental measurement is shown in Figure 7-6. The comparison reveals that the efficiency of the converter obtained during simulation studies is close to the estimated or mathematically calculated frequency. However, the efficiency measured from experimental setup is a bit lower than anticipated value. The reason of this minor difference could be the difference in ideal and practical values of the components, accuracy of the test equipment, probable loose connections due to test and measurement points and last but not the least the human error. However, the difference is not substantial but falls within acceptable values. The total output current $I_{o,max}$ for this comparison is taken as 1.15A with I_{o1}, 0.85A and I_{o2}, 0.3 A. The inductor current ripple is taken as ΔI_L is 0.345A.

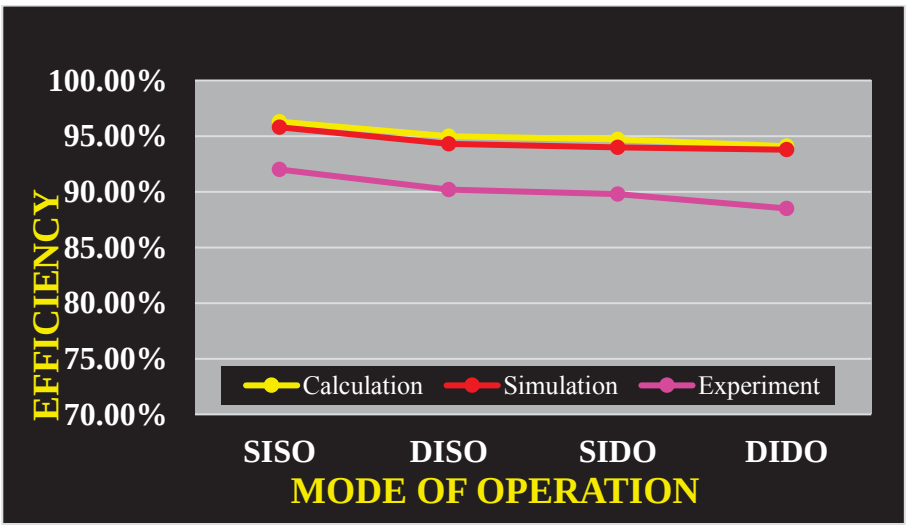

Figure 7-6 Comparison of calculated, simulated and measured efficiency

7.2 Stability Analysis

The MIMO system is considered to be a stable system if all of its poles are strictly inside the stability region i.e. inside the unit disc for discrete-time systems [161] whereas the relative stability can be defined as the measure of how far the system is from instability. The relative stability of a system relates to its gain and phase margins. The gain margin defined as "the increment of loop gain required to drive the feedback system into instability" [157]. The primary condition for a stable loop is that the total loop gain must be unity when the total open loop phase shift must be below 360° at a given crossover frequency and the amount by which the total phase shift is less than 360° is known as phase margin. For a stable system, both the phase and gain margin must be positive [162]. The switching converters can become unstable and may show an undesirable response in a close loop system. This problem can be overcome by adding a compensator network to increase the phase margin and shape the loop transfer function to get a desired transient response.

An appropriate method to determine the stability of the presented converter is a Bode Plot analysis. A Bode plot is the plot of phase and gain magnitude versus the frequency which provides accurate results when the open loop system is stable and the magnitude response has no more than one zero-crossing (crossover) frequency. As a recommended design practice, the phase margin must be at least 60° and gain margin should be greater than 6dB to ensure the stability of close loop switching converter [162].

Control system and design of compensation network has been presented in Chapter 4. In the following section, the Bode plot of the converter with the designed compensation network have been presented to validate the stability of the converter in several modes of operation. The dynamic performance of the converter has been obtained by tuning the coefficients k_i and k_p of a PI controller and obtaining Bode plots. A MATLAB/Simulink model is developed, as shown in Figure 7-7 and Figure 7-8, to represent a switching model of the multiport converter based on its state-space description. The state-space equations are shown in Figure 7-9. The parameters used for this simulation study are shown in Table 7-7. The developed Simulink is used to perform the following functions

- Develop close loop model and plot loop gain frequency response and run time domain simulations based on average converter model.
- Construct large signal model and perform Time-domain simulations of the obtained average converter model.
- To perform small-signal linearization of average converter model to obtain and plot converter's frequency response.
- Design compensator and tune the coefficient to obtain stable response

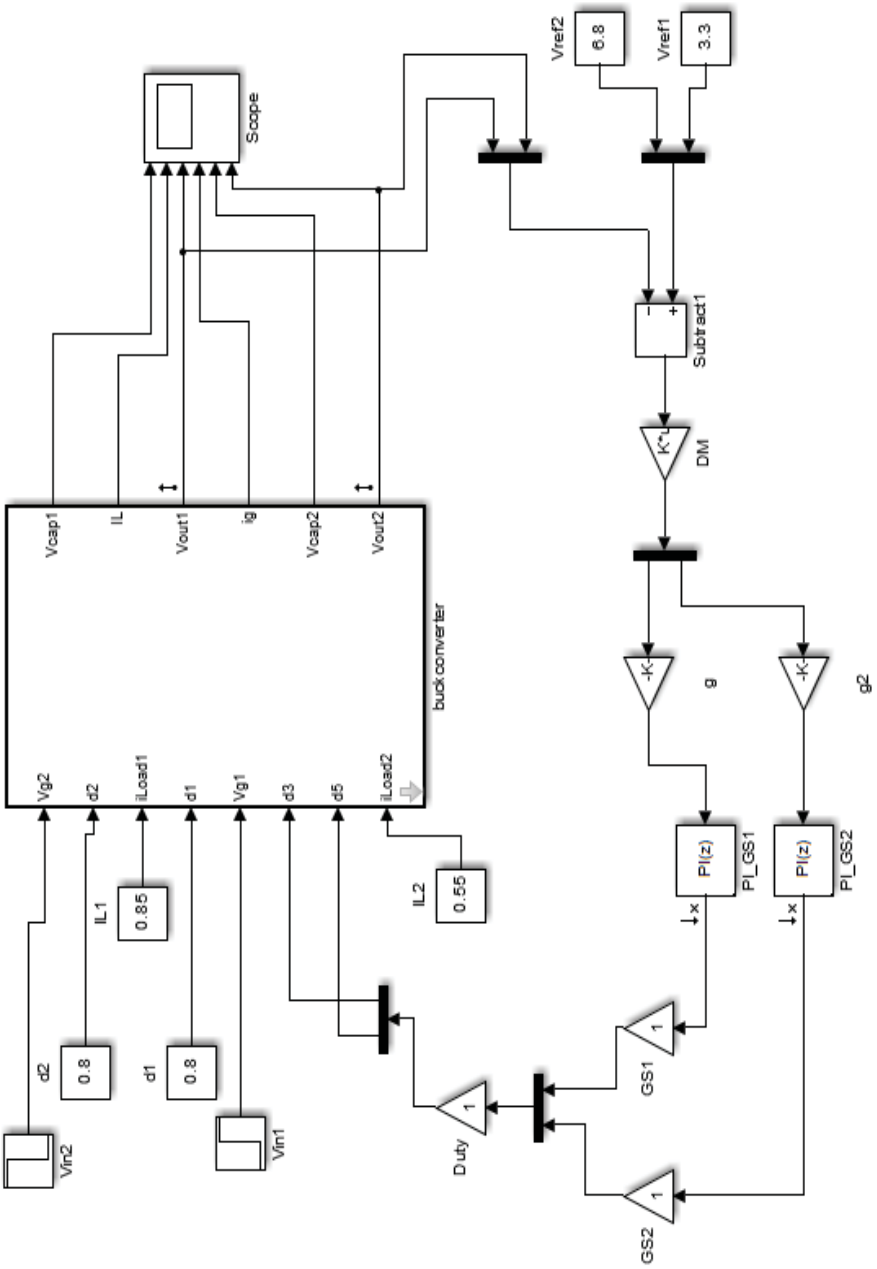

Figure 7-7 Simulink model of Multiport Converter for time and frequency domain analysis

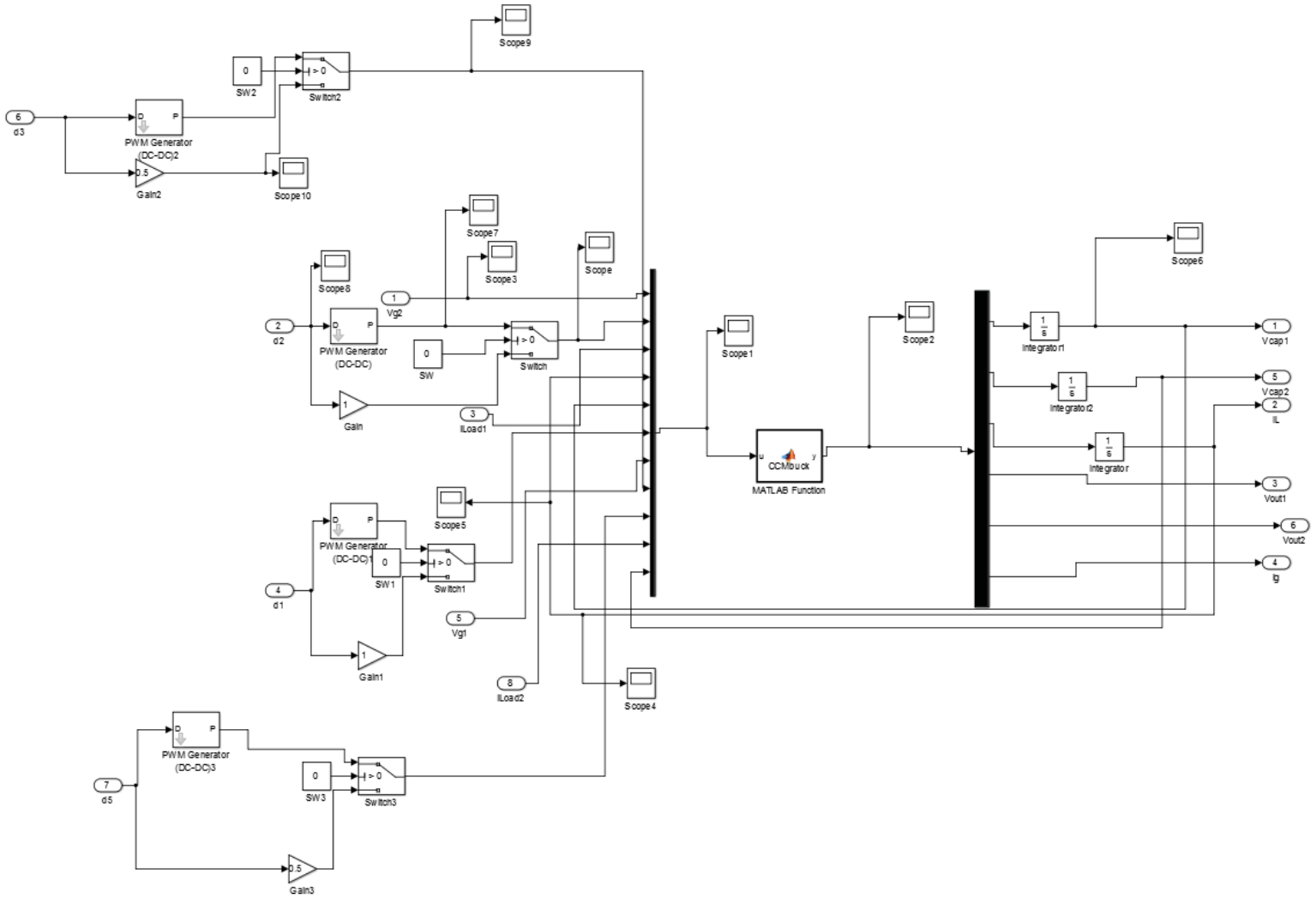

Figure 7-8 Simulink model of Multiport Converter for time and frequency domain analysis (Sub System)

Table 7-6 Multiport Converter Parameters block

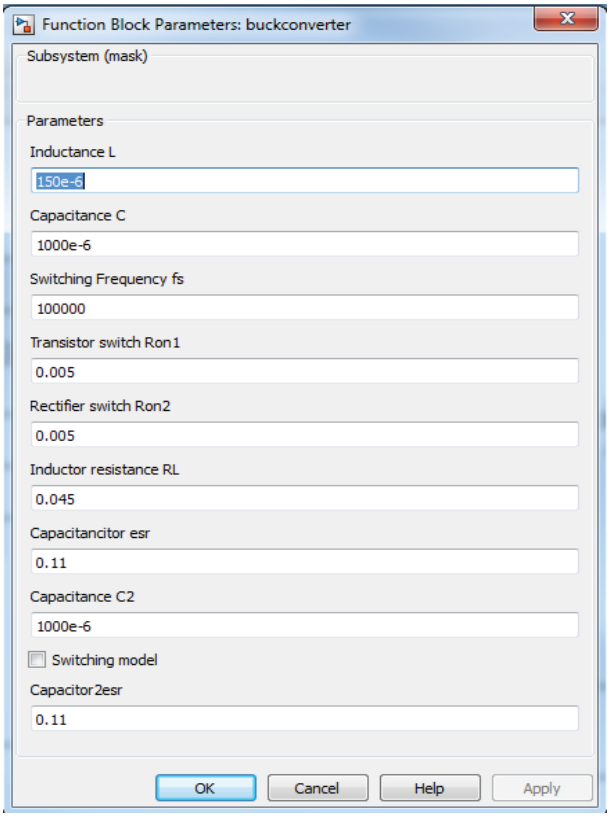

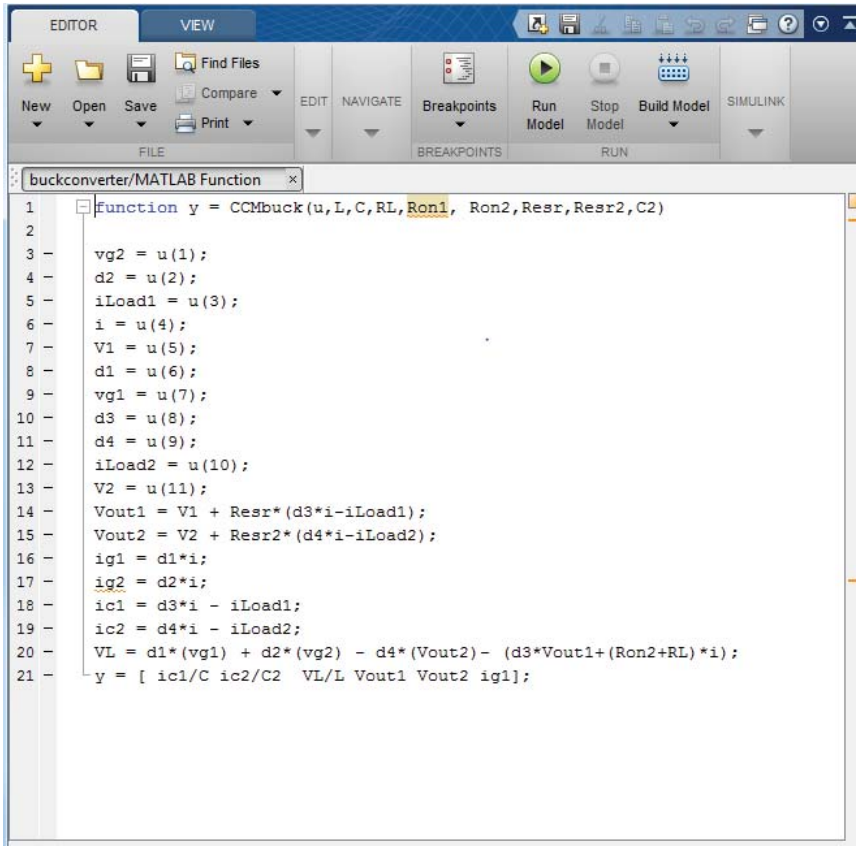

Figure 7-9 Multiport Converter State Equations Block

Open loop bode plots are shown in Figure 7-10 to 7-18. Analysis of the bode plots reveals that by the introduction of a pre-compensator (decoupling matrix) and tuning the PI coefficients, the system shows stable response with the desired phase margin between 60° to 80° and the gain margin greater than 6db at a reasonable cut off frequency under different modes of operations.

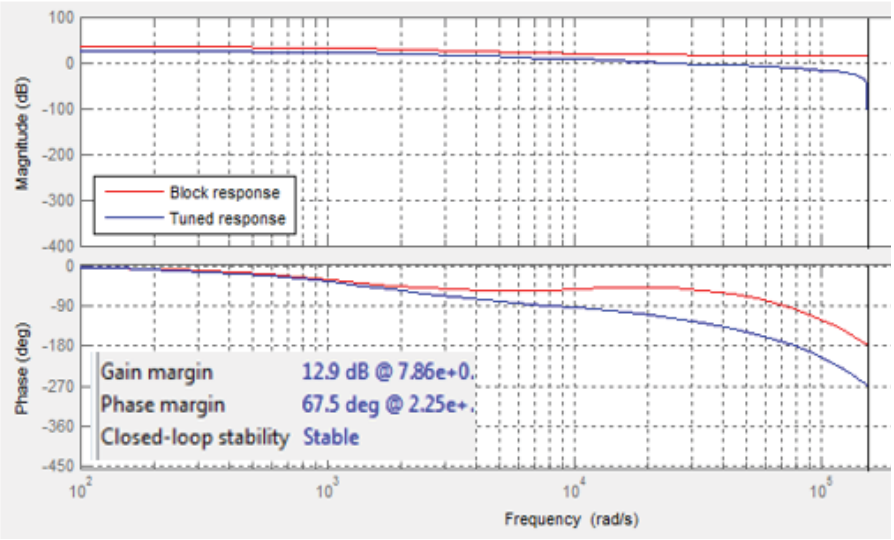

Figure 7-10 Bode Plot for Single Input-Dual output mode v_{o1}/d_5

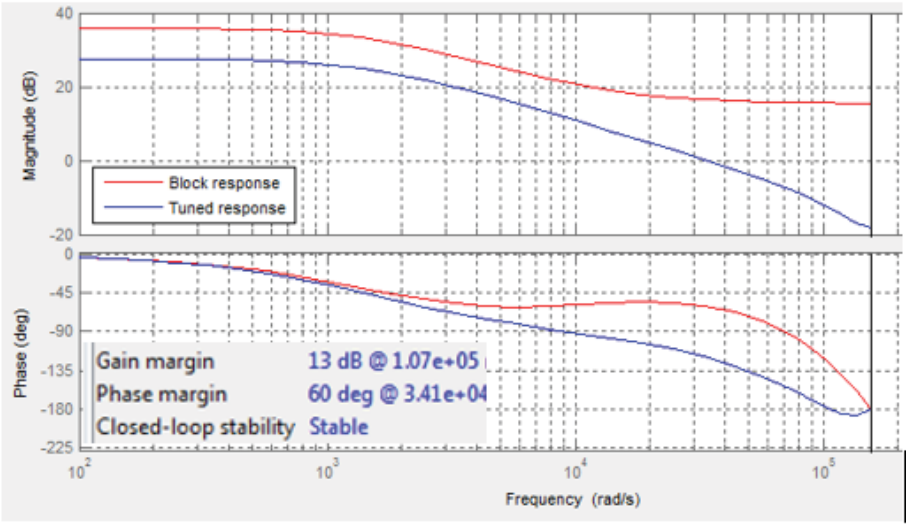

Figure 7-11 Bode Plot for Single Input-Dual output mode v_{o2}/d_5

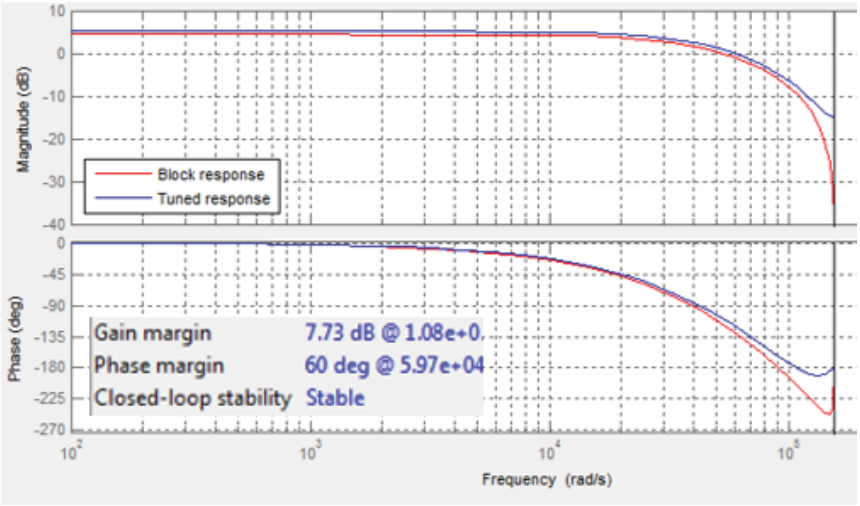

Figure 7-12 Bode Plot for Single Input-Dual output mode v_{o2}/d_3

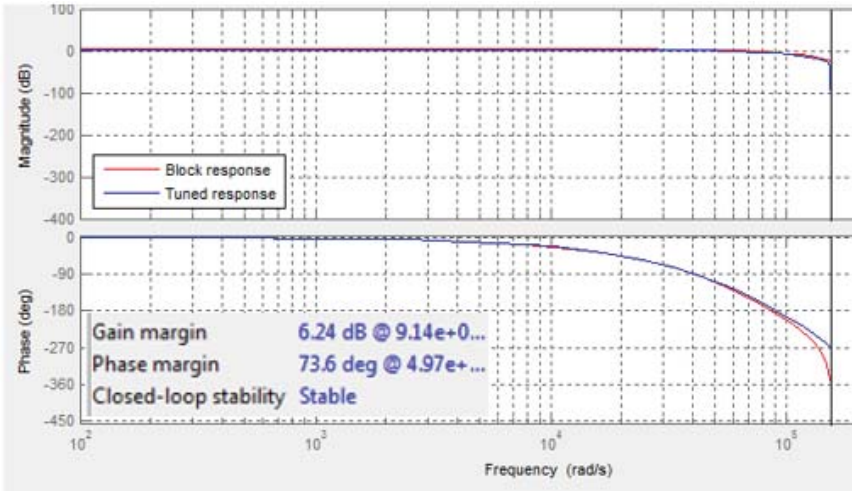

Figure 7-13 Bode Plot for Single Input-Dual output mode v_{o1}/d_3

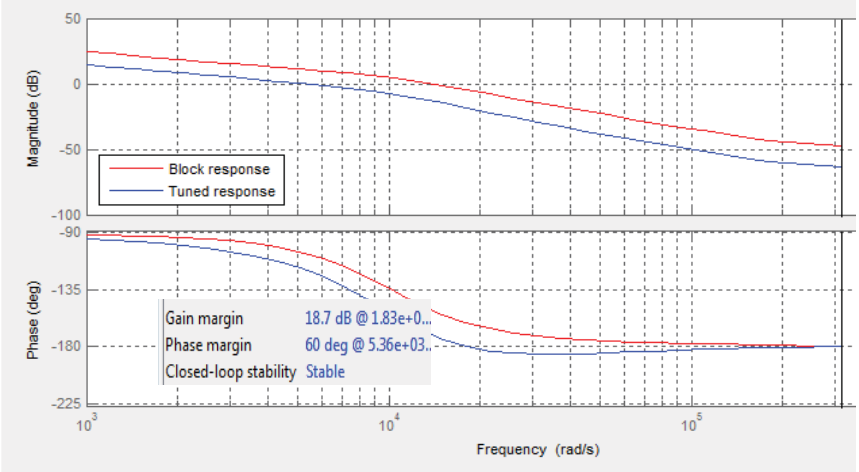

Figure 7-14 Bode Plot for Dual Input-Single output mode v_{o1}/d_5

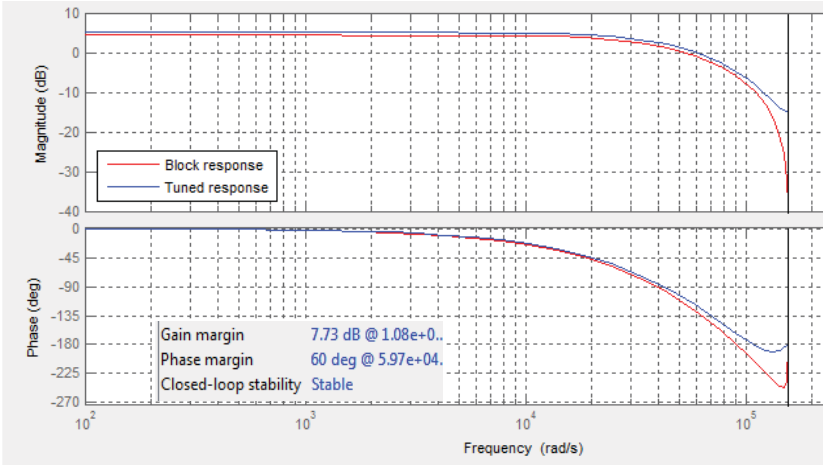

Figure 7-15 Bode Plot for Dual Input-Dual output mode V_{o1}/d_5

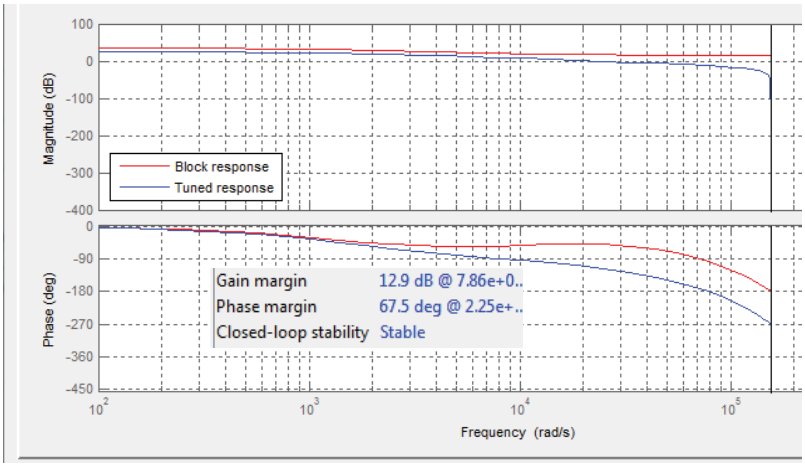

Figure 7-16 Bode Plot for Dual Input-Dual output mode V_{o2}/d_5

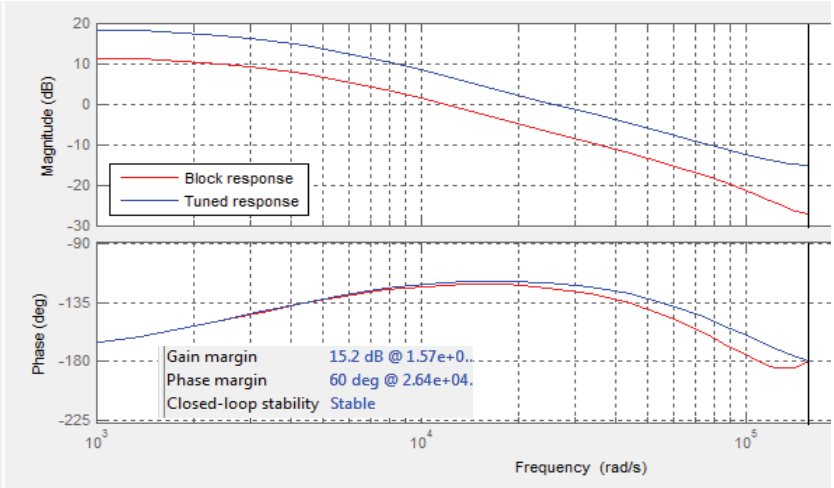

Figure 7-17 Bode Plot for Dual Input-Dual output mode V_{o1}/d_3

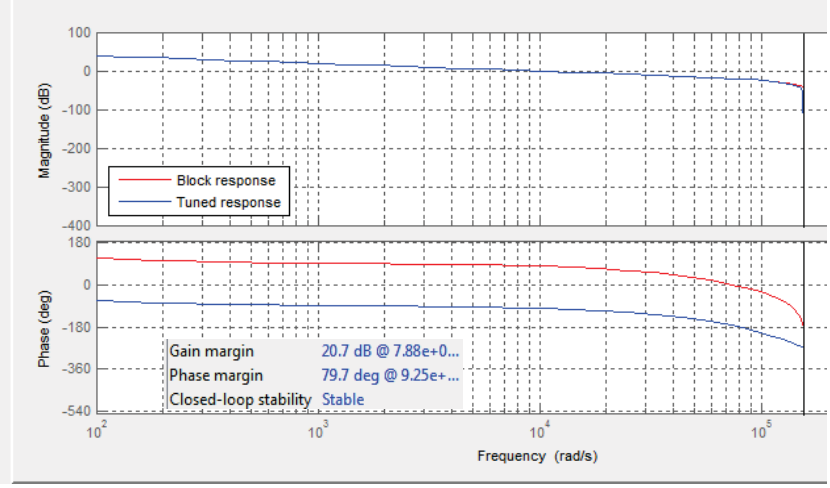

Figure 7-18 Bode Plot for Dual input- Dual output mode V_{O2}/d_3

7.3 Voltage Regulation

Experimental results for the converter's operation under different operating conditions have been presented in chapter 6. In this section, further experimental results are presented to show the response of the converter under variable source voltage and load current conditions. Furthermore, the response of the controller and compensation network to input perturbations and variation in loading conditions is also examined.

7.3.1 Line Regulation

The main purpose of the converter is to provide the regulated voltage to energize the loads despite of any variations in the source voltage. Figure 7-19 represents that the input voltage is reduced from 9.3 volts to 8.1 volts. (Here Vin represents voltage of both the sources Vin_1 + Vin_2). However, the controller quickly responds to the input perturbation and increase the duty cycle d_5 to keep the output voltage V_{o1} at 3.3 V. Figure 7-20 shows the increase in input voltage from 7.5V to 9.5V. The controller responds to the increase in input voltage and decreases the duty cycle d_5 to regulate the output voltage V_{o1} to a desired value of 3.3V. Similarly, Figure 7-21 shows another decrease in input voltage from 9.5V to 8.5V however due to fast response of the controller the output voltage V_{o1} is kept at a required value of 3.3V. Likewise the other output voltage V_{o2} is also regulated at the desired value of 6.8V by duty cycle d_3 as shown in Figure 7-22, despite of all the fluctuations in the input voltage.

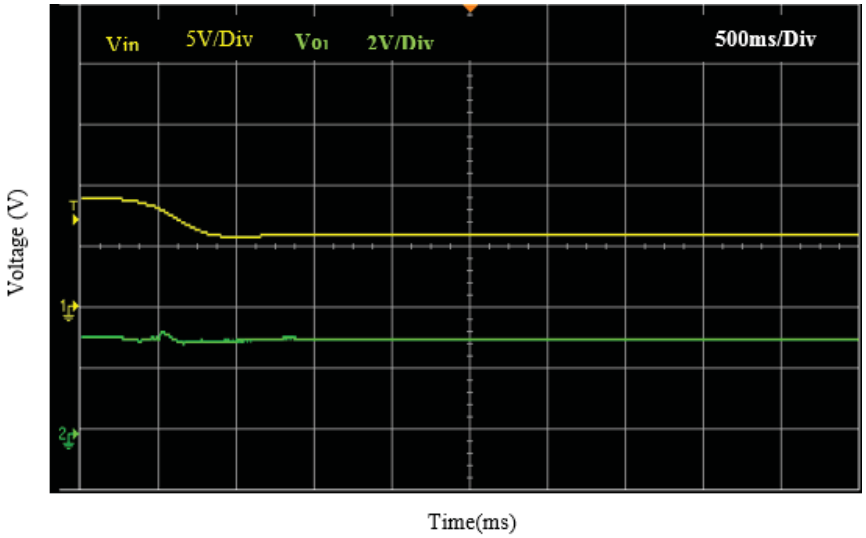

Figure 7-19 Output voltage V_{o1} regulation due to decrease in input voltage

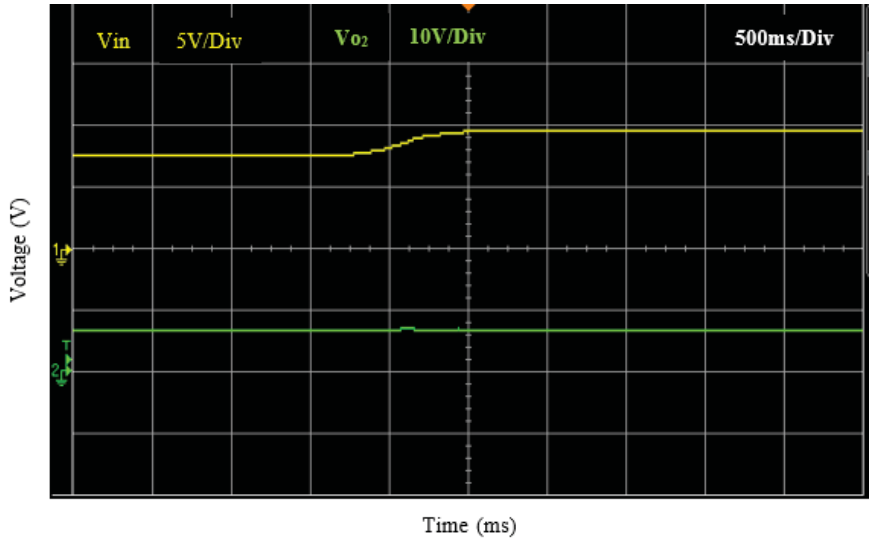

Figure 7-20 Output voltage V_{o1} regulation due to increase in input voltage

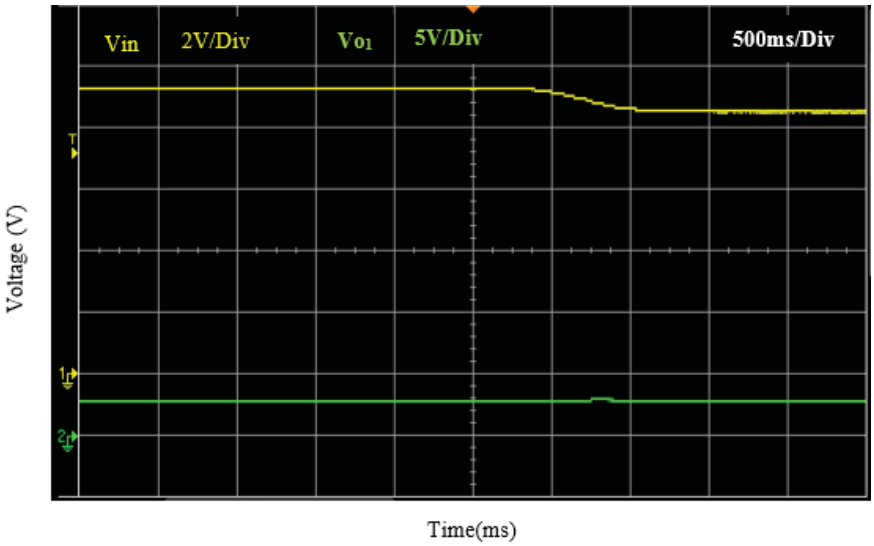

Figure 7-21 Output voltage V_{o1} regulation due to decrease in input voltage

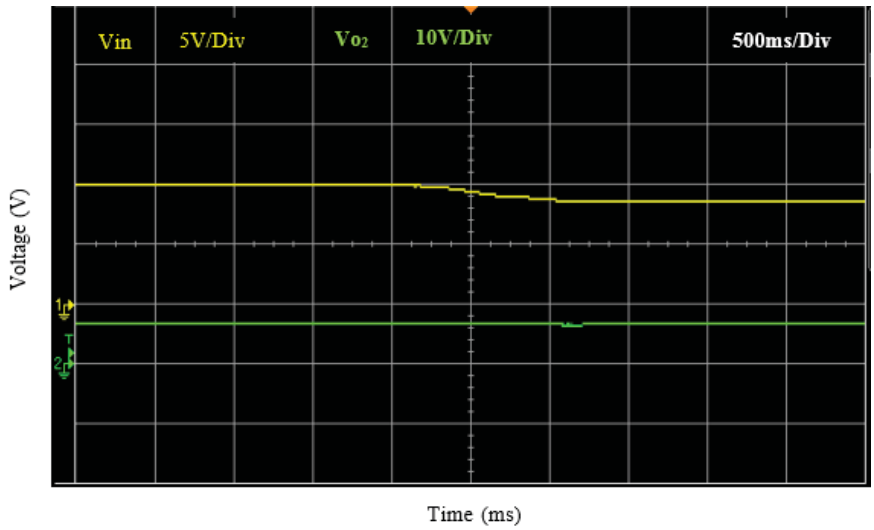

Figure 7-22 Output voltage V_{o2} regulation due to decrease in input voltage

7.3.2 Load Regulation

The compensation network in the controller has been designed to quickly respond to any perturbations in the source voltage and load current by adjusting the duty cycles to keep the output voltage constant at required values all the times. In order to observe the behavior of the converter and performance of the controller, the load current for output one is increased from 340mA to 460mA thus increasing the total load current from 1.19A to 1.31A. Figure 7-23 shows that no change has been observed in output voltage V_{o1} due to increase in its load current. Similarly Figure 7-24 shows that the output voltage V_{o2} also did not show any deviations and remains constant during the variation in the load current of other output port. However, there is an increase in inductor current, as shown in Figure 7-25, due to increase in load current at output port one.

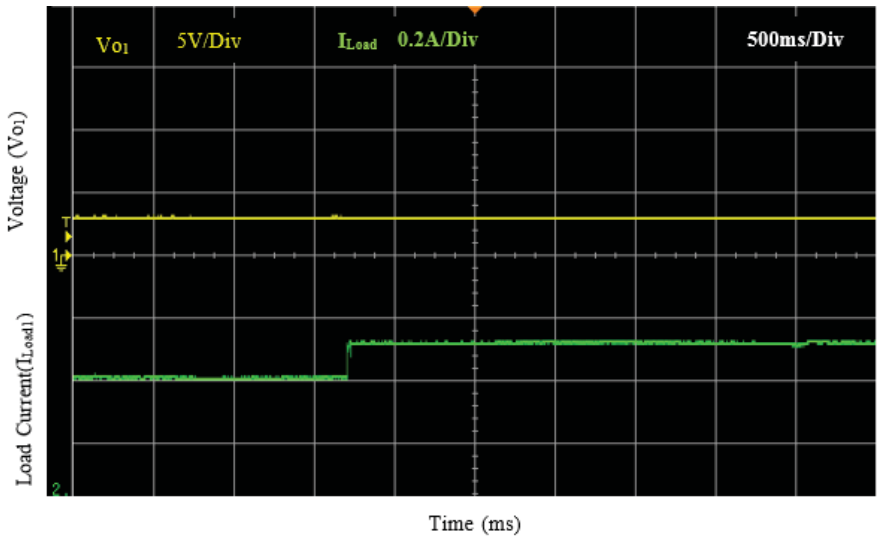

Figure 7-23 Output voltage V_{o1} regulation due to decrease in load Current

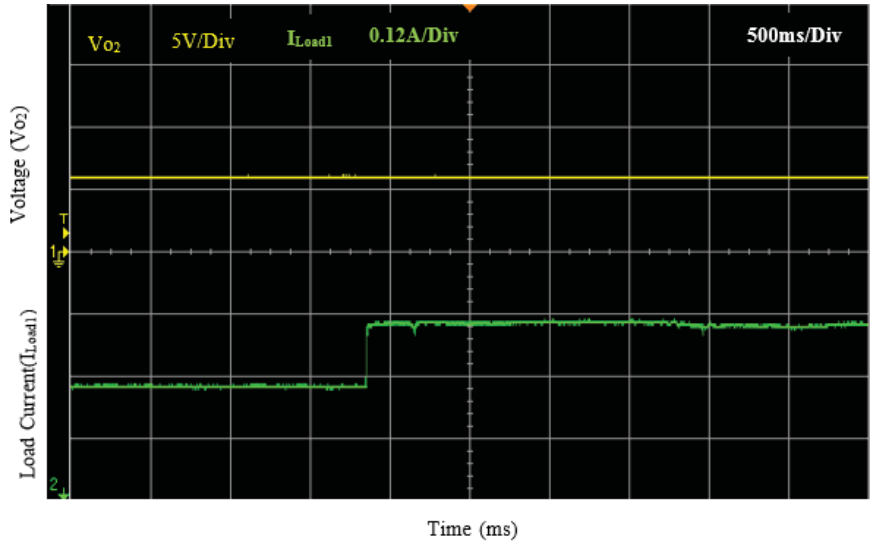

Figure 7-24 Output voltage V_{o2} regulation due to increase in load current

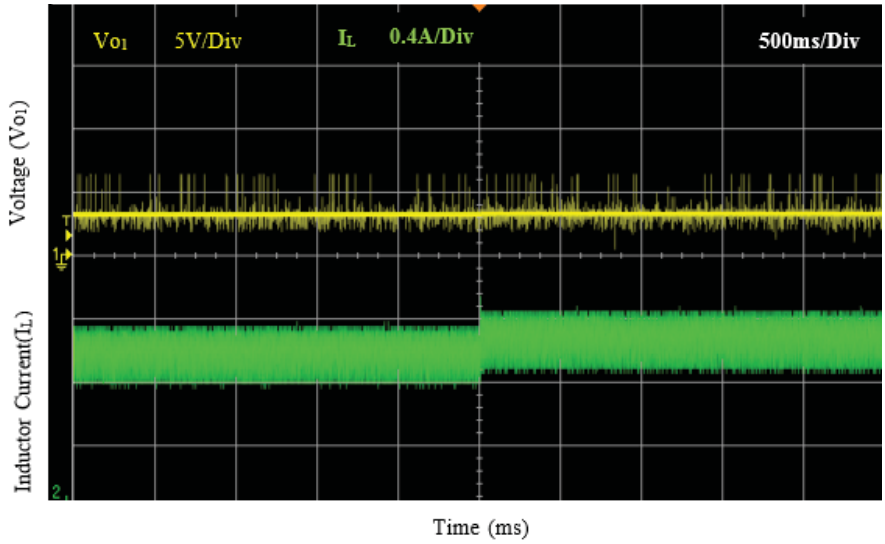

Figure 7-25 Increase in Inductor current due to increase in load current

7.3.3 Cross Regulation

Cross regulation is the major problem in the multioutput converters wherein any variations on one of the output port may affect the other output. In the presented topology, the cross-regulation problem has been minimum due to the reasons that one of the output port is used to charge the battery at constant voltage so there is no variation in the output voltage. Furthermore, any effect on cross coupling due to any variations on port one is also lessened by designing an appropriate compensation network. Results presented in the above figure (From 7-19 to 7-24) show that no cross-regulation problem has been observed during the entire operation of the converter.

7.4 Comparison of new topology with the other work

The comparison of newly presented multiport DC-DC converter topology is made with the other topologies presented in the literature. The comparison has been made in terms of reliability, efficiency, number of components and size.

7.4.1 Reliability

The primary objective of the power electronics interface is to harvest maximum power from ambient energy source and to transfer it to load in the form of a regulated supply, without any interruption. Due to irregular behavior of the renewable energy sources, a constant power from these sources in never guaranteed therefore, multiple sources are integrated to constitute a reliable power system. However, if the power electronics interface is unable to utilize multiple sources at the same time, the benefit of multiple interface is lost to some extent. For instance, if more than one source is available at a time and PE interface could exploit only one of them at a time as in case of topologies presented in [71], [73], [83], [87] and [88] or cannot store the surplus energy as in case of topologies presented in [66], [72],[84]-[101], the energy from other source remains un utilized. Furthermore, when the sources are not available, the load remains without power. Moreover, if the PE holds only one source to power up the load and to charge the battery as in case of three port converters presented in [69], [123], [126]-[129] and in case of absence of source neither load is energized nor battery is charged hence makes the system less reliable.

The advantage of the newly presented topology over the topologies presented in the literature is that it can house multiple sources at the input and these can be utilized individually and simultaneously. In addition to that, the surplus energy if available, can be stored and can be used to energize the load when the sources are not available or unable to independently power up the load. Hence the uninterrupted power supply to the load is guaranteed and the system is highly reliable as compared to other topologies presented in the literature.

7.4.2 Number of Components/size

The offered solution for the multiport interface of renewable energy sources employs only one inductor which not only reduces the components count but also reduces the overall size of the PE interface and makes it easy to control in contrast with the topologies presented in literature. In addition, this topology has multi input-multi

output interface and has a bidirectional storage port. Table 7-5 presents a comparison of presented topology with the topologies presented in the cited literature, in terms of input, output, storage ports and number of inductors. The presented topology has clear advantage over the others.

7.4.3 Efficiency

Comprehensive efficiency analysis of the multiport topology in different modes of operation has been presented in section 7.1. A comparison of converter's efficiency with the existing topologies is shown in table 7-6. It is evident that despite of new converter's multi input and multi-output ports and capacity to accommodate a storage device, the presented topology is highly energy efficient as compared to the other topologies presented in the literature.

7.5 Conclusion

This chapter presents a critical analysis of the mathematical, simulation and experimental results obtained in chapter 3,5 and 6 respectively. Power transfer efficiency of the new topology is calculated for different modes and under different conditions by considering all the losses in the components of the circuitry. The calculated efficiency is then compared with the efficiency measured during simulation and experimental studies and results are presented. Stability analysis of the converter is also conducted and results are presented in this chapter. A comparison of the presented topology, in terms of its efficiency, reliability, size and number of components is made with the topologies cited in the literature. It is concluded that the presented topology is highly efficient power electronics interface for integration of renewable energy sources in low power applications.

Table 7-7 Comparison of Converter with other topologies

Converter Ports and components	**Converter Structure**				
	Multi Input		**Multi Output**	**Three Port**	**This Work**
	[84], [85] [90]-[92] [100]-102]	[86]-[89] [94],[97],[103]	[122], [125]	[69], [128]-[131]	
Input ports	2	2	1	1	2
Output port	1	1	2	2	2
Storage port	0	0	0	1*	1*
Inductors	2	1	1	1	1
Power Switches	2-6	2-5	2	3-5	5

Table 7-8 Efficiency Comparison

Topology	**Reference**		**Efficiency %**	
Single input Dual output	[104]	[110]	77	96
	[105]	[111]	89.04	94.5 (1.1A)
	[106]	[112]	95	90
	[107]		92	
	[108]		95	
	[109]		93	
	This Work		94.7%	
Dual input-Single output	[85]		96	
	[91]		95	
	[92]		95	
	This Work		95	
Multi Input- Multi Output	[123]		85	
	[125]		83	
	This Work		93.78	

Chapter 8

8 Conclusions and Future Work

8.1 Conclusions

In this research, a multi-port power electronics circuitry is presented for a standalone hybrid energy system in low power applications. The circuitry based on a non-isolated DC-DC buck converter, consists of multiple input and output ports. It integrates two renewable energy sources, a bidirectional port connects a storage device which acts as a load when both the sources are present and the available power is more than the requirement of load and acts as a source in case of absence of renewable sources. A variable load can be connected to the other output port. The advantages of the newly presented topology over the existing topologies are

- The converter has high power transfer efficiency in all the modes of operation and under different loading conditions
- The topology is highly reliable and the uninterrupted supply of power is ensured even in the absence of renewable energy sources
- It has less components as compared to most of the existing topologies
- The use of single inductor not only reduces the size but also makes the control easy
- A simple control scheme can control the topology.
- Multiple sources can be connected at the input ports.
- Input sources can be employed independently and concurrently.
- It can power up multiple loads with different voltage levels.
- In addition to provide regulated output to the load, this converter can harvest maximum power from the input sources.
- Surplus energy can be stored in the battery and made available in the absence of renewable energy sources.

The aim of this research was to identify the limitations in the existing multiport interface for integration of multiple renewable energy sources, and to contribute a significant addition in the existing knowledge by presenting a novel topology.

An extensive literature review is conducted which results in identification of limitations in existing multiport converter topologies. Based on the identified research gape, a new topology of a single inductor non-Isolated DC-DC buck converter is presented. The new topology is analyzed mathematically followed by simulation results and validated by the experimental results on the model.

A sequential methodology adopted to carry out this research is summarized as follows:
In the first chapter, the background of the research area is presented. A brief discussion is made on the potential problems associated with conventional power generating systems along with the opportunities and challenges for employing renewable energy sources. An overview of power electronics interface is also presented. Statement of research problem is defined, research methodology chalked out and potential research contributions are also recognized.

A comprehensive literature review of multiport non-isolated PE converters is presented in the second chapter. The extensive literature review guides to the identification of knowledge gap and provides bases to carry out further research in the area and to present a viable solution to address the issues identified during the literature review.

A new topology of multi-port non-isolated DC-DC buck converter to overcome the drawbacks of existing multiport converters is introduced in the chapter three. The architecture of the new topology is explained and its advantages over the existing converters are highlighted. Detailed mathematical analysis is conducted and presented. Design of different components of the converter is also covered in this chapter.

Chapter four, explores several control schemes employed to control the multiport converters in renewable energy applications. A control scheme based on decoupling control for multi input multi output systems, adopted for this research work is presented and small signal model of the converter for linear analysis is presented.

Development of simulation platform to test the new topology is covered by chapter five. In this chapter design parameters for simulation studies are defined and the operation of the converter in different modes of operation is critically analysed.

Different operating conditions are applied and behaviour of the converter is judged. Open loop and closed loop simulation results are also presented in this chapter.

Finalization of design parameters, selection of components and development of low power prototype model for novel multiport DC-DC buck converter is presented in chapter six. The presented topology is tested for different modes of operation under different conditions and results are presented to authenticate the analytical and simulation results presented in chapter three and chapter five.

Critical analysis of the results obtained in chapter three (mathematical), five (simulation) and six (experimental) is performed and presented in the seven. The obtained results thoroughly investigated in terms of Power transfer efficiency in different modes of operation and under different source and load conditions. Stability analysis of the converter is also discussed in this chapter. Finally, the comparison of the presented topology, in terms of its efficiency, reliability, size and components count is made with the topologies cited in the literature to prove the novelty of this multiport interface.

8.2 Future Opportunities

In this research, a low voltage and low power single inductor DC-DC buck converter is developed. The developed converter has two input ports, a storage port, and a load port. The developed converter can be used only in low power applications. So, there is an opportunity to carry out the further research and to develop a circuitry for medium to high power applications. A transformerless converter topology to integrate multiple energy sources in medium to high power application would be a potential significant contribution in the area.

The developed prototype model of the new topology integrates two sources at the input. The topology can be extended to accommodate more renewable energy sources, hence further enhancing the reliability of the power system by ensuring continuous power to the load despite of irregular availability of the renewable energy sources.

The scope of this work was confined to power up two different loads with different voltage level requirements. In the future work, the outputs may be increased and this topology can be extended to simultaneously power up more than two loads with different regulated voltages.

A PI control scheme with a decoupling controller is employed in this work. However future work may be carried out to use other linear and nonlinear control techniques to propose a more robust control scheme for multiport interface.

References

[1] U.S. Energy Information Administration, "Annual Energy Outlook 2015," *Integr. Int. Energy Anal.*, vol. 1, pp. 1–244, 2015.

[2] International Energy Agency (IEA), "World Energy Outlook 2016," 2016.

[3] A. Merabet, K. T. Ahmed, H. Ibrahim, R. Beguenane, and A. M. Y. M. Ghias, "Energy Management and Control System for Laboratory Scale Microgrid Based Wind-PV-Battery," *IEEE Trans. Sustain. Energy*, vol. 8, no. 1, pp. 145–154 January 2017.

[4] F. Spertino, A. Ciocia, V. Cocina, and P. Di Leo, "Renewable Sources with Storage for Cost-Effective Solutions to Supply Commercial Loads," in Proc. *Power Electron. Electr. Drives Autom. Motion Sympo.*, pp. 242–247, 2016.

[5] J. Chen and H. E. Garcia, "Economic optimization of operations for hybrid energy systems under variable markets," *j. Appl. Energy*, vol. 177, pp. 11–24, 2016.

[6] M. C. Mira, Z. Zhang, A. Knott, and M. A. E. Andersen, "Analysis , Design , Modeling , and Control of an for Hybrid Renewable Energy Systems," *IEEE TTrans Power Electro.*, vol. 32, no. 2, pp. 1138–1155, February 2017.

[7] J. Paska, P. Biczel, and M. Kłos, "Hybrid power systems – An effective way of utilising primary energy sources," *J. Renew. Energy*, vol. 34, no. 11, pp. 2414–2421, March, 2009.

[8] A. Le, A. Giourdjian, A. Frankyan, and V. Mandany, "Design , Sizing and Operation of a Hybrid Renewable Energy System for Farming," in Proc. *IEEE Power Energy Soc. Innov. Smart Grid Tech. conf.*, pp. 1–5, 2016.

[9] I. R. H. Mahmoudi, "The control strategy for a hybrid wind-photovoltaic system with compressed air storage element," in Proc. *Electr. Inf. Technol.*, pp. 89–92, 2016.

[10] O. Nadjemi, T. Nacer, A. Hamidat, and H. Salhi, "Optimal hybrid PV/wind energy system sizing: Application of cuckoo search algorithm for Algerian dairy farms," *Renew. Sustain. Energy Rev.*, vol. 70, pp. 1352–1365, 2017.

[11] V. Das, S. Padmanaban, K. Venkitusamy, R. Selvamuthukumaran, F. Blaabjerg, and P. Siano, "Recent advances and challenges of fuel cell based power system architectures and control – A review," *J. Renew. Sustain. Energy Rev.*, vol. 73, no., pp. 10–18, November 2016.

[12] E. Baleke Ssekulima, M. B. Anwar, A. Al Hinai, M. Shawky, and E. Moursi, "Wind speed and solar irradiance forecasting techniques for enhanced renewable energy integration with the grid: a review," *IET Renew. Power Gener.*, vol. 10, pp. 885–898, 2016.

[13] A. Thalamttathu Thankappan, S. P. Simon, P. S. R. Nayak, K. Sundareswaran, and N. P. Padhy, "Pico-hydel hybrid power generation system with an open well energy storage," *IET Gener. Transm. Distrib.*, vol. 11, no. 3, pp. 740–749,

2017.

[14] S. Barakat, "Viability Study of Grid Connected PV / Wind / Biomass Hybrid Energy System for a Small Village in Egypt," in Proc. *IEEE Middle East Power Syst. Conf.*, pp. 46–51, 2016.

[15] M. K. Shahzad, A. Zahid, T. ur Rashid, M. A. Rehan, M. Ali, and M. Ahmad, "Techno-economic feasibility analysis of a solar-biomass off grid system for the electrification of remote rural areas in Pakistan using HOMER software," *J. Renew. Energy*, vol. 106, pp. 264–273, 2017.

[16] A. Haddad, M. Ramadan, M. Khaled, and K. Chahine, "An investigation on coupling fuel cell and photovoltaic systems for power generation," in Proc. *IEEE Adv. Comput. Tools Eng. Appl.*, pp. 37–42, 2016.

[17] V. S. Tejwani and B. N. Suthar, "Control Strategy for Utility Interactive Hybrid PV Hydrogen System," in Proc. *IEEE Power Energy Gen. meerting*, pp. 1–5, 2016.

[18] H. Fathabadi, "Novel high-efficient unified maximum power point tracking controller for hybrid fuel cell/wind systems," *J. Appl. Energy*, vol. 183, pp. 1498–1510, 2016.

[19] P. Suhane, S. Rangnekar, A. Mittal, and A. Khare, "Sizing and performance analysis of standalone wind-photovoltaic based hybrid energy system using ant colony optimisation," *J. IET Renew. Power Gener.*, vol. 10, no. 7, pp. 964–972, 2016.

[20] L. Ali, "Impact of Annual Load Growth on Selecting the Suitable Sustainable Standalone System for an Off-Grid Town in Western Australia," in Proc. *IEEE Power Syst. Technol. Conf.*, pp. 1–5, 2016.

[21] J. Philip, C. Jain, K. Kant, B. Singh, S. Mishra, A. Chandra, and K. Al-Haddad, "Control and Implementation of a Standalone Solar Photovoltaic Hybrid System," *IEEE Trans. Ind. Appl.*, vol. 52, no. 4, pp. 3472–3479, 2016.

[22] L. Wang, Q.-S. Vo, and A. V Prokhorov, "Dynamic Stability Analysis of a Hybrid Wave and Photovoltaic Power Generation System Integrated into a Distribution Power Grid," *IEEE Trans. Sustain. Energy*, vol. PP, no. 99, pp. 404–413, 2016.

[23] S. A. Zaid and A. M. Kassem, "Review, analysis and improving the utilization factor of a PV-grid connected system via HERIC transformerless approach," *J. Renew. Sustain. Energy Rev.*, vol. 73, pp. 1061–1069, 2017.

[24] A. C. Luna, N. L. Diaz, J. C. Vasquez, and J. M. Guerrero, "Mixed-Integer-Linear-Programming-Based Energy Management System for Hybrid PV-Wind-Battery Experimental Verification," *J. IEEE Trans Power Electron.*, vol. 32, no. 4, pp. 2769–2783, 2017.

[25] B. Mangu, S. Akshatha, D. Suryanarayana, and B. G. Fernandes, "Grid-Connected PV-Wind-Battery-Based Bidirectional DC-DC Converter for Household Applications," *IEEE J. Emerg. Sel. Top. Power Electron.*, vol. 4,

no. 3, pp. 1086–1095, 2016.

[26] A. Aktas, K. Erhan, S. Ozdemir, and E. Ozdemir, "Experimental investigation of a new smart energy management algorithm for a hybrid energy storage system in smart grid applications," *J. Electr. Power Syst. Res.*, vol. 144, pp. 185–196, 2017.

[27] S. Kim, J. Jeon, C. Cho, J. Ahn, and S. Kwon, "Dynamic Modeling and Control of a Grid-Connected Hybrid Generation System With Versatile Power Transfer," *IEEE Trans. Ind. Electron.*, vol. 55, no. 4, pp. 1677–1688, April 2008.

[28] O. M. Toledo, D. Oliveira Filho, and A. S. A. C. Diniz, "Distributed photovoltaic generation and energy storage systems: A review," *J. Renew. Sustain. Energy Rev.*, vol. 14, no. 1, pp. 506–511, January 2010.

[29] Walling, R A Reigh et al., "Summary of Distributed Resources Impact on Power Delivery Systems," *J. IEEE Trans. Energy Conversion.*, vol. 23, no. 3, pp. 1636–1644, July 2008.

[30] J. a. P. Lopes, N. Hatziargyriou, J. Mutale, P. Djapic, and N. Jenkins, "Integrating distributed generation into electric power systems: A review of drivers, challenges and opportunities," *J. Electr. Power Syst. Res.*, vol. 77, no. 9, pp. 1189–1203, July 2007.

[31] P. N. Vovos, A. E. Kiprakis, A. R. Wallace, and G. P. Harrison, "Centralized and distributed voltage control: Impact on distributed generation penetration," *IEEE Trans. Power Syst.*, vol. 22, no. 1, pp. 476–483, February 2007.

[32] K. Malmedal, B. Kroposki, P. K. Sen, and D. Ph, "Distributed Energy Resources and Renewable Energy in Distribution Systems : Protection Considerations and Penetration Levels," in Proc. *Annu. meeitng Ind. Appl. Soc.*, pp. 1–8, 2008.

[33] B. Kruimer and W. L. Kling, "Integration Issues of Distributed Generation in Distribution Grids," *IEEE Proceedings*, vol. 99, no. 1, 2011.

[34] B. Muruganantham, R. Gnanadass, and N. P. Padhy, "Challenges with renewable energy sources and storage in practical distribution systems," *J. Renew. Sustain. Energy Rev.*, vol. 73, pp. 125–134, 2017.

[35] J. P. Ram, N. Rajasekar, and M. Miyatake, "Design and overview of maximum power point tracking techniques in wind and solar photovoltaic systems: A review," *J. Renew. Sustain. Energy Rev.*, vol. 73, pp. 1138–1159, 2017.

[36] J. M. Carrasco, L. G. Franquelo, E. Bialasiewicz, Jan TGalván, R. C. P. Guisado, M. Ángeles, M. Prats, J. I. León, and N. Moreno-alfonso, "Power-Electronic Systems for the Grid Integration of Renewable Energy Sources : A Survey," *J. IEEE Trans. Ind. Electron.*, vol. 53, no. 4, pp. 1002–1016, August 2006.

[37] B. Kroposki, C. Pink, R. Deblasio, H. Thomas, M. Simoes, and P. K, "Benefits of Power Electronic Interfaces for Distributed Energy Systems," *IEEE Trans.*

Energy Conversion, vol. 25, no. 3, pp. 901–908, September 2010.

[38] Y. Xue, L. Chang, S. B. Kjær, J. Bordanau, and S. Toshihisa, "Topologies of Single-Phase Inverters for Small Distributed Power Generators : An Overview," *IEEE Transation Power Electron.* vol. 19, no. 5, pp. 1305–1314, September 2004.

[39] P. Szczešniak and J. Kaniewski, "Power electronics converters without DC energy storage in the future electrical power network," *J. Electr. Power Syst. Res.*, vol. 129, pp. 194–207, 2015.

[40] J. He, B. Liang, and Y. W. Li, "Simultaneous Microgrid Voltage and Current Harmonics Compensation Using Coordinated Control of Dual-Interfacing-Converters," *IEEE Trans. Power Electron.*, vol. 32, no. c, pp. 2647–2660. April 2017.

[41] S. Chakraborty, B. Kramer, and B. Kroposki, "A review of power electronics interfaces for distributed energy systems towards achieving low-cost modular design," *J. Renew. Sustain. Energy Rev.*, vol. 13, no. 9, pp. 2323–2335, 2009.

[42] A. Chakraborty, "Advancements in power electronics and drives in interface with growing renewable energy resources," *J. Renew. Sustain. Energy Rev.*, vol. 15, no. 4, pp. 1816–1827, May 2011.

[43] L. Costa, G. Buticchi, M. Liserre, and A. F. Src, "A Fault-Tolerant Series-Resonant DC–DC Converter," *IEEE Trans. Power Electron.*, vol. 32, no. 2, pp. 900–905, February 2017.

[44] H. Kim, H. Cha, H. F. Ahmed, B. Choi, and Heung-Geun Kim, "Isolated Double Step-Down DC – DC Converter With Improved ZVS Range and No Transformer Saturation Problem," *IEEE Trans. Power Electron.*, vol. 32, no. 3, pp. 1792–1804, March 2017

[45] O. Kirshenboim and M. M. Peretz, "High-Efficiency Nonisolated Converter With Very High Step-Down Conversion Ratio," *Trans. Power Electron.*, vol. 32, no. 5, pp. 3683–3690, May 2017.

[46] S. Du, B. Wu, D. Xu, and N. R. Zargari, "A Transformerless Bipolar Multistring DC–DC Converter Based on Series-Connected Modules," *IEEE Trans. Power Electron.*, vol. 32, no. 2, pp. 1006–1017, February 2017.

[47] W. Li and X. He, "Review of nonisolated high-step-up DC/DC converters in photovoltaic grid-connected applications," *IEEE Trans. Ind. Electron.*, vol. 58, no. 4, pp. 1239–1250, 2011.

[48] B. Sri Revathi and M. Prabhakar, "Non isolated high gain DC-DC converter topologies for PV applications A comprehensive review," J. *Renew. Sustain. Energy Rev.*, vol. 66, pp. 920–933, 2016.

[49] K. I. Hwu, W. Z. Jiang, and P. Y. Wu, "An Expandable Two-Phase Interleaved Ultrahigh Step-Down Converter with Automatic Current Balance," J. *IEEE Trans. Power Electron.*, vol. 8993, no. c, pp. 1–1, 2017.

[50] H. L. Do, "Zero-voltage-switching synchronous buck converter with a coupled

inductor," *IEEE Trans. Industrial Electron.*, vol. 6, no. 4, pp. 1556–1563, August 2011.

[51] F. Marvi, E. Adib, and H. Farzanehfard, "Zero voltage switching interleaved coupled inductor synchronous buck converter operating at boundary condition," *IET Power Electron.*, vol. 9, no. 1, pp. 126–131, 2016.

[52] M. Esteki, B. Poorali, E. Adib, and H. Farzanehfard, "Interleaved Buck Converter with Continuous Input Current, Extremely Low Output Current Ripple, Low Switching Losses, and Improved Step-Down Conversion Ratio," *IEEE Trans. Ind. Electron.*, vol. 62, no. 8, pp. 4769–4776, 2015.

[53] M. H. Taghvaee, M. A. M. Radzi, S. M. Moosavain, H. Hizam, and M. Hamiruce Marhaban, "A current and future study on non-isolated DC-DC converters for photovoltaic applications," *J. Renew. Sustain. Energy Rev.*, vol. 17, pp. 216–227, 2013.

[54] C.-C. Lin, G. W. Wu, and L.-S. Yang, "Study of a non-isolated bidirectional DC–DC converter," *IET Power Electron.*, vol. 6, no. 1, pp. 30–37, 2013.

[55] A. K. Rathore, D. R. Patil, and D. Srinivasan, "Non-isolated Bidirectional Soft-Switching Current-Fed LCL Resonant DC/DC Converter to Interface Energy Storage in DC Microgrid," *IEEE Trans. Ind. Appl.*, vol. 52, no. 2, pp. 1711–1722, April 2016.

[56] E. Durán, J. M. Andújar, F. Segura, and A. J. Barragán, "A high-flexibility DC load for fuel cell and solar arrays power sources based on DC-DC converters," *J. Appl. Energy*, vol. 88, no. 5, pp. 1690–1702, 2011.

[57] Z. Chen, "PI and sliding mode control of a Cuk converter," *IEEE Trans. Power Electron.*, vol. 27, no. 8, pp. 3695–3703, 2012.

[58] M. M. Algazar, H. AL-monier, H. A. EL-halim, and M. E. E. K. Salem, "Maximum power point tracking using fuzzy logic control," *J. Electr. Power Energy Syst.*, vol. 39, no. 1, pp. 21–28, 2012.

[59] S. J. Chiang, "Modeling and Control of PV Charger System With SEPIC Converter," *IEEE Trans.Industrial Electron.*, vol. 56, no. 11, pp. 4344–4353, November 2009.

[60] J. C. Rosas-Caro, V. M. Sanchez, R. F. Vazquez-Bautista, L. J. Morales-Mendoza, J. C. Mayo-Maldonado, P. M. Garcia-Vite, and R. Barbosa, "A novel DC-DC multilevel SEPIC converter for PEMFC systems," *J. Hydrogen Energy*, vol. 41, no. 48, pp. 6–13, 2016.

[61] M. Chen, F. Gao, R. Li, and X. Li, "A Dual-Input Central Capacitor DC/DC Converter for Distributed Photovoltaic Architectures," *IEEE Trans. Ind. Appl.*, vol. 53, no. 1, pp. 305-318, February 2017.

[62] A. Urtasun and D. D. C. Lu, "Control of a Single-Switch Two-Input Buck Converter for MPPT of Two PV Strings," *IEEE Trans. Ind. Electron.*, vol. 62, no. 11, pp. 7051–7060, January 2015.

[63] Z. Rehman, I. Al-Bahadly, and S. Mukhopadhyay, "Multiinput DC–DC

converters in renewable energy applications – An overview," *J. Renew. Sustain. Energy Rev.*, vol. 41, pp. 521–539, January 2015.

[64] S. Khosrogorji, M. Ahmadian, H. Torkaman, and S. Soori, "Multi-input DC/DC converters in connection with distributed generation units A review," *J. Renew. Sustain. Energy Rev.*, vol. 66, pp. 360–379, 2016.

[65] N. Zhang, D. Sutanto, and K. M. Muttaqi, "A review of topologies of three-port DC-DC converters for the integration of renewable energy and energy storage system," *J. Renew. Sustain. Energy Rev.*, vol. 56, pp. 388–401, 2016.

[66] J. Hui, A. Bakhshai, and P. K. Jain, "A Hybrid Wind-Solar Energy System : A New Rectifier Stage Topology," in Pro. *IEEE Appl. Power Electron. Conf. Expo.,* pp. 155–161, 2010.

[67] F. Guo, L. Fu, X. Zhang, C. Yao, H. Li, and J. Wang, "A Family of Quasi-Switched-Capacitor Circuit-Based Dual-Input DC/DC Converters for Photovoltaic Systems Integrated with Battery Energy Storage," *IEEE Trans. Power Electron.*, vol. 31, no. 12, pp. 8237–8246, 2016.

[68] W. Jiang and B. Fahimi, "Multi-port Power Electric Interface for Renewable Energy Sources," in Proc *IEEE Appl. power Electron. conf.,* pp. 347–352, 2009.

[69] Y. Chen, A. Q. Huang, and X. Yu, "A High Step-Up Three-Port DC – DC Converter for Stand-Alone PV / Battery Power Systems," *IEEE Trans.Power Electron.*, vol. 28, no. 11, pp. 5049–5062, 2013.

[70] Z. Zhang, R. Pittini, M. A. E. Andersen, and O. C. Thomsena, "A Review and Design of Power Electronics Converters for Fuel Cell Hybrid System Applications," *J. Energy Procedia*, vol. 20, pp. 301–310, January 2012.

[71] R. R. Ahrabi, H. Ardi, M. Elmi, and A. Ajami, "A Novel Step-Up Multiinput DC – DC Converter for Hybrid Electric Vehicles Application," *IEEE Trans Power Electron*.,vol. 32, no. 5, pp. 3549–3561, May 2017.

[72] F. Akar, Y. Tavlasoglu, E. Ugur, B. Vural, and I. Aksoy, "A Bidirectional Non Isolated Multi Input DC-DC Converter for Hybrid Energy Storage Systems in Electric Vehicles," *IEEE Trans. Veh. Technol.*, vol. 65 pp 7944-7955, no. 10, October 2016.

[73] L. Solero and A. Lidozzi, "Design of Multiple-Input Power Converter for Hybrid Vehicles," *IEEE Trans.Power Electron.*, vol. 20, no. 5, pp. 1007–1016, September 2005.

[74] A. Hintz, U. R. Prasanna, and K. Rajashekara, "Novel Modular Multiple-Input Bidirectional DC – DC Power Converter (MIPC) for," *IEEE Trans. Ind. Electron.*, vol. 62, no. 5, pp. 3163–3172, May 2015.

[75] M. Marchesoni and C. Vacca, "New DC–DC Converter for Energy Storage System Interfacing in Fuel Cell Hybrid Electric Vehicles," *IEEE Trans. Power Electron.*, vol. 22, no. 1, pp. 301–308, January 2007.

[76] H. Wu, C. Wan, K. Sun, and Y. Xing, "A high step-down multiple output

converter with wide input voltage range based on quasi two-stage architecture and dual-output LLC resonant converter," *IEEE Trans. Power Electron.*, vol. 30, no. 4, pp. 1793–1796, April 2015.

[77] Z. Qian and O. Abdel-rahman, "Modeling and Control of Three-Port DC / DC Converter Interface for Satellite Applications," *IEEE Trans. Power ELlectronics*, vol. 25, no. 3, pp. 637–649, March 2010.

[78] Z. Nie, B. Bekiarov, and A. Emadi, "An On-Line UPS System with Power Factor Correction and Electric Isolation Using BIFRED Converter," in Proc. *IEEE Ind. Electron. Conf.*, vol. 1, pp. 361–366, 2003.

[79] Y. Shen, X. Sun, W. Li, X. Wu, and B. Wang, "A Modified Dual Active Bridge Converter with Hybrid Phase-Shift Control for Wide Input Voltage Range," *IEEE Trans. Power Electron.*, vol. 31, no. 10, pp. 6884–6900, 2016.

[80] H. R. Nielsen, M. a. E. Andersen, Z. Zhang, and O. C. Thomsen, "Dual-input isolated full-bridge boost dc–dc converter based on the distributed transformers," *IET Power Electron.*, vol. 5, no. 7, pp. 1074–1083, August 2012.

[81] L. Corradini, D. Seltzer, D. Bloomquist, R. Zane, D. Maksimović, and B. Jacobson, "Zero voltage switching technique for bidirectional dc/dc converters," *IEEE Trans. Power Electron.*, vol. 29, no. 4, pp. 1585–1594, 2014.

[82] Z. Zhang, O. C. Thomsen, M. A. E. Andersen, and A. S. F. M. Technique, "Modeling and Control of a Dual-Input Isolated Full-Bridge Boost Converter," in Proc. *Asia Int. Model. Simul. Conf.*, pp. 2017–2023, 2012.

[83] A. Sivaprasad, S. Kumaravel, and S. Ashok, "Integration of Solar PV / BatteryHybrid System Using Dual Input DC-DC Converter," in Proc. *Int. Conf. Power Energy Syst. Sustain. Energy*, pp. 0–4, 2016.

[84] N. Katayama, S. Tosaka, T. Yamanaka, M. Hayase, K. Dowaki, and S. Kogoshi, "New Topology for DC – DC Converters Used in Fuel Cell – Electric Double Layer Capacitor Hybrid Power Source Systems for Mobile Devices," *IEEE Trans. Ind. Appl.*, vol. 52, no. 1, pp. 313–321, February 2016.

[85] M. Azizi, M. Mohamadian, and R. Beiranvand, "A New Family of Multi-Input Converters Based on Three Switches Leg," *IEEE Trans. Ind. Electron.*, vol. 63, no. 11, pp. 6812–6822, November 2016.

[86] Y. Chen, Y. Liu, and S. Lin, "Double-Input PWM DC/DC Converter for High/Low Voltage Sources," *IEEE Trans. Industr. Electron*., vol. 53, no. 53, pp. 1538–1545, October 2006.

[87] K. P. Yalamanchili and M. Ferdowsi, "Review of Multiple Input DC-DC Converters for Electric and Hybrid Vehicles," in Proc. *IEEE Veh. Power Propuls. Conf.*, pp. 552–555, 2005.

[88] B. G. Dobbs and P. L. Chapman, "A multiple-input DC-DC converter topology," *IEEE Power Electron. Lett.*, vol. 99, no. 1, pp. 6–9, March 2003.

[89] A. Khaligh, "A Multiple-Input DC–DC Converter Topology," *IEEE Trans.Power Electron.*, vol. 24, no. 3, pp. 862–868, March 2009.

[90] M. Marchesoni and C. Vacca, "New DC–DC Converter for Energy Storage System Interfacing in Fuel Cell Hybrid Electric Vehicles," *IEEE Trans. Power Electron.*, vol. 22, no. 1, pp. 301–308, January 2007.

[91] R. Wai, C. Lin, J. Liaw, and Y. Chang, "Newly Designed ZVS Multi-Input Converter," *IEEE Trans. Ind. Electron.*, vol. 58, no. 2, pp. 555–566, February 2011.

[92] R. Wai, C. Lin, and B. Chen, "High-Efficiency DC – DC Converter With Two Input Power Sources," *IEEE Trans. Power Electron. Electron.*, vol. 27, no. 4, pp. 1862–1875, April 2012.

[93] D. Lee, M. Lee, D. Hyun, and I. Choy, "New Zero-Current-Transition PWM DC / DC Converters without current stress," *IEEE Trans. Power Electron.*, vol. 18, no. 1, pp. 95–104, January 2003.

[94] K. P. Yalamanchili, M. Ferdowsi, and K. Corzine, "New Double Input DC-DC Converters for Automotive Applications," in Proc. *IEEE Veh. Power Propuls. Conf.*, pp. 1–6, 2006.

[95] M. Gavriş, O. Cornea, and N. Muntean, "Multiple Input DC-DC Topologies in Renewable Energy Systems - A General Review," in Proc. *Renewable Energy Sources Explo. Sympo*., pp. 123–128, 2011.

[96] Y. Liu and Y. Chen, "A Systematic Approach to Synthesizing Multi-Input DC–DC Converters," *IEEE Trans Power Electron.*, vol. 24, no. 1, pp. 116–127, January 2009.

[97] L. Kumar and S. Jain, "A multiple source DC/DC converter topology," *J. Electr. Power Energy Syst.*, vol. 51, pp. 278–291, October 2013.

[98] A. Kwasinski, "Identification of Feasible Topologies for Multiple-Input DC–DC Converters," *IEEE Trans. Power Electron.*, vol. 24, no. 3, pp. 856–861, March 2009.

[99] Y. Li, X. Ruan, D. Yang, F. Liu, and C. K. Tse, "Synthesis of Multiple-Input DC / DC Converters," *IEEE Tran. Power Electron.*, vol. 25, no. 9, pp. 2372–2385, September 2010.

[100] N. Muntean, M. Gavris, and O. Cornea, "Dual input hybrid DC-DC converters," in Proc. *IEEE Int. Comput. as a Tool Conf.*, pp. 1–4, 2011.

[101] O. Cornea, N. Muntean, R. Teodorescu, and M. L. Gavris, "Dual input hybrid buck LC converter for a mixed wind and PV array generation system," in Proc. *Power Electron. Motion Control Conf.*, pp. DS1b.22–1–DS1b.22–6, Sep. 2012.

[102] M. Gavris, O. Cornea, and N. Muntean, "Dual input hybrid buck LC converter," in Proc. *Power Electron. Electr. Drives, Autom. Motion Sympo.*, vol. 2, pp. 309–314, 2012.

[103] S. Kumaravel and Ashok S, "Design and Analysis of Multiple Input Power Conditioner for SolarPV / Wind Hybrid Energy System," *IEEE Region 10 Conf. TENCON 2011*, pp. 883–887, 2011.

[104] G. Zhang, B. Zhang, Z. Li, Y. Zhang, and S. Chen, "A Novel Single-Input-Dual-Output Impedance Network Converter," *IEEE J. Emerg. Sel. Top. Power Electron.*, to be published.

[105] X. Liu, J. Xu, Z. Chen, and N. Wang, "Single-inductor dual-output buck-boost power factor correction converter," *IEEE Trans. Ind. Electron.*, vol. 62, no. 2, pp. 943–952, February 2015.

[106] W. H. Yang, C. H. Lin, K. H. Chen, C. L. Wey, Y. H. Lin, J. R. Lin, T. Y. Tsai, and J. L. Chen, "95% light-load efficiency single-inductor dual-output DC-DC buck converter with synthesized waveform control technique for USB type-C," *IEEE Symp. VLSI Circuits, Dig. Tech. Pap.*, pp. 9–10, September 2016.

[107] J. Kim and C. Chulwoo, "A single-inductor 8-channel output DC-DC boost converter with time-limited power distribution control and single shared hysteresis comparator," in Proc. *Asia South Pacific Des. Autom. Conf.* vol. 60, no. 12, pp. 33–34, 2014.

[108] A. S. J, "Design Of Integrated ZVS Single-Inductor Synchronous Buck Converter For Multiload Applications," in Proc. *Electr. Electron. Optim. Tech. Conf.,* pp. 4835–4840, 2016.

[109] E. Bonizzonil, F. Borghettil, and P. Malcovati, "A 200mA 930/O Peak Efficiency Single-inductor Dual-Output DC-DC Buck Converter," in Proc. *IEEE Int. Solid -State Circuits Conf.*, pp. 526–528, 2007.

[110] H. A. Yang, W. H. Yang, K. H. Chen, C. L. Wey, Y. H. Lin, C. C. Lee, J. R. Lin, T. Y. Tsai, and S. C. Lai, "A 96%-efficiency and 0.5%-current-cross-regulation single-inductor multiple floating-output LED driver with 24b color resolution," in Proc. *IEEE Solid-State Circuits Conf.*, vol. 59, pp. 230–231, 2016.

[111] Y. Ye and K. W. Eric Cheng, "Single-switch single-inductor multi-output pulse width modulation converters based on optimised switched-capacitor," J. *IET Power Electron.*, vol. 8, no. 11, pp. 2168–2175, 2015.

[112] O. Ray, A. P. Josyula, S. Mishra, and A. Joshi, "Integrated Dual-Output Converter," *IEEE Trans. Ind. Electron.*, vol. 62, no. 1, pp. 371–382, January 2015.

[113] K. Lin, C. Huang, D. Chen, and K. H. Liu, "Modeling and Design of Feedback Loops for a Buck Converter," in Proc. *IEEE, Power Electron. Spec. Conf. 2008*, pp. 3389–3395, 2008.

[114] M. Belloni, E. Bonizzoni, and F. Maloberti, "On the design of single-inductor double-output DC-DC buck, boost and buck-boost converters," in Proc. *15th IEEE Electron. Circuits Syst. Conf.,* pp. 626–629, 2008.

[115] D. Kwon and G. A. Rincón-mora, "Single-Inductor–Multiple-Output Switching DC–DC Converters," *IEEE Trans. Circuits Syst.*, vol. 56, no. 8, pp. 614–618, August 2009.

[116] M. A. Rojas-gonz and S. Edgar, "An Integrated Dual-Output Buck Converter

Based on Sliding Mode Control," *IEEE Third Lat. Am.. Circuits Syst Symp.,* pp. 1–4, 2012.

[117] W. Xu, Y. Li, X. Gong, Z. Hong, and D. Killat, "A Dual-Mode Single-Inductor Dual-Output Switching Converter With Small Ripple," *IEEE Trans.Power Electron.*, vol. 25, no. 3, pp. 614–623, March 2010.

[118] B. Bahrani, J. D. Dasika, M. Saeedifard, A. Karimi, and A. Rufer, "Multivariable Control of Single-Inductor," *IEEE Trans. Power Electron.*, pp. 2061-2070, April 2014.

[119] M. Belloni, E. Bonizzoni, and F. Maloberti, "On the design of single-inductor multiple-output DC-DC buck converters," in Proc. *IEEE Circuits Syst. sympo.,* pp. 3049–3052, 2008.

[120] E. C. dos Santos, "Dual-output dc–dc buck converters with bidirectional and unidirectional characteristics," *IET J.Power Electron.*, vol. 6, no. 5, pp. 999–1009, May 2013.

[121] E. C .Santos, "Single-Input Dual-Output Dc-Dc Buck Converter," in Proc. *IEEE Ind. Electron. sympo.,* vol. 3, pp. 496–502, 2012.

[122] P. Davis and K. V Aathira, "Transformer-less DIDO DC-DC Converter for EV ' s," in Proc. *Electr. Electron. Optim. Tech. Conf.,* pp. 400–404, 2016.

[123] Y. Lu, S. Yao, B. Shao, and P. Brokaw, "A 200nA single-inductor dual-input-triple-output (DITO) converter with two-stage charging and process-limit cold-start voltage for photovoltaic and thermoelectric energy harvesting," in Proc. *IEEE Solid-State Circuits Conf.*, vol. 59, pp. 368–369, 2016.

[124] E. Babaei and O. Abbasi, "Structure for multi-input multi-output dc–dc boost converter," *J. IET Power Electron.*, vol. 9, no. 1, pp. 9–19, 2016.

[125] G. Yu, K. W. R. Chew, Z. C. Sun, H. Tang, and L. Siek, "A 400 nW Single-Inductor Dual-Input-Tri-Output DC-DC Buck-Boost Converter With Maximum Power Point Tracking for Indoor Photovoltaic Energy Harvesting," *J. Solid-State Circuits*, vol. 50, no. 11, pp. 2758–2772, 2015.

[126] A. Nahavandi, M. T. Hagh, M. B. B. Sharifian, and S. Danyali, "A nonisolated multiinput multioutput DC-DC boost converter for electric vehicle applications," *IEEE Trans. Power Electron.*, vol. 30, no. 4, pp. 1818–1835, April 2015.

[127] M. Jafari, G. Hunter, and J. G. Zhu, , "A New Topology of Multi-Input Multi-Output Buck-Boost DC-DC Converter for Microgrid Applications," in Proc, *Power and Energy Conf*., pp. 286–291, 2012.

[128] Z. Zhoul, H. Wul, and V. Xingl, ""A Non-Isolated Three-Port Converter for Stand-Alone Renewable Power System," in Proc. *IEEE Electron. Soc. conf.,* vol. 3, no. c, pp. 3352–3357, 2012.

[129] H. Wu, Y. Xing, Y. Xia, and K. Sun, "A family of non-isolated three-port converters for stand-alone renewable power system," in Proc.,*Pro. IEEE Ind. Electron. Soc. Conf.,* vol. 3, pp. 1030–1035, 2011.

[130] S. Ding, H. Wu, Y. Xing, Y. Fang, and X. Ma, "Topology and control of a family of non-isolated three-port DC-DC converters with a bidirectional cell," in Proc. *IEEE Appl. Power Electron. Conf.,* no. c, pp. 1089–1094, 2013.

[131] H. Wu, K. Sun, S. Ding, and Y. Xing, "Topology Derivation of Nonisolated Three-Port DC–DC Converters From DIC and DOC," *IEEE Trans.Power Electron.*, vol. 28, no. 7, pp. 3297–3307, July 2013.

[132] S. H. Hosseini, S. K. Haghighian, S. Danyali, and H. Aghazadeh, "Multi-input dc boost converter supplied by a hybrid PV/Wind turbine power systems for street lighting application connected to the grid," in Proc. *Univ. Power Eng. Conf.,* pp. 1–6, Sep. 2012.

[133] F. Nejabatkhah, S. Danyali, S. H. Hosseini, M. Sabahi, and S. M. Niapour, "Modeling and Control of a New Three-Input DC–DC Boost Converter for Hybrid PV/FC/Battery Power System," *IIEEE Trans.Power Electron.*, vol. 27, no. 5, pp. 2309–2324, May 2012.

[134] H. Shao, X. Li, C.-Y. Tsui, and W.-H. Ki, "A Novel Single-Inductor Dual-Input Dual-Output DC – DC Converter With PWM Control for Solar Energy Harvesting System," *IEEE Trans. Very Large Scale Inte.*, vol. 22, no. 8, pp. 1693–1704, August 2014.

[135] W. Xiao, N. Ozog, and W. G. Dunford, "Topology Study of Photovoltaic Interface for Maximum Power Point Tracking," *IEEE Trans.Power Electron.*, vol. 54, no. 3, pp. 1696–1704, June 2007.

[136] E. Durán, J. Galán, and J. M. Andújar, "Comparative Analysis of Buck-Boost Converters used to obtain I-V Characteristic Curves of Photovoltaic Modules," in Proc. *IEEE Power Electron. Spec. Conf.,* pp. 2036–2042, 2008.

[137] M. H. Taghvaee, M. a. M. Radzi, S. M. Moosavain, H. Hizam, and M. Hamiruce Marhaban, "A current and future study on non-isolated DC–DC converters for photovoltaic applications," *J.Renewable Sustain. Energy Rev.*, vol. 17, pp. 216–227, January 2013.

[138] S. H. Choung and A. Kwasinski, "Multiple-Input DC-DC Converter Topologies Comparison," *IEEE Ind. Electron Conf.,* pp 2369-2364*, 2008*.

[139] S. Poshtkouhi, V. Palaniappan, M. Fard, and O. Trescases, "A General Approach for Quantifying the Benefit of Distributed Power Electronics for Fine Grained MPPT in Photovoltaic Applications Using 3-D Modeling," *IEEE Trans.Power Electron.*, vol. 27, no. 11, pp. 4656–4666, November 2012.

[140] Abraham I. Pressman, Keith Billings, Taylor Morey, *Switching Power Supply Design, Third Ed. Mc Graw Hill, New York,* 2009.

[141] D. Schelle and J. Castorena, "Buck-Converter Design Demystified," in Proc. *Power Electron. Tech. Conf.*, pp. 46–53, 2006.

[142] Maxim Integrated App. Note 4332, "How to Design an Efficient DC-DC Converter Using the DS1875 PWM Controller," pp. 1–8, 2012.

[143] M. Bella, F. Prieto, S. P. Litrán, J. Manuel, and E. Gómez, "New Single-Input,

Multiple output Converter Tiopologies," *IEEE Ind. Electron. Mag.*, vol. 10, no. 2, pp. 6–20, June 2016.

[144] M. Du and H. Lee, "A single-inductor dual-input dual-output buck regulator with enhanced power-delivery capability for portable battery management system," in Proc. *Midwest. Circuits Syst. Symp.*, vol. 1, pp. 1141–1144, 2010.

[145] M. H. Huang and K. H. Chen, "Single-inductor multi-output (SIMO) DC-DC converters with high light-load efficiency and minimized cross-regulation for portable devices," *IEEE J. Solid-State Circuits*, vol. 44, no. 4, pp. 1099–1111, April 2009.

[146] Z. Shen, X. Chang, W. Wang, X. Tan, N. Yan, and H. Min, "CCM with low cross regulation," *IEEE Trans. Power Electron.*, vol. 27, no. 4, pp. 1917–1925, April 2012.

[147] D. Ma, W. H. Ki, C. Y. Tsui, and P. K. T. Mok, "Single-inductor multiple-output switching converters with time-multiplexing control in discontinuous conduction mode," *IEEE J. Solid-State Circuits*, vol. 38, no. 1, pp. 89–100, January 2003.

[148] D. Ma, W.-H. Ki, and C.-Y. Tusi, "A pesudo-CCM/DCM SIMO switching converterwith freewhelling switching," *IEEE J. Solid state Circuits*, vol. 38, no. 6, pp. 1007–1014, 2002.

[149] Y. Zhang and D. Ma, "A fast-response hybrid SIMO power converter with adaptive current compensation and minimized cross-regulation," *IEEE J. Solid-State Circuits*, vol. 49, no. 5, pp. 1242–1255, 2014.

[150] D. Trevisan, P. Mattavelli, and P. Tenti, "Digital control of single-inductor dual-output dc-dc converters in continuous-conduction mode," in Proc. *IEEE Power Electron. Spec. Conf.*, vol. 2005, pp. 2616–2622, 2005.

[151] D. Trevisan, P. Mattavelli, and P. Tenti, "Digital control of single-inductor multiple-output step-down DC-DC converters in CCM," *IEEE Trans. Ind. Electron.*, vol. 55, no. 9, pp. 3476–3483, September 2008.

[152] a. Pizzutelli and M. Ghioni, "Novel control technique for single inductor multiple output converters operating in CCM with reduced cross-regulation," in Proc. *IEEE Appl. Power Electron. Conf. Expo.,* pp. 1502–1507, 2008.

[153] J. D. Dasika, B. Bahrani, M. Saeedifard, and A. Karimi, "Multivariable Control of Single-Inductor," *IEEE Trans. Power Electron.,* vol. 29, no. 4, pp. 2061–2070, April 2014.

[154] P. Patra, J. Ghosh, and A. Patra, "Control scheme for reduced cross-regulation in single-inductor multiple-output DC-DC converters," *IEEE Trans. Ind. Electron.*, vol. 60, no. 11, pp. 5095–5104, November 2013.

[155] B. Wang, V. Kanamarlapudi, L. Xian, X. Peng, K. Tan, and P. So, "Model Predictive Voltage Control for Single-Inductor Multiple-Output DC-DC Converter with Reduced Cross Regulation," *IEEE Trans. Ind. Electron.*, vol. 63, no. 7, pp. 4187–4197, July 2016.

[156] W. Huang, J. A. Abu Qahouq, and Z. Dang, “CCM-DCM Power-Multiplexed Control Scheme for Single-Inductor Multiple-Output DC-DC Power Converter with No Cross-Regulation,” *IEEE Trans. Ind. Appl.*, vol. 9994, no. c, pp. 1–1, 2016.

[157] S. Ang and Alejandro Oliva, “Power-Switching Converters,” *Third ed. CRC Press London*,2011.

[158] R. W. Erickson and Dragan Maksimovic, "Fundamentals of Power Electronics*"* *Second ed. Academic Publishers New York*, 2000.

[159] K. Åström and R. Murray, “Feedback systems: an introduction for scientists and engineers,” pp. 412, 2008.

[160] G. C. Goodwin, S. F. Graebe, and M. E. Salgado, “Control System Design,” *Prentice Hill ,New Jersey* ,2001.

[161] J. Peffer, “Linear Feedback Controls The essentials,” *First ed. Elsevier, London* .2013.

[162] A. Riccobono and E. Santi, “Comprehensive review of stability criteria for DC power distribution systems,” *IEEE Trans. Ind. Appl.*, vol. 50, no. 5, pp. 3525–3535, October 2014.

Appendix A: DRC 16 Statement of Contribution

DRC 16

MASSEY UNIVERSITY
GRADUATE RESEARCH SCHOOL

STATEMENT OF CONTRIBUTION
TO DOCTORAL THESIS CONTAINING PUBLICATIONS

(To appear at the end of each thesis chapter/section/appendix submitted as an article/paper or collected as an appendix at the end of the thesis)

We, the candidate and the candidate's Principal Supervisor, certify that all co-authors have consented to their work being included in the thesis and they have accepted the candidate's contribution as indicated below in the *Statement of Originality*.

Name of Candidate: Zubair Rehman

Name/Title of Principal Supervisor: A. Prof. Ibrahim Al-Bahadly

Name of Published Research Output and full reference:

Z. Rehman, I. H. Al-Bahadly and S. C. Mukhopadhyay "Multi input DC-DC Converters in Renewable Energy Applications- An Overview," Journal of Renewable and Sustainable Energy Reviews, 41, pp 521-539 January 2015.

In which Chapter is the Published Work: Chapter 2

Please indicate either:

- The percentage of the Published Work that was contributed by the candidate: 100%

  and / or
- Describe the contribution that the candidate has made to the Published Work:

Zubair Rehman Digitally signed by Zubair Rehman Date: 2017.03.29 08:59:32 +13'00'

Candidate's Signature _____ Date _____

Ibrahim Al-Bahadly Digitally signed by Ibrahim Al-Bahadly DN: cn=Ibrahim Al-Bahadly, o=Massey University, ou=SEAT, email=i.h.albahadly@massey.ac.nz, c=NZ Date: 2017.03.29 09:30:45 +13'00'

Principal Supervisor's signature _____ Date _____

GRS Version 3– 16 September 2011

MASSEY UNIVERSITY
GRADUATE RESEARCH SCHOOL

STATEMENT OF CONTRIBUTION TO DOCTORAL THESIS CONTAINING PUBLICATIONS

(To appear at the end of each thesis chapter/section/appendix submitted as an article/paper or collected as an appendix at the end of the thesis)

We, the candidate and the candidate's Principal Supervisor, certify that all co-authors have consented to their work being included in the thesis and they have accepted the candidate's contribution as indicated below in the *Statement of Originality*.

Name of Candidate: Zubair Rehman

Name/Title of Principal Supervisor: A. Prof. Ibrahim Al-Bahadly

Name of Published Research Output and full reference:

Z. Rehman, I. H. Al-Bahadly and S. C. Mukhopadhyay "Renewable Energy Harvesting for low Power Wireless Monitoring Networks", Journal of Clean Energy Technologies 2016. (Accepted for publication in journal)

In which Chapter is the Published Work: Chapter 2,3,5 & 6

Please indicate either:

- The percentage of the Published Work that was contributed by the candidate: 100%

  and / or
- Describe the contribution that the candidate has made to the Published Work:

Zubair Rehman Digitally signed by Zubair Rehman Date: 2017.03.29 09:02:44 +13'00'

Candidate's Signature _____ Date _____

Ibrahim Al-Bahadly Digitally signed by Ibrahim Al-Bahadly DN: cn=Ibrahim Al-Bahadly, o=Massey University, ou=SEAT, email=i.h.albahadly@massey.ac.nz, c=NZ Date: 2017.03.29 09:31:32 +13'00'

Principal Supervisor's signature _____ Date _____

GRS Version 3– 16 September 2011

MASSEY UNIVERSITY
GRADUATE RESEARCH SCHOOL

STATEMENT OF CONTRIBUTION TO DOCTORAL THESIS CONTAINING PUBLICATIONS

(To appear at the end of each thesis chapter/section/appendix submitted as an article/paper or collected as an appendix at the end of the thesis)

We, the candidate and the candidate's Principal Supervisor, certify that all co-authors have consented to their work being included in the thesis and they have accepted the candidate's contribution as indicated below in the *Statement of Originality*.

Name of Candidate: Zubair Rehman

Name/Title of Principal Supervisor: A. Prof. Ibrahim Al-Bahadly

Name of Published Research Output and full reference:

Z. Rehman, I. H. Al-Bahadly and S. C. Mukhopadhyay "Dual Input-Dual Output Single Inductor dc-dc Converter", Proceedings of 41st International Annual Conference of the IEEE Industrial Electronics Society, IECON 2015, pp 004848-004853, 2015.

In which Chapter is the Published Work: Chapter 2, 3, 5 & 6

Please indicate either:

- The percentage of the Published Work that was contributed by the candidate: 100%

  and / or
- Describe the contribution that the candidate has made to the Published Work:

Zubair Rehman Digitally signed by Zubair Rehman Date: 2017.03.29 09:05:24 +13'00'

Candidate's Signature _____ Date _____

Ibrahim Al-Bahadly Digitally signed by Ibrahim Al-Bahadly DN: cn=Ibrahim Al-Bahadly, o=Massey University, ou=SEAT, email=i.h.albahadly@massey.ac.nz, c=NZ Date: 2017.03.29 09:32:15 +13'00'

Principal Supervisor's signature _____ Date _____

GRS Version 3– 16 September 2011

MASSEY UNIVERSITY
GRADUATE RESEARCH SCHOOL

STATEMENT OF CONTRIBUTION TO DOCTORAL THESIS CONTAINING PUBLICATIONS

(To appear at the end of each thesis chapter/section/appendix submitted as an article/paper or collected as an appendix at the end of the thesis)

We, the candidate and the candidate's Principal Supervisor, certify that all co-authors have consented to their work being included in the thesis and they have accepted the candidate's contribution as indicated below in the *Statement of Originality*.

Name of Candidate: Zubair Rehman

Name/Title of Principal Supervisor: A. Prof. Ibrahim Al-Bahadly

Name of Published Research Output and full reference:

Z. Rehman, I. H. Al-Bahadly and S. C. Mukhopadhyay "Dual Input-Dual Output Single Inductor dc-dc Converter for Renewable Energy Applications," Proceedings of 4th International Conference on Renewable Energy and Research Applications ICRERA, pp 783-788, 2015.

In which Chapter is the Published Work: 2,3,4,5 & 6

Please indicate either:

- The percentage of the Published Work that was contributed by the candidate: 100%

  and / or
- Describe the contribution that the candidate has made to the Published Work:

Zubair Rehman Digitally signed by Zubair Rehman Date: 2017.03.29 09:07:07 +13'00'

Candidate's Signature _____ Date _____

Ibrahim Al-Bahadly Digitally signed by Ibrahim Al-Bahadly DN: cn=Ibrahim Al-Bahadly, o=Massey University, ou=IEAT, email=i.h.albahadly@massey.ac.nz, c=NZ Date: 2017.03.29 09:32:52 +13'00'

Principal Supervisor's signature _____ Date _____

GRS Version 3– 16 September 2011

MASSEY UNIVERSITY
GRADUATE RESEARCH SCHOOL

STATEMENT OF CONTRIBUTION TO DOCTORAL THESIS CONTAINING PUBLICATIONS

(To appear at the end of each thesis chapter/section/appendix submitted as an article/paper or collected as an appendix at the end of the thesis)

We, the candidate and the candidate's Principal Supervisor, certify that all co-authors have consented to their work being included in the thesis and they have accepted the candidate's contribution as indicated below in the *Statement of Originality*.

Name of Candidate: Zubair Rehman

Name/Title of Principal Supervisor: A. Prof. Ibrahim Al-Bahadly

Name of Published Research Output and full reference:

Z. Rehman, I. H. Al-Bahadly and S.C.Mukhopadhyay, "A Non-Isolated DC-DC converter for Renewable Energy Based Portable Measuring Instruments," Proceedings of IEEE Instrumentation and Measurement Technology Conference I2MTC pp. 936-941, 2013.

In which Chapter is the Published Work: Chapter 2,3 & 5

Please indicate either:

- The percentage of the Published Work that was contributed by the candidate: 100%

  and / or

- Describe the contribution that the candidate has made to the Published Work:

Zubair Rehman Digitally signed by Zubair Rehman Date: 2017.03.29 09:09:06 +13'00'

Candidate's Signature _____ Date

Ibrahim Al-Bahadly Digitally signed by Ibrahim Al-Bahadly DN: cn=Ibrahim Al-Bahadly, o=Massey University, ou=IEAT, email=i.h.albahadly@massey.ac.nz, c=NZ Date: 2017.03.29 09:33:31 +13'00'

Principal Supervisor's signature _____ Date

GRS Version 3– 16 September 2011

Appendix B: Altium Model for Multiport Converter

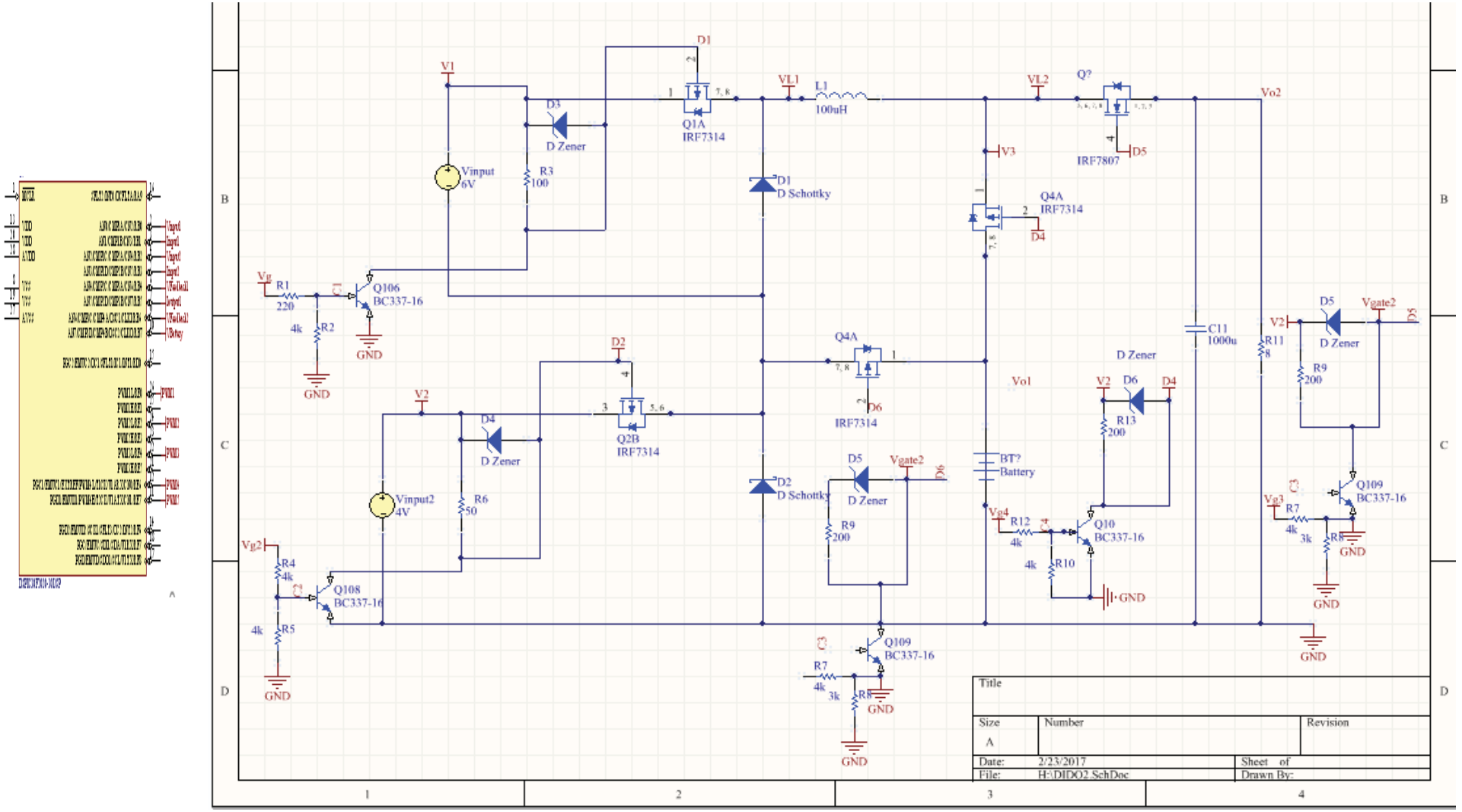

Digital Controller DSPIC 30F2020

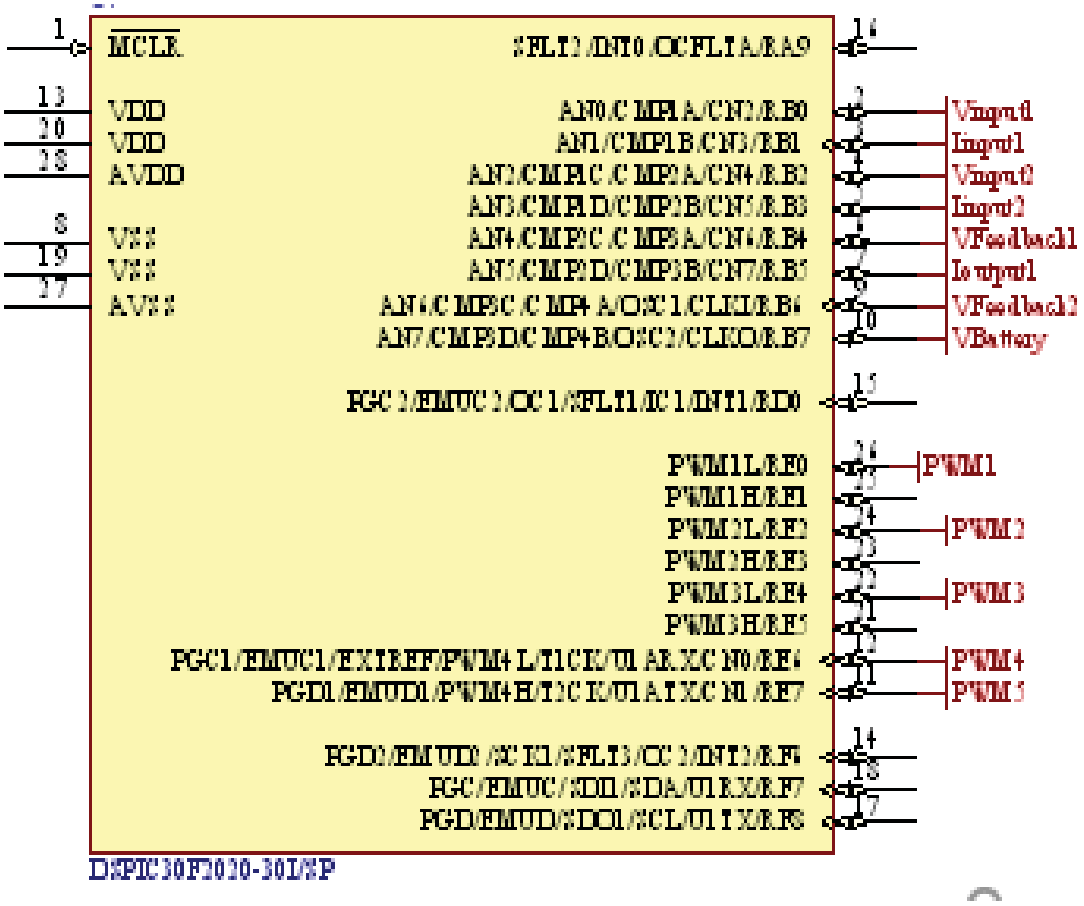

Appendic C: Altium Simulation Results in DIDO mode

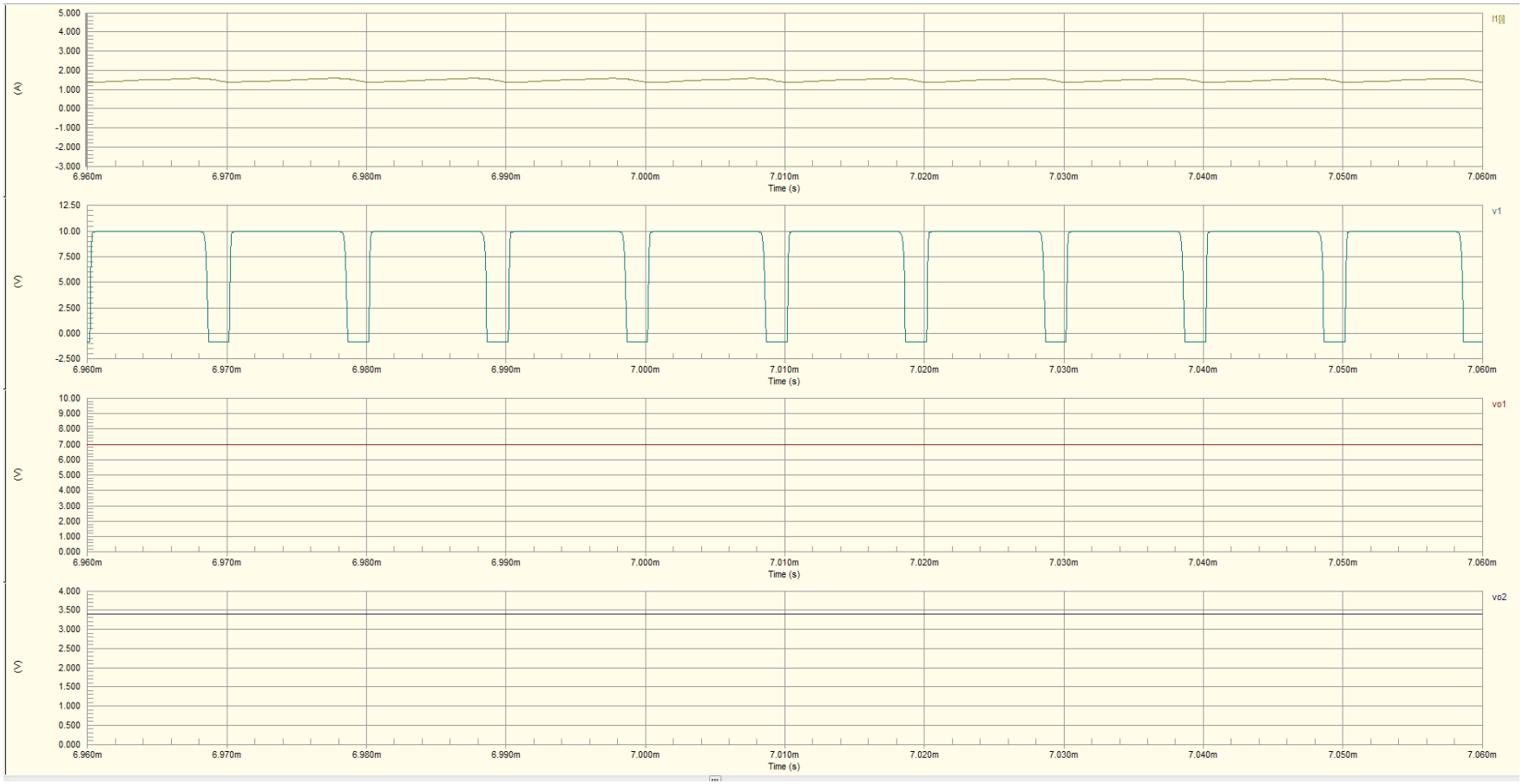
I1[i]
(A)
5.000
4.000
3.000
2.000
1.000
0.000
-1.000
-2.000
-3.000
v1
(V)
12.50
10.00
7.500
5.000
2.500
0.000
-2.500
vo1
(V)
10.00
9.000
8.000
7.000
6.000
5.000
4.000
3.000
2.000
1.000
0.000
vo2
(V)
4.000
3.500
3.000
2.500
2.000
1.500
1.000
0.500
0.000
6.960m
6.970m
6.980m
6.990m
7.000m
7.010m
7.020m
7.030m
7.040m
7.050m
7.060m
Time (s)

Appendix D: Computer Program to control the converter

```
#include "p30F2020.h"
_FOSCSEL(FRC_PLL)
_FOSC(CSW_FSCM_OFF & FRC_HI_RANGE & OSC2_CLKO)
_FPOR(PWRT_128)
_FGS(CODE_PROT_OFF)

unsigned int output;
double error;
double setpoint;
double measured_value;
double integral;
double error;
double dt;
double output_pi;
double Kp;
double Ki;
double previous_error ;
double duty_cycle ;
int16_t out1;

unsigned int output1;
double error1;
double setpoint1;
double measured_value1;
double integral1;
double error1;
```

```
double dt;
double output_pi1;
double Kp1;
double Ki1;
double previous_error1 ;
double duty_cycle1;
int16_t out2;

int main(void)
{
PTPER = 9350;
IOCON1bits.PENH= 1;
IOCON1bits.PENL= 1;
IOCON1bits.POLH= 0;
IOCON1bits.POLL= 0;
IOCON1bits.PMOD= 1;
IOCON1bits.OVRENH = 0;
IOCON1bits.OVRENL = 0;
TRGCON1bits.TRGDIV = 0;
TRGCON1bits.TRGSTRT= 0;
TRIG1 = 7480;
PWMCON1bits.FLTSTAT = 0;
PWMCON1bits.CLSTAT = 0;
PWMCON1bits.TRGSTAT = 0;
PWMCON1bits.FLTIEN = 0;
PWMCON1bits.CLIEN = 0;
PWMCON1bits.TRGIEN = 0;
PWMCON1bits.ITB= 0;
PWMCON1bits.MDCS = 0;
```

```
PWMCON1bits.DTC= 2;
PWMCON1bits.XPRES = 0;
PWMCON1bits.IUE = 0;
PDC1 = 7480;
PHASE1 = 0;
DTR1    = 0;
ALTDTR1 = 0;
IOCON2bits.PENH= 1;
IOCON2bits.PENL= 1;
IOCON2bits.POLH= 0;
IOCON2bits.POLL= 0;
IOCON2bits.PMOD= 1;
IOCON2bits.OVRENH = 0;
IOCON2bits.OVRENL = 0;
TRGCON2bits.TRGDIV = 3;
TRGCON2bits.TRGSTRT= 2;
TRIG2 = 200;
PWMCON2bits.FLTSTAT = 0;
PWMCON2bits.CLSTAT = 0;
PWMCON2bits.TRGSTAT = 0;
PWMCON2bits.FLTIEN = 0;
PWMCON2bits.CLIEN = 0;
PWMCON2bits.TRGIEN = 0;
PWMCON2bits.ITB= 0;
PWMCON2bits.MDCS = 0;
PWMCON2bits.DTC= 2;
PWMCON2bits.XPRES = 0;
PWMCON2bits.IUE = 0;
PDC2 = 1870;
```

```
PHASE1 = 0;
 DTR2    = 64;
 ALTDTR2 = 64;
IOCON3bits.PENH= 1;
IOCON3bits.PENL= 1;
IOCON3bits.POLH= 0;
IOCON3bits.POLL= 0;
IOCON3bits.PMOD= 1;
IOCON3bits.OVRENH = 0;
IOCON3bits.OVRENL = 0;
TRGCON3bits.TRGDIV = 0;
TRGCON3bits.TRGSTRT= 0;
TRIG3 = 7840;
PWMCON3bits.FLTSTAT = 0;
PWMCON3bits.CLSTAT = 0;
PWMCON3bits.TRGSTAT = 0;
PWMCON3bits.FLTIEN = 0;
PWMCON3bits.CLIEN = 0;
PWMCON3bits.TRGIEN = 0;
PWMCON3bits.ITB= 0;
PWMCON3bits.MDCS = 0;
PWMCON3bits.DTC= 2;
PWMCON3bits.XPRES = 0;
PWMCON3bits.IUE = 0;
PDC3 = 5610;
PHASE3 = 0;
ADCONbits.ADSIDL = 0;
ADCONbits.FORM = 0;
ADCONbits.EIE = 1;
```

```
ADCONbits.ORDER = 0;
ADCONbits.SEQSAMP = 1;
ADCONbits.ADCS = 5;
ADPCFG = 0xFFFC;
ADSTAT = 0;
ADCPC0bits.TRGSRC0 = 0x4;
ADCPC0bits.IRQEN0 = 1;
 ADCPC0bits.TRGSRC0 = 0x4;
ADCPC0bits.IRQEN0 = 1;
ADCONbits.ADON = 1;

IFS0bits.ADIF = 0;
IPC2bits.ADIP = 4;
IEC0bits.ADIE = 1;

PTCON = 0x8000;

error=0;
measured_value=0;
integral=0;
error=0;
dt=0.000010;
Kp= 0.00038;
Ki=1.66;
previous_error=0;
duty_cycle=0;
error1=0;
measured_value1=0;
integral1=0;
```

```
dt=0.000010;
Kp1=0.005;
Ki1=1.5;
previous_error1=0 ;
duty_cycle1=0 ;

TRISEbits.TRISE3=0;
while(1);
}

void __attribute__((interrupt, no_auto_psv)) _ADCInterrupt()
{
int channel0Result;

IFS0bits.ADIF = 0;
ADSTATbits.P0RDY = 0;
channel0Result = ADCBUF0;

     PORTEbits.RE3=1;
      setpoint= 395;
      measured_value=(double)channel0Result;
      error = setpoint - measured_value;
      integral = integral + error*dt;
      output_pi = Kp*error + Ki*integral;
      previous_error = error;
      duty_cycle = output_pi;

int channel2Result;
PORTEbits.RE3=0;
```

```
       // if (duty_cycle > 0.8) {duty_cycle = 0.8;}
      // if (duty_cycle < 0.2) {duty_cycle = 0.2;}
        PDC1=(duty_cycle)*9350;
        PDC1 = (PDC1 >= 7480) ? 7480 :
 ((PDC1 <= 1870) ? 1870 : PDC1);
       setpoint1= 200;
      measured_value1=(double)channel2Result;
       error1 = setpoint1 - measured_value1;
       integral1 = integral1 + error1*dt;
       output_pi1 = Kp*error1 + Ki*integral1;
       previous_error = error1;
        duty_cycle1 = output_pi1;

if (duty_cycle1 > 0.8) {duty_cycle1 = 0.8;}
       if (duty_cycle1 < 0.2) {duty_cycle1 = 0.2;}
      PDC2=(duty_cycle1*9350);
PDC2 = 6545;
/* Update the Duty cycle with value read from AN1
   PDC value will be such that 7F >= PDC2 >= 3F0 */
       PDC2 = (out2 >= 7480) ? 7480 :
 ((out2 <= 1870) ? 1870 : out2);
PDC3 = 7000;
       PDC1 =channel0Result;
       PDC2 =channel2Result;
            (channel0Result >= 0x03F0) ? 0x03F0 :
((channel0Result <= 0x007F) ? 0x007F : channel0Result);
}
```